

Distribution Agreement

In presenting this thesis or dissertation as a partial fulfillment of the requirements for an advanced degree from Emory University, I hereby grant to Emory University and its agents the non-exclusive license to archive, make accessible, and display my thesis or dissertation in whole or in part in all forms of media, now or hereafter known, including display on the world wide web. I understand that I may select some access restrictions as part of the online submission of this thesis or dissertation. I retain all ownership rights to the copyright of the thesis or dissertation. I also retain the right to use in future works (such as articles or books) all or part of this thesis or dissertation.

Signature:

Qiushi Yin

April 16, 2010

Date

**Polyoxometalates as Water Oxidation Catalysts
and Their Use in Light-Driven Water Splitting**

By

Qiushi Yin
Bachelor of Science and Master of Science

Chemistry

Craig L. Hill
Advisor

Cora MacBeth
Committee Member

Tianquan Lian
Committee Member

Aaron Abrams
Committee Member

Accepted:

Lisa A. Tedesco, Ph. D.
Dean of the James T. Laney School of Graduate Studies

Date

**Polyoxometalates as Water Oxidation Catalysts
and Their Use in Light-Driven Water Splitting**

By

Qiushi Yin

Advisor: Craig L. Hill, Ph. D.

An Abstract of
A thesis submitted to the Faculty of the
James T. Laney School of Graduate Studies of Emory University
in partial fulfillment of the requirements for the degree of
Bachelor of Science and Master of Science
in Chemistry
2010

Abstract

Polyoxometalates as Water Oxidation Catalysts and Their Use in Light-Driven Water Splitting

By Qiushi Yin

Transition-metal substituted polyoxometalates are used to construct molecular analogues of heterogeneous metal-oxide clusters. The importance of these ligand-stabilized all-inorganic metal-oxide clusters originate from both their functionality and their molecular nature, which provides a system for mechanistic studies of metal-oxide water oxidation catalysis. Investigations were made to explain two polyoxometalates' ability to oxidize water at low overpotential with efficient redox leveling. Chapter I summarizes recent findings on the chemistry of a tetra-ruthenium polyoxometalate and includes studies of its rich redox chemistry. Chapter II describes discovery of a tetra-cobalt polyoxometalate water oxidation catalyst and discusses its possible electronic structure. Chapter III illustrates that molecular water oxidation catalysts can be interfaced efficiently with photo-driven systems to capture light energy.

**Polyoxometalates as Water Oxidation Catalysts
and Their Use in Light-Driven Water Splitting**

By

Qiushi Yin

Advisor: Craig L. Hill, Ph. D.

A thesis submitted to the Faculty of the
James T. Laney School of Graduate Studies of Emory University
in partial fulfillment of the requirements for the degree of
Bachelor of Science and Master of Science
in Chemistry
2010

Acknowledgements

When I first joined Dr. Hill's lab in the November of 2007, I did not imagine that I would come to live and breathe chemistry the way I do today. I am eternally grateful to those who have inspired and encouraged my love for chemistry. I set upon my path in life now thanks to those who have made my research experience exceptionally enjoyable.

I was not born a scientist. I thank my parents for giving me my first set of books: biographies of the greatest scientists, which, in retrospect, enkindled my desire to be a research scientist. I was able to follow this desire in large part thanks to the opportunities my father works tirelessly to afford me and the unwavering support my mother unfailingly gave me, even after her passing.

My undergraduate education did not truly begin until after I joined the Hill lab. I thank all its members, who are each both teacher and friend. In particular, I thank Yurii Gueletii for his immense reservoir of knowledge, wisdom, and hands-on experience. His patient mentoring sculpted me into an experimentalist, and his love for laboratory science in old age fills me with optimism about my own future.

I thank Dr. Hill for providing me the incredible opportunity to work in his lab. He has consistently been the perfect mixture of hands-on and hands-off research advisor. His mentoring style has allowed me to flourish by focusing me on the broad scientific ideas while allowing me to work on, and resolve, the finer details. Moreover, I have benefitted greatly by learning from his vast experience in communicating and managing scientific research.

I would also like to thank my other advisors and committee members: Dr. MacBeth for always being there and willing to help as well as her unbridled love

of inorganic chemistry; Dr. Lian for exposing me to material science and physical chemistry; Dr. Abrams for keeping math fun and for taking the time to read my thesis; Dr. Weinschenk for teaching a memorable orgo class and making my decision to major in chemistry a no-brainer.

Lastly, I would like to thank Emory University for providing a first-class education and for giving me these opportunities with zero financial burdens. I will graduate, proud to be an Emory alumnus.

In closing, I hope that my career will be a worthy reflection of all who have touched my life, whether they are mentioned in this far-too-brief acknowledgement or not.

Table of Contents

Abstract

Acknowledgements

List of Figures

List of Tables

Chapter I	Redox Properties of a Polyoxometalate Water Oxidation Catalyst, $[\text{Ru}_4\text{O}_4(\text{OH})_2(\text{H}_2\text{O})_4(\text{SiW}_{10}\text{O}_{36})_2]^{10-}$, and corresponding Implications in its Oxidation Chemistry.....	1
	Introduction	3
	Experimental	7
	Results and Discussion	8
Chapter II	Discovery and Identification of a Carbon-Free Molecular Cobalt Oxide Water Oxidation Catalyst and Its Characterization	27
	Introduction	29
	Experimental	30
	Results and Discussion	40
Chapter III	Coupling of Photosensitizers with Molecular Water Oxidation Catalysts for use in Artificial Photosynthesis, and Light-driven Water Splitting via Photoelectrochemical Cells.....	72

Introduction	74
Experimental	76
Results and Discussion	78

List of Figures

Chapter I

Figure 1.1	Energy density diagram	5
Figure 1.2	A chemical scheme for water splitting.....	6
Figure 1.3	UV-Vis spectra of 1 in 0.1 M H ₂ SO ₄	9
Figure 1.4	Voltammogram of 1 in 0.2 M pH 2 lithium sulfate buffer	10
Figure 1.5	<i>E</i> _{1/2} values of 1(n) as a function of the redox state	11
Figure 1.6	Absorption spectra of 1(+2) in 0.1 M H ₂ SO ₄	13
Figure 1.7	Time profile of the absorbance at $\lambda = 445$ nm.	14
Figure 1.8	The UV-visible absorption spectra of reduced 1(-2)	15
Figure 1.9	The absorbance at 445 nm of a reduced 20 μ M 1(-2) at r.t.....	16
Figure 1.10	The absorbance at 445 nm of a reduced 20 μ M 1(-2) at 45°C.....	17

Chapter II

Figure 2.1	Thermogravimetric Analysis (TGA) of crystalline Na₁₀-2	31
Figure 2.2	FT-Infrared spectrum of 2	32
Figure 2.3	UV-Visible spectrum of 1 mM 2 in pH 8	33
Figure 2.4	³¹ P NMR of a post catalytic solution containing 2	39
Figure 2.5	Cyclic voltammogram of 2 at pH 8.....	42

Figure 2.6	X-ray structure of Na₁₀-2	44
Figure 2.7	Structure of cobalt-containing polytungstate complexes 2-9	46
Figure 2.8	Hyperbolic fit of O ₂ yield versus catalyst concentration	48
Figure 2.9	UV-Visible spectra showing cobalt titration using bpy	51
Figure 2.10	³¹ P NMR of 2 at pH 8	53
Figure 2.11	³¹ P NMR of 2 at pH 3.5	54
Figure 2.12	³¹ P NMR of 2 at pH 6	55
Figure 2.13	³¹ P NMR of 2 at pH 9	56
Figure 2.14	CV showing catalyst 2 maintaining activity after use	61
Figure 2.15	CV showing Co(aq.) ²⁺ does not maintaining activity after use	62

Chapter III

Figure 3.1	A scheme for light-driven water oxidation	75
Figure 3.2	Time-profile of light-driven O ₂ yield with 2 and persulfate	80
Figure 3.3	Structure of [Ru(mptpy) ₂] ⁴⁺	80
Figure 3.4	Time-profile of light-driven O ₂ yield using [Ru(mptpy) ₂] ⁴⁺	82
Figure 3.5	A scheme for photoelectrochemical splitting of water	83
Figure 3.6	Electronic spectra of a Fe ₂ O ₃ film with and without 1	84
Figure 3.7	Reaction scheme for the functionalization of SMO surface.	85
Figure 3.8	Reflectance IR spectrum of functionalized Fe ₂ O ₃ surface.....	85
Figure 3.9	Photocurrent obtained using the photoelectrochemical cell	86
Figure 3.10	UV-visible spectrum of Cr-O modified TiO ₂ surface.....	88

List of Tables

Chapter 2

Table 2.1	Crystal data and refinement parameters for Na₁₀-2	35
Table 2.2	Co-containing POMs as potential WOCs	41
Table 2.3	The effect of bpy on the catalytic activity of 2 and Co(aq) ²⁺	58

Chapter I

Redox Properties of a Polyoxometalate Water Oxidation Catalyst, [Ru₄O₄(OH)₂(H₂O)₄(SiW₁₀O₃₆)₂]¹⁰⁻, and Corresponding Implications in its Oxidation Chemistry

Published in part in “Structural, Physicochemical, and Reactivity Properties of an All-Inorganic, Highly Active Tetraruthenium Homogeneous Catalyst for Water Oxidation,” *J. Am. Chem. Soc.* **2009**, *131*, 17360–17370.

With Geletii, Y. V.; Besson, C.; Hou, Y.; Musaeu, D. G.; Quinonero, D.; Cao, R.; Hardcastle, K. I.; Proust, A.; Kogerler P.; Hill C. L.

Abstract

Due to the push for clean renewable fuel, water oxidation catalysts have garnered much attention because of its essential role in water splitting. Some interesting characteristics of an all-inorganic water oxidation catalyst, $[\text{Ru}_4\text{O}_4(\text{OH})_2(\text{H}_2\text{O})_4(\text{SiW}_{10}\text{O}_{36})_2]^{10-}$, are described and discussed here. In particular, the tetra-ruthenium core is able to accommodate multiple electronic charges and thus has multiple accessible redox states. Moreover, the four-electron oxidation associated with water oxidation chemistry was identified and is shown to be within a short potential range, demonstrating a redox leveling effect. Unlike most known redox leveling effects, which are attributed to proton coupled electron transfer, this molecule seems to have this characteristic due to its metal-oxo frame and appears to resemble a molecular capacitor.

Introduction

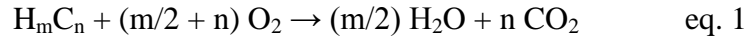
The impending energy crisis is much more than apocalyptic noise. It is based upon scientific models which unanimously point to the need to rapidly develop a renewable energy economy.¹⁻²² The issue with our current petroleum-dependent energy economy is two-fold. Fossil fuels are a limited resource: they are reservoirs of millions of years of photosynthetic hydrocarbon production, and are raw ingredients in many modern necessities.^{13,15,20-22} Also important are the effects burning hydrocarbons has on the global climate by producing the greenhouse gas, CO₂. Current models predict that, unless new means of renewable energy are obtained, energy shortage will significantly limit our quality of life within the century and CO₂ production will cause irreversible change to Earth's climate in 50 years.^{3-6,9,13,18,22,23}

Nuclear energy and solar energy are the only two sources of energy scalable to meet our growing energy demands.^{3,4,6,8,9,13,17,21,24} Serious scientific and engineering problems plaguing fusion power plants make them virtually unattainable within our lifetime.^{8,10,13,17,24-27} The only viable option for establishing a renewable and sustainable energy economy must therefore be solar-based.^{1,2,6,10-14,19-22,24,28} Approximately 1366 Wm⁻² of sunlight reaches the upper atmosphere of Earth and 239 Wm⁻² of that energy reaches Earth's surface as harvestable light. We currently consume about 16 TW globally, or 0.032 Wm⁻².^{3,29} Theoretically, sunlight contains more than enough energy to sustain our need for it.

The issue, however, is one of energy conversion. Energy in the form of electromagnetic radiation does us little good.^{10,11,13,16,22} We require energy that can be used to move our cars, run our computers, and heat our homes. In other words, our modern energy needs requires the instant conversion of stored energy into kinetic, thermal, electrical, or light energy. As such, the most efficient and sensible course of action is to convert solar energy into chemical energy, which can then be stored and released on demand.

When converting solar energy into chemical energy. Two main issues must be considered: energy density and accessibility.^{1,6,14,28} Figure 1.1 shows an energy density diagram. While metals may release large quantities of energy when oxidized, this energy is not readily accessible or recyclable. Batteries, on the other hand, can be easily paired with a photovoltaic cell to store energy. However, their charging and discharging rates are limited.³⁰ More importantly, batteries have extremely poor energy densities. In both regards, hydrocarbons are ideal candidates for storage of chemical energy.^{11,31-33} Whether hydrogen can be used effectively is of debate. It must be noted that these compounds only “store” energy when coupled with an oxidizer in redox reactions. In summary, light energy is captured by forming a kinetically stable oxidant/reductant pair.

A hydrogen-based economy is clearly the most promising form of renewable energy (whether hydrogen is best stored as diatomic hydrogen, a hydrocarbon, or even hydrides is beyond the scope of this thesis). However, all energy stored in this form requires the air-abundant oxygen as an oxidant. The energy generating reaction therefore is of the general form expressed in eq. 1.



Storing energy in a hydrogen economy must involve the splitting of water.

This redox reaction can be separated into two half-reactions, the oxidation of water and the reduction of water. Water can be reduced to covalent hydrogen bonds in the form of any of the previously described chemicals (e.g. eqs. 2-4). Conversely, water must invariably be oxidized to oxygen in such a scheme (eq. 5).

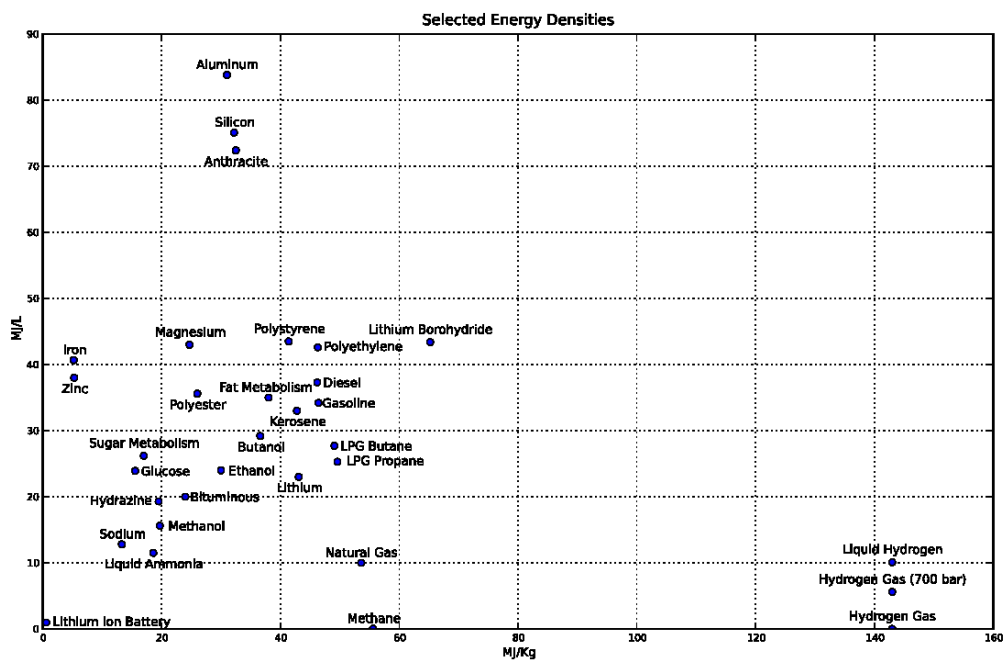
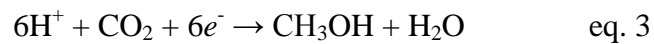


Figure 1.1 Energy density diagram of hydrogen storage chemicals by volume (y-axis) and by mass (x-axis).

The redox reactions store potential energy in chemical bonds, this energy must be captured using a photosensitizing device.^{1,10,12-14,17,20-22,24,28,34} This scheme is summarized in figure 1.2. Water oxidation is a critical reaction in such a scheme and is arguably the more difficult of the two half reactions.^{22,35-42} Therefore, the development of new water oxidation catalysts (WOCs) and understanding of existing WOCs are of great importance.

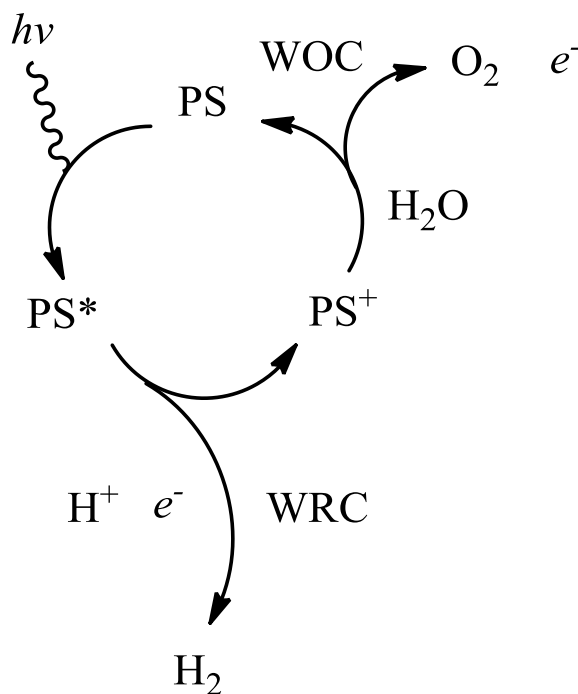


Figure 1.2 A generalized chemical scheme for water splitting. PS: photosensitizer, PS*: photoexcited photosensitizer, PS⁺: oxidized photosensitizer, WOC: water oxidation catalyst, WRC: water reduction catalyst.

The oxidizing potentials required for water oxidation ($1.229V - 0.059V \times pH$ at $25\text{ }^\circ C$) inevitably leads to the decomposition of organic complexes.³⁶⁻⁵³ The development of oxidation-resistant WOCs is necessary if the

scheme shown in figure 1.2 is to become applicable. The Hill group previously reported an all-inorganic WOC, $[\text{Ru}_4\text{O}_4(\text{OH})_2(\text{H}_2\text{O})_4(\text{SiW}_{10}\text{O}_{36})_2]^{10-}$ (**1**).^{38,42} In this chapter, I will discuss studies related to the understanding of this complex.

Experimental

Synthesis of $\text{Rb}_8\text{K}_2[\text{Ru}_4\text{O}_4(\text{OH})_2(\text{H}_2\text{O})_4(\text{SiW}_{10}\text{O}_{36})_2] \cdot 25\text{H}_2\text{O}$

$\text{Rb}_8\text{K}_2[\text{Ru}_4\text{O}_4(\text{OH})_2(\text{H}_2\text{O})_4(\text{SiW}_{10}\text{O}_{36})_2]$ (**Rb₈K₂-1**) was synthesized from a mixture of ruthenium trichloride and potassium γ -decatungstosilicate. Commercially available RuCl_3 and freshly prepared $\text{K}_8[\text{SiW}_{10}\text{O}_{36}]$ were mixed in a 1:2 molar ratio and dissolved in water to give an approximately 10 mM final concentration of **1**, giving a brown solution. The pH was adjusted from *ca.* 2.6 to 1.6 with the drop-wise addition of 6M HCl. After additional stirring, RbCl was then added slowly until small amounts of precipitates formed. The precipitate was redissolved with the addition of water. This solution was filtered and the filtrate left at room temperature (r.t.). Crystalline brown plates of **Rb₈K₂-1** was collected after 24 hours. The structure of **1** was confirmed using elemental analysis, infrared spectroscopy, x-ray crystallography, and UV-Visible spectroscopy.

Stoichiometric chemical oxidation and reduction of 1

UV-visible studies of the one- and two-electron reduced forms of **1**, the resting oxidation state of **1**, and the one- and two-electron oxidized forms of **1**, **1(-2)**, **1(-1)**, **1(0)**, **1(+1)**, **1(+2)**, respectively, were done through the reversible redox titrations of complex **1**. In a typical experiment, $>10 \mu\text{M}$ solution of **1** in acidic conditions ($\text{pH} < 2$) were titrated using 1 mM cerium ammonium nitrate as an oxidant or 1 mM tin (II) sulfate as a reductant.

Instrumentation

Cyclic voltammograms (CVs) were obtained at room temperature in buffered solutions using BAS CV-50W voltammetric analyzer. An Ag/AgCl (saturated NaCl) reference electrode from BAS was used. Potentials in the CV are reported relative to the NHE by the addition of 200 mV to the BAS electrode values. CVs were all obtained under Ar.

Infrared spectra (2% sample in KBr) were recorded on a Nicolet 510 FTIR spectrometer. UV-visible absorption spectra were acquired using an Agilent 8453 spectrophotometer equipped with a diode-array detector and with a magnetic stirrer and temperature controller (Agilent 89090A).

Hi-Tech KinetAsyst™ Stopped Flow SF-61SX2 equipped with a diode array detector operating in wavelength range 400-700 nm was used in precision kinetics studies. Timescales: from 0-0.4 s up to 0-400 s. Optical path length is 1 cm.

Results and Discussion

As reported, all characterizations of the crystalline **1** are consistent with the Ru₄O₆ core having the oxidation state Ru₄^{IV,IV,IV,IV}O₆ (**1(0)**).³⁸ Stoichiometric titration of **1** in acidic medium using cerium (IV) ammonium nitrate as an oxidant and tin (II) sulfate as a reductant shows reversible four-electron transfer, which can be followed by UV-Vis spectroscopy. The oxidized species, (**1(+1)** and **1(+2)**) and reduced (**1(-1)** and **1(-2)**) species have characteristic UV-Vis spectra (figure 1.3). It was observed that all five species seen in the UV-Visible absorption spectra are relatively stable within an hour at ambient temperature.

The cyclic voltammogram (CV) of **1** shows four anodic and cathodic peaks between 400 mV and 1000 mV (figure 1.4). Bulk electrolysis at these potentials and characterization using UV-Vis spectroscopy allows the assignments shown in figure 1.5.³⁸ These assignments indicate that it is thermodynamically impossible for **1(+2)** to oxidize water in acidic medium. Along with the fact that **1(+2)** is relatively stable in water, this is evidence that **1(+2)** is not the water oxidizing species. The actual water oxidizing species is in a higher oxidation state. In fact, either **1(+3)** or **1(+4)** might be capable of water evolution. Additional kinetics studies and extrapolation from figure 1.5 indicate that **1(+4)** evolves oxygen in the chemical water oxidation system reported in previous literature.³⁸

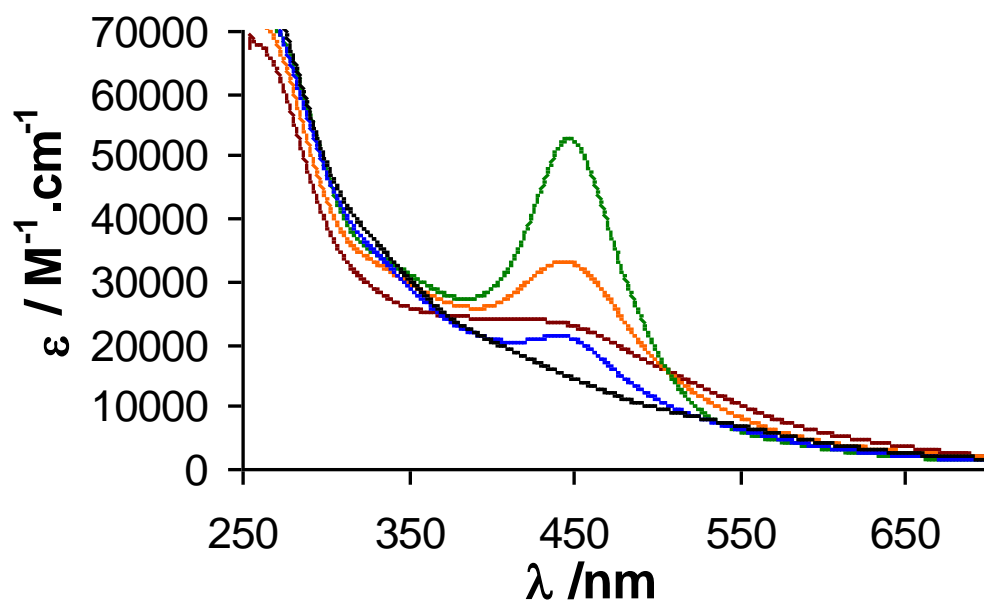


Figure 1.3 UV-Vis spectra of **1** in 0.1 M H₂SO₄. Green: **1(0)**, Blue: **1(+1)**, Black: **1(+2)**, Orange: **1(-1)**, Brown: **1(-2)**.

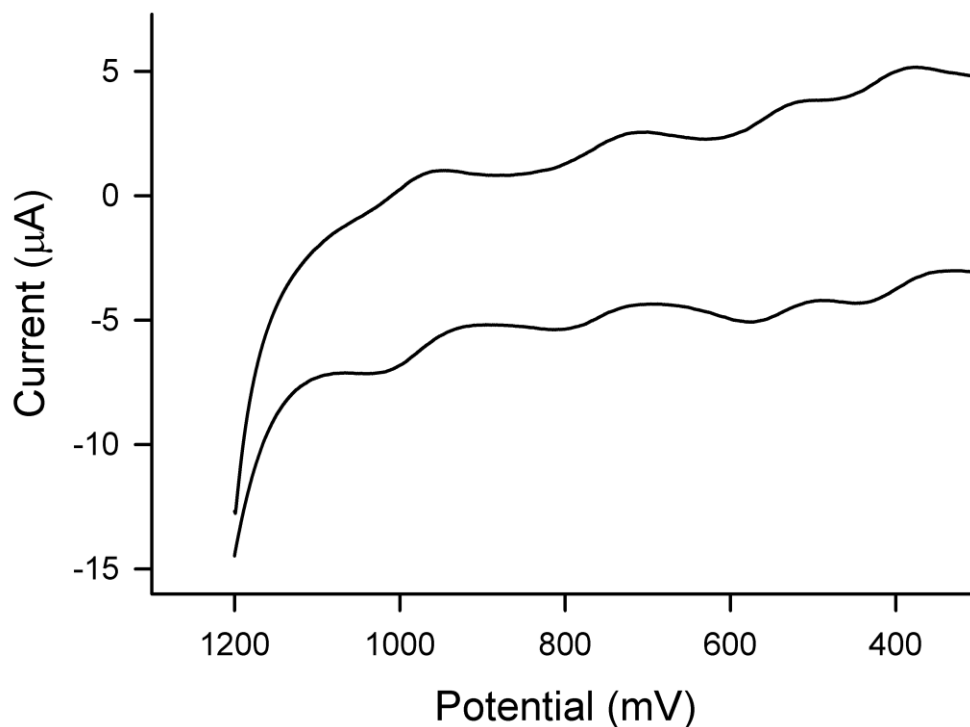


Figure 1.4 Voltammogram of **1** in 0.2 M pH 2 lithium sulfate buffer.

An interesting property of complex **1** is the redox leveling seen in figure 1.5. Specifically, the multiple redox states are relatively close in energy. Since each oxidative step in the catalytic system is done at the same potential, redox leveling allows more accessible oxidation states with less wasted potential energy. Surprisingly, this redox leveling effect does not appear to come from proton coupled electron transfer (PCET) because no direct pH dependence is observed.^{38,54-60} Acid-base titrations indicate that **1(0)** has a pK_a between 3 and 4. Deprotonation at higher pH causes a shift in the redox potentials of all redox states by approximately 400 mV.

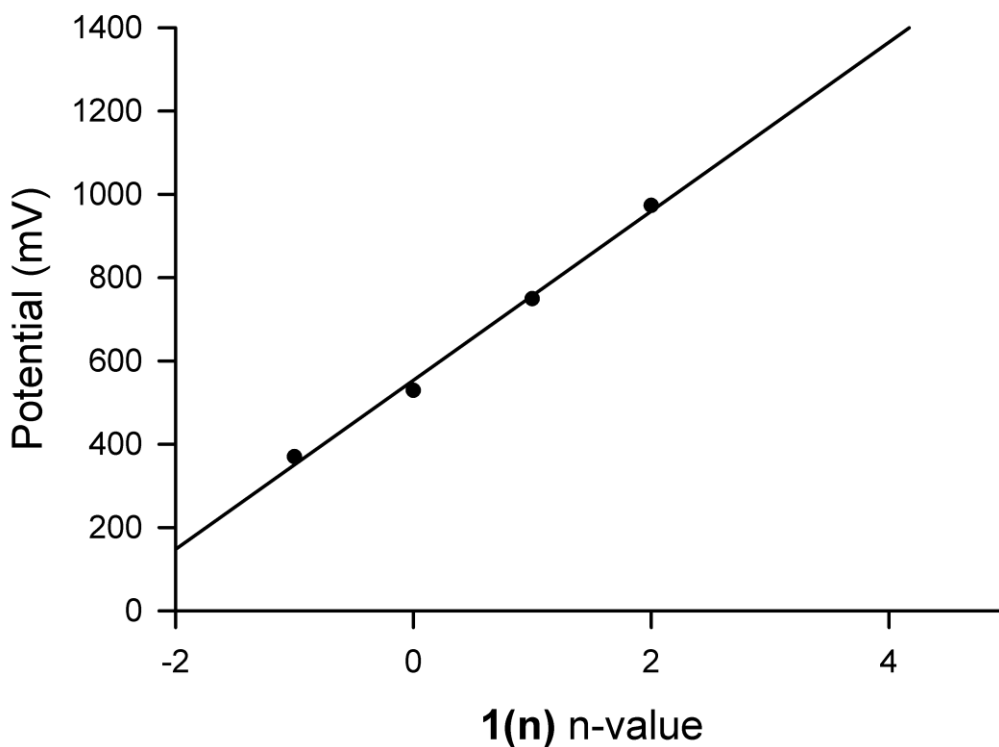
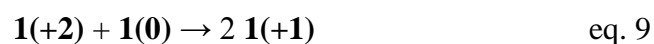
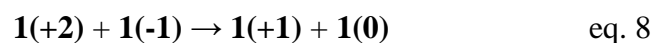
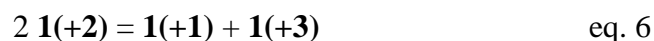


Figure 1.5 Plot of the $E_{1/2}$ values in figure 1.4 as a function of the redox state of complex $1(n)$, where n is the number of electrons removed from the $\text{Ru}^{\text{IV,IV,IV,IV}}$ core structure. Linear regression is also shown; fit has a Pearson r -value of 0.997.

Redox leveling in this system requires an alternative explanation than PCET. The linear dependence of the redox leveled potentials on the charge of the Ru_4O_6 core is consistent with a coulomb staircase. This behavior is consistent with that of a capacitor, taking the continuum dielectric approximation.⁶¹⁻⁶⁵ Conceptualizing complex **1** as a “molecular capacitor” has several major implications. Chiefly, the redox chemistry of the Ru_4O_6 core can be explained using only electrostatic effects. This would require that frontier molecular orbital energies to remain virtually unchanged throughout the redox events. This is most

characteristic of bulk metal-based materials with delocalized d-electrons forming continuous energy bands rather than discrete molecular orbitals. Thus, it would seem that complex **1** better approximates a quantum confined semiconducting metal-oxide rather than a discrete molecular species. An obvious explanation of this interpretation is that complex **1** is a large enough molecular species and its multi-metal-oxo composition is capable of delocalizing charge density such that the HOMOs of **1(n)** are closely spaced ($n = -1 \dots +4$).

Stoichiometric oxidation of **1(0)** to **1(+2)** using cerium ammonium nitrate shows an immediate decrease in λ_{\max} (figure 1.3). Monitoring the oxidized solution shows a slow increase in λ_{\max} (figure 1.6). The UV-vis spectrum resembles that of **1(+1)** after 16 hours. Redox titration of this final solution indicates that the initial **1(+2)** solution had become 1-electron reduced. A time profile of this reaction is shown in figure 1.7. This result indicates that it may be possible for **1(+3)** to oxidize water via disproportionation of **1(+2)**. Albeit an extremely slow reaction, it is nonetheless feasible for such a reaction to proceed thermodynamically, giving the final products of oxygen and **1(+1)**. A proposed reaction scheme is summarized in eq. 6 to eq. 9. Kinetic fitting of figure 1.7 to this mechanism is consistent but uninformative given the number of variables.³⁸



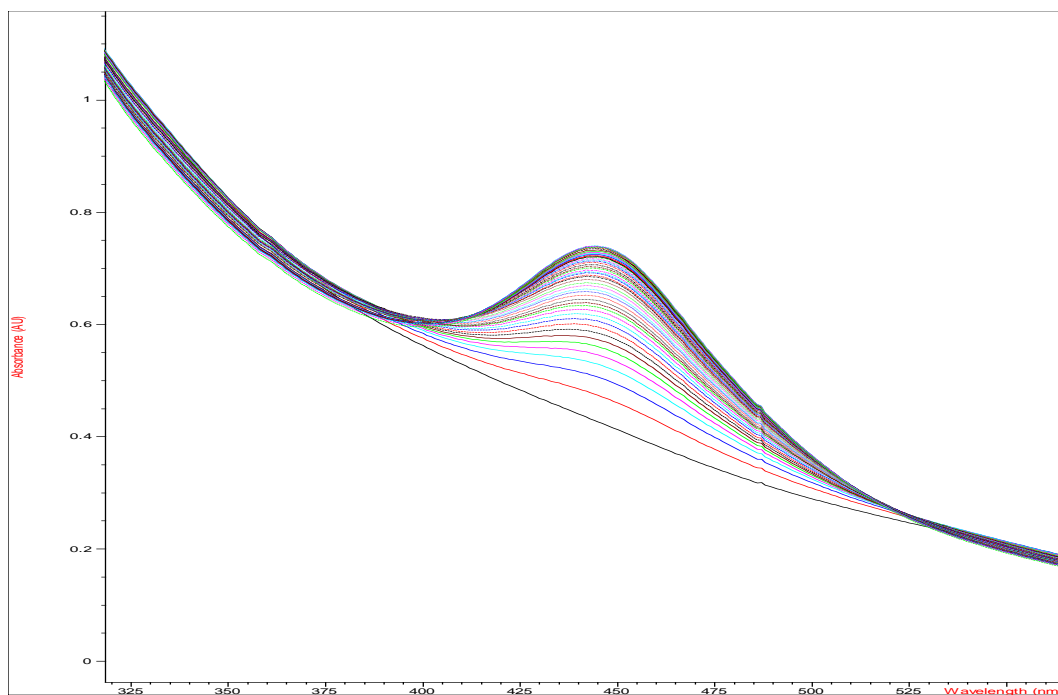


Figure 1.6 The absorption spectra of 40 μM of **1(+2)** in 0.1 M H₂SO₄ taken at 20 minute intervals.

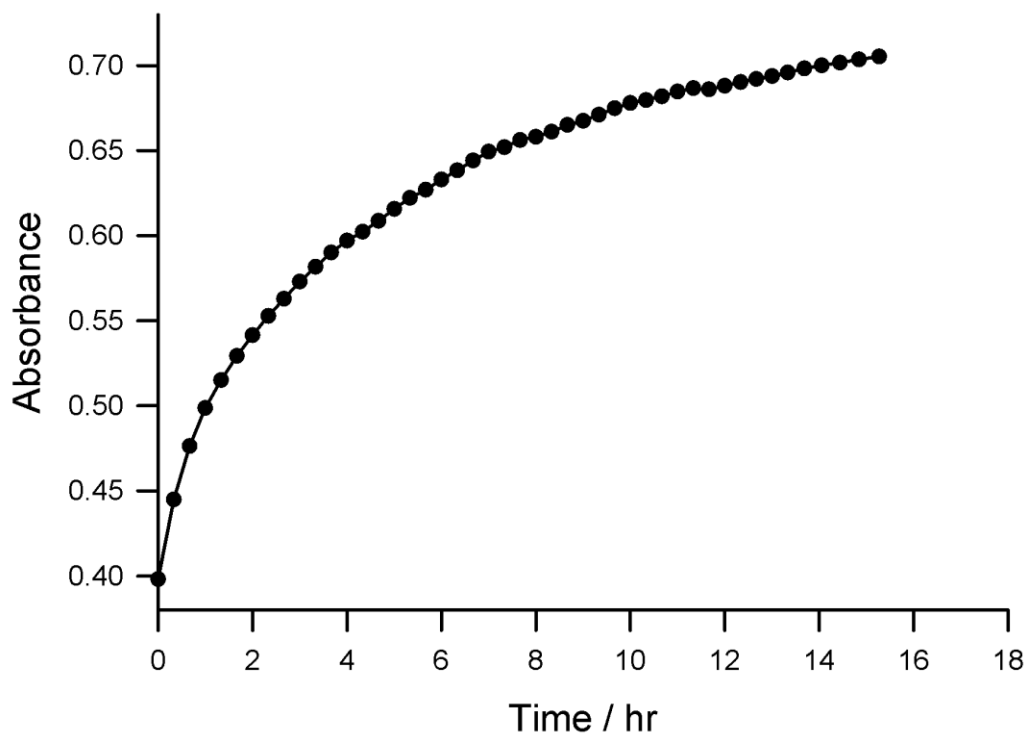


Figure 1.7 Time profile of the absorbance at $\lambda = 445$ nm.

Equally interesting are the behavior of complex **1** in its low oxidation states. Approximately one molar equivalent of SnSO_4 (two electron equivalent) was added to a solution of **1(0)**, reducing it to **1(-2)**. A solution of this species is stable via UV-vis spectroscopy in the absence of dioxygen (argon purged). If oxygen was bubbled through the solution, the UV/Vis absorption spectra of the solutions changes over time (figure 1.8). The full regeneration of the characteristic peak of **1(0)** at 445 nm with time indicates that the reduced species was two-electron oxidized. Since oxygen is the only plausible oxidizing agent, it is reasonable to surmise that we are seeing the stoichiometric reduction of oxygen

by **1(-2)**. At ambient temperature, the reaction is completed in about 8 hours (figure 1.9). The initial induction period in figure 1.8 is attributed to over reduction using SnSO_4 . At 45°C , the reaction rate is significantly lowered (figure 1.10), consistent with oxygen being a reactive moiety. The zeroth-order reaction kinetics indicates a strong dependence on oxygen concentration. This result implies that **1(-2)** should be capable of oxygen activation. However, additional experiments by other individuals have so far yielded negative results.

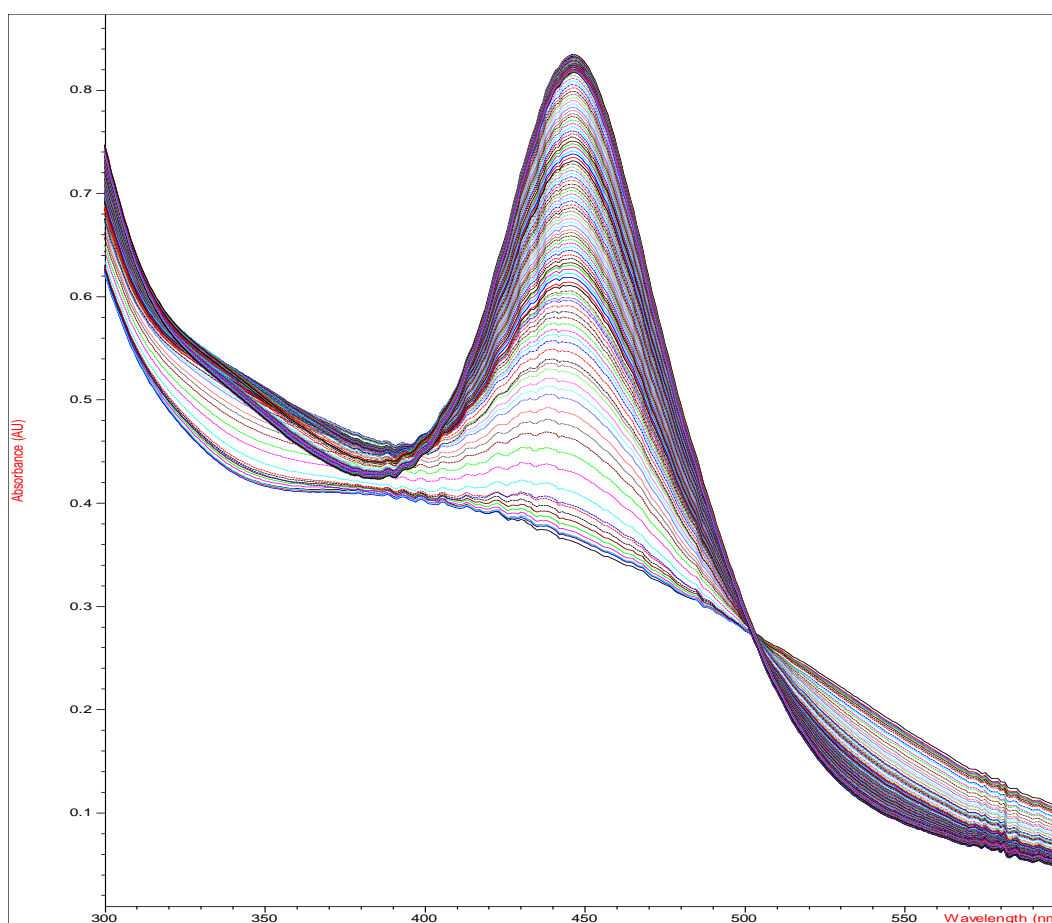


Figure 1.8 The UV-visible absorption spectra of reduced 20 μM **1(-2)** in 0.1 M H_2SO_4 taken at 5 minute intervals.

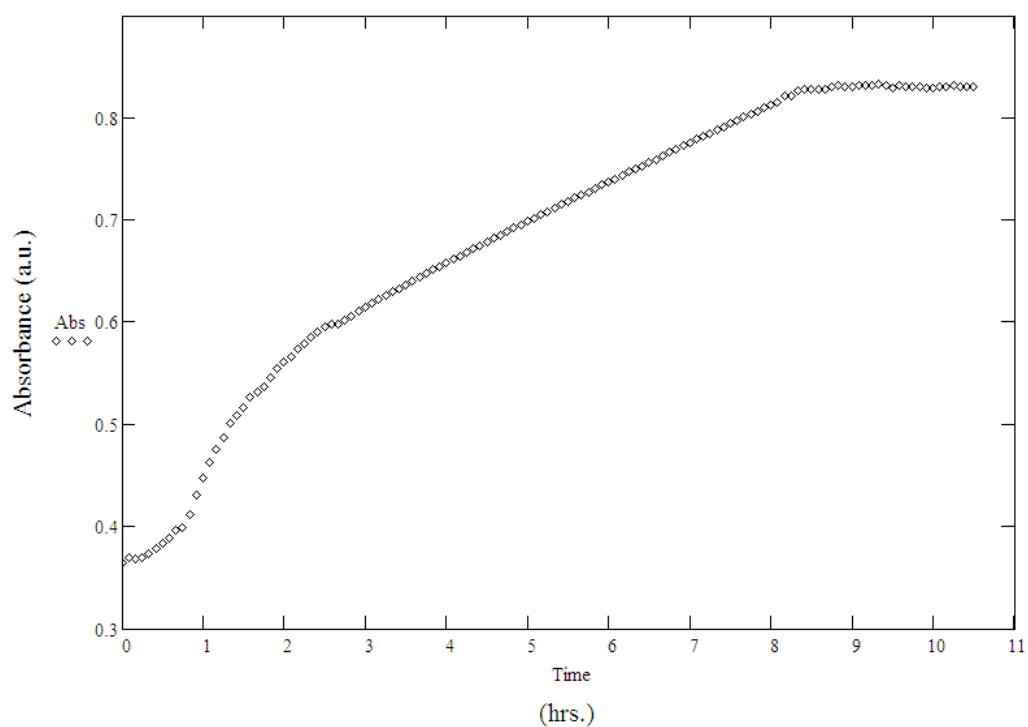


Figure 1.9 The absorbance at 445 nm of a reduced 20 μM **1(-2)** solution at 25°C with respect to time in hours. Reaction vessel was saturated with oxygen.

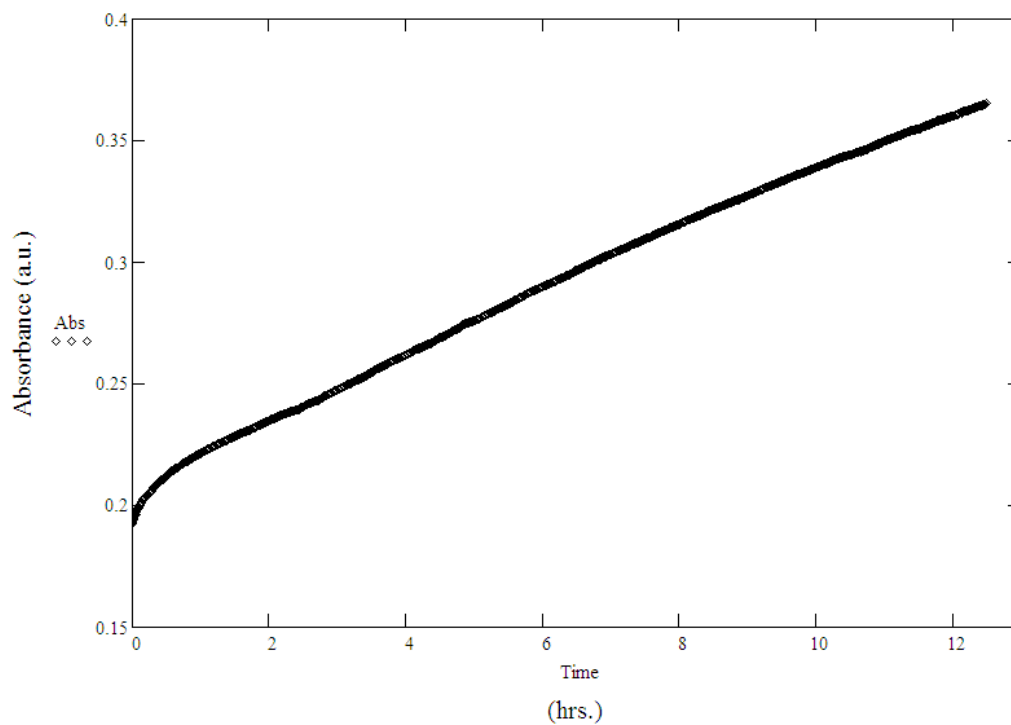


Figure 1.10 The absorbance at 445 nm of a reduced 20 μM **1(-2)** solution at 45°C with respect to time in hours. Reaction vessel was saturated with oxygen.

References

- 1 Materials for clean energy. *Nature* **414**, 331-331 (2001).
- 2 The future is not black. *Nat Mater* **5**, 159-159 (2006).
- 3 Energy Information Administration. International Energy Outlook 2009. *U.S. Department of Energy* (2009).
- 4 International Energy Agency. Key World Energy Statistics. *IEA* (2008).
- 5 Office of Global Change. Fourth U.S. Climate Action Report. *U.S. Department of State* (2007).
- 6 Chow, J., Kopp, R. J. & Portney, P. R. Energy Resources and Global Development. *Science* **302**, 1528-1531 (2003).
- 7 da Silva, C. G. The fossil energy/climate change crunch: Can we pin our hopes on new energy technologies? *Energy* **35**, 1312-1316, doi:10.1016/j.energy.2009.11.013 (2010).
- 8 Edwards, J. D. Crude Oil and Alternate Energy Production Forecasts for the Twenty-First Century: The End of the Hydrocarbon Era. *AAPG Bulletin* **81**, 1292-1305 (1997).
- 9 Heinberg, R. *Blackout: Coal, Climate and the Last Energy Crisis*. (New Society Publishers, 2009).
- 10 Hoffert, M. I., Caldeira, K., Benford, G., Criswell, D. R., Green, C., Herzog, H., Jain, A. K., Kheshgi, H. S., Lackner, K. S., Lewis, J. S., Lightfoot, H. D., Manheimer, W., Mankins, J. C., Mauel, M. E., Perkins, L. J., Schlesinger, M. E., Volk, T. & Wigley, T. M. L. Advanced Technology

- Paths to Global Climate Stability: Energy for a Greenhouse Planet. *Science* **298**, 981-987, doi:10.1126/science.1072357 (2002).
- ¹¹ Johansson, T. B., Kelly, H., Reddy, A. K. N. & Williams, R. H. *Renewable energy: Sources for fuels and electricity*. (1993).
- ¹² Oak Ridge National Laboratory. Basic Research Needs To Assure A Secure Energy Future. *U.S. Department of Energy* (2008).
- ¹³ Lewis, N. S. Powering the Planet. *MRS Bulletin* **32**, 208-820 (2007).
- ¹⁴ Painuly, J. P. Barriers to renewable energy penetration; a framework for analysis. *Renewable Energy* **24**, 73-89, doi:Doi: 10.1016/s0960-1481(00)00186-5 (2001).
- ¹⁵ Pimentel, D., Hurd, L. E., Bellotti, A. C., Forster, M. J., Oka, I. N., Sholes, O. D. & Whitman, R. J. Food Production and the Energy Crisis. *Science* **182**, 443-449, doi:10.1126/science.182.4111.443 (1973).
- ¹⁶ Pimentel, D., Rodrigues, G., Wang, T., Abrams, R., Goldberg, K., Staecker, H., Ma, E., Brueckner, L., Trovato, L., Chow, C., Govindarajulu, U. & Boerke, S. Renewable Energy: Economic and Environmental Issues. *BioScience* **44**, 536-547 (1994).
- ¹⁷ Rosa, A. d. *Fundamentals of Renewable Energy Processes*. (Academic Press, 2009).
- ¹⁸ Solomon, S., Qin, D., Manning, M., Chen, Z., Marquis, M., Averyt, K. B., Tignor, M. & Miller, H. L. Climate Change 2007: The Physical Science Basis. *Intergovernmental Panel on Climate Change (IPCC)* (2007).

- ¹⁹ Srinivasan, S., Mosdale, R., Stevens, P. & Yang, C. Annual Review of Energy and the Environment-Fuel Cells: Reaching the Era of Clean and Efficient Power Generation in the Twenty-First Century. *Annual Reviews* **24**, 281-328 (1999).
- ²⁰ Turner, J. A. A Realizable Renewable Energy Future. *Science* **285**, 687-689, doi:10.1126/science.285.5428.687 (1999).
- ²¹ Twidell, J. & Weir, T. *Renewable Energy Resources*. (Taylor & Francis, 2006).
- ²² Lewis, N. S. & Nocera, D. G. Powering the planet: Chemical challenges in solar energy utilization. *Proc. Nat. Acad. Sci.* **103(43)**, 15729-15735 (2006).
- ²³ Parmesan, C. & Yohe, G. A globally coherent fingerprint of climate change impacts across natural systems. *Nature* **421**, 37-42 (2003).
- ²⁴ Barnham, K. W. J., Mazzer, M. & Clive, B. Resolving the energy crisis: nuclear or photovoltaics? *Nat Mater* **5**, 161-164 (2006).
- ²⁵ Bloom, E. E. The challenge of developing structural materials for fusion power systems. *Journal of Nuclear Materials* **258-263**, 7-17 (1998).
- ²⁶ Bloom, E. E., Zinkle, S. J. & Wiffen, F. W. Materials to deliver the promise of fusion power - progress and challenges. *Journal of Nuclear Materials* **329-333**, 12-19 (2004).
- ²⁷ Moyer, M. Fusion's False Dawn. *Scientific American* (2010).

- 28 Balzani, V., Credi, A. & Venturi, M. Photochemical Conversion of Solar Energy. *ChemSusChem* **1**, 26-58, doi:DOI: [10.1002/cssc.200700087](https://doi.org/10.1002/cssc.200700087) (2008).
- 29 Froehlich, C. Solar Irradiance Variability Since 1978. Revision of the PMOD Composite during Solar Cycle 21. *Space Science Reviews* **125**, 53-65 (2006).
- 30 Tarascon, J. M. & Armand, M. Issues and challenges facing rechargeable lithium batteries. *Nature* **414**, 359-367 (2001).
- 31 Farrell, A. E., Plevin, R. J., Turner, B. T., Jones, A. D., O'Hare, M. & Kammen, D. M. Ethanol Can Contribute to Energy and Environmental Goals. *Science* **311**, 506-508, doi:10.1126/science.1121416 (2006).
- 32 Pimentel, D. Ethanol fuels: Energy security, economics, and the environment. *Journal of Agricultural and Environmental Ethics* **4**, 1-13 (1991).
- 33 Ragauskas, A. J., Williams, C. K., Davison, B. H., Britovsek, G., Cairney, J., Eckert, C. A., Frederick, W. J., Jr., Hallett, J. P., Leak, D. J., Liotta, C. L., Mielenz, J. R., Murphy, R., Templer, R. & Tschaplinski, T. The Path Forward for Biofuels and Biomaterials. *Science* **311**, 484-489, doi:10.1126/science.1114736 (2006).
- 34 Granqvist, C. G., Niklasson, G. A. & Azens, A. Electrochromics: Fundamentals and energy-related applications of oxide-based devices. *Applied Physics A: Materials Science & Processing* **89**, 29-35 (2007).

- 35 Eisenberg, R. & Gray, H. B. Preface on Making Oxygen. *Inorg. Chem.* **47**,
1697-1699 (2008).
- 36 Kanan, M. W. & Nocera, D. G. In Situ Formation of an Oxygen-Evolving
Catalyst in Neutral Water Containing Phosphate and Co^{2+} . *Science* **321**,
1072-1075, doi:[10.1126/science.1162018](https://doi.org/10.1126/science.1162018) (2008).
- 37 Kanan, M. W., Surendranath, Y. & Nocera, D. G. Cobalt–phosphate
oxygen-evolving compound. *Chem. Soc. Rev.* **38**, 109-114 (2009).
- 38 Geletii, Y. V., Besson, C., Hou, Y., Yin, Q., Musaev, D. G., Quinero, D.,
Cao, R., Hardcastle, K. I., Proust, A., Kögerler, P. & Hill, C. L. Structural,
Physicochemical and Reactivity Properties of an All-Inorganic, Highly
Active Tetraruthenium Homogeneous Catalyst for Water Oxidation. *J. Am.*
Chem. Soc. **131**, 17360-17370 (2009).
- 39 Yin, Q., Tan, J. M., Besson, C., Geletii, Y. V., Musaev, D. G., Kuznetsov,
A. E., Luo, Z., Hardcastle, K. I. & Hill, C. L. A fast soluble carbon-free
molecular water oxidation catalyst based on abundant metals. *Science*,
Printed online March 11, 2010, doi:[10.1126/science.1185372](https://doi.org/10.1126/science.1185372) (2010).
- 40 Tagore, R., Crabtree, R. H. & Brudvig, G. W. Oxygen Evolution Catalysis
by a Dimanganese Complex and Its Relation to Photosynthetic Water
Oxidation. *Inorganic Chemistry* **47**, 1815-1823, doi:[10.1021/ic062218d](https://doi.org/10.1021/ic062218d)
(2008).
- 41 Yagi, M. & Kaneko, M. Molecular Catalysts for Water Oxidation.
Chemical Reviews **101**, 21-36, doi:[10.1021/cr980108l](https://doi.org/10.1021/cr980108l) (2000).

- 42 Geletii, Y. V., Botar, B., Kögerler, P., Hillesheim, D. A., Musaev, D. G. & Hill, C. L. An All-Inorganic, Stable, and Highly Active Tetra­ruthenium Homogeneous Catalyst for Water Oxidation. *Angew. Chem. Int. Ed.* **47**, 3896-3899. Selected as the VIP Article by the reviewers and editor. Published online 3893/3820/3808 DOI: 3810.1002/anie.200705652, doi:DOI: 10.1002/anie.200705652 (2008).
- 43 Gersten, S. W., Samuels, G. J. & Meyer, T. J. Catalytic Oxidation of Water by an Oxo-Bridged Ruthenium Dimer. *J. Am. Chem. Soc.* **104**, 4029-4030 (1982).
- 44 Wada, T., Tsuge, K. & Tanaka, K. Electrochemical Oxidation of Water to Dioxygen Catalyzed by the Oxidized Form of the Bis(ruthenium-hydroxo) Complex in H₂O *Angew. Chem. Int. Ed.* **39**, 1479-1482 (2000).
- 45 Limburg, J., Vrettos, J. S., Chen, H., Paula, J. C. d., Crabtree, R. H. & Brudvig, G. W. Characterization of the O₂-Evolving Reaction Catalyzed by [(terpy)(H₂O)Mn^{III}(O)₂Mn^{IV}(OH₂)(terpy)](NO₃)₃ (terpy) 2,2':6,2"-Terpyridine). *J. Am. Chem. Soc.* **123**, 423-430 (2001).
- 46 Hurst, J. K. Water oxidation catalyzed by dimeric μ-oxo bridged ruthenium diimine complexes. *Coord. Chem. Rev.* **249**, 313-328 (2005).
- 47 Zong, R. & Thummel, R. A New Family of Ru Complexes for Water Oxidation. *J. Am. Chem. Soc.* **127**, 12802-12803 (2005).
- 48 Muckerman, J. T., Polyansky, D. E., Wada, T., Tanaka, K. & Fujita, E. Water Oxidation by a Ruthenium Complex with Noninnocent Quinone

- Ligands: Possible Formation of an O-O Bond at a Low Oxidation State of the Metal. *Inorg. Chem.* **47**, 1787-1802 (2008).
- ⁴⁹ Brimblecombe, R., Swiegers, G. F., Dismukes, G. C. & Spiccia, L. Sustained Water Oxidation Photocatalysis by a Bioinspired Manganese Cluster. *Angew. Chem. Int. Ed.* **47**, 7335-7338 (2008).
- ⁵⁰ Romain, S., Bozoglian, F., Sala, X. & Llobet, A. Oxygen—Oxygen Bond Formation by the Ru-Hbpp Water Oxidation Catalyst Occurs Solely via an Intramolecular Reaction Pathway. *J. Am. Chem. Soc.* **131**, 2768-2769 (2009).
- ⁵¹ Kohl, S. W., Weiner, L., Schwartsburd, L., Konstantinovski, L., Shimon, L. J. W., Ben-David, Y., Iron, M. A. & Milstein, D. Consecutive Thermal H₂ and Light-Induced O₂ Evolution from Water Promoted by a Metal Complex. *Science* **324**, 74-77 (2009).
- ⁵² Hull, J. F., Balcells, D., Blakemore, J. D., Incarvito, C. D., Eisenstein, O., Brudvig, G. W. & Crabtree, R. H. Highly Active and Robust Cp* Iridium Complexes for Catalytic Water Oxidation. *J. Am. Chem. Soc.* **131**, 8730-8731 (2009).
- ⁵³ Kunkely, H. & Vogler, A. Water Splitting by Light with Osmocene as Photocatalyst. *Angew. Chem. Int. Ed.* **48**, 1685-1687, doi:10.1002/anie.200804712 (2009).
- ⁵⁴ Cady, C. W., Crabtree, R. H. & Brudvig, G. W. in *Photosynthesis. Energy from the Sun* 377-381 (2008).

- 55 Wang, T., Brudvig, G. & Batista, V. S. Characterization of Proton Coupled Electron Transfer in a Biomimetic Oxomanganese Complex: Evaluation of the DFT B3LYP Level of Theory. *Journal of Chemical Theory and Computation* **6**, 755-760, doi:10.1021/ct900615b.
- 56 Dismukes, G. C., Brimblecombe, R., Felton, G. A. N., Pryadun, R. S., Sheats, J. E., Spiccia, L. & Swiegers, G. F. Development of Bioinspired Mn₄O₄ Cubane Water Oxidation Catalysts: Lessons from Photosynthesis. *Accounts of Chemical Research* **42**, 1935-1943, doi:10.1021/ar900249x (2009).
- 57 Thorp, H. H., Sarneski, J. E., Brudvig, G. W. & Crabtree, R. H. Proton-coupled electron transfer in manganese complex [(bpy)₂Mn(O)₂Mn(bpy)₂]³⁺. *Journal of the American Chemical Society* **111**, 9249-9250, doi:10.1021/ja00208a029 (1989).
- 58 Mayer, J. M. PROTON-COUPLED ELECTRON TRANSFER: A Reaction Chemist's View. *Annual Review of Physical Chemistry* **55**, 363-390, doi:doi:10.1146/annurev.physchem.55.091602.094446 (2004).
- 59 Cukier, R. I. & Nocera, D. G. PROTON-COUPLED ELECTRON TRANSFER. *Annual Review of Physical Chemistry* **49**, 337-369, doi:doi:10.1146/annurev.physchem.49.1.337 (1998).
- 60 Huynh, M. H. V. & Meyer, T. J. Proton-Coupled Electron Transfer. *Chemical Reviews* **107**, 5004-5064, doi:10.1021/cr0500030 (2007).
- 61 Roth, J. D., Lewis, G. J., Safford, L. K., Jiang, X., Dahl, L. F. & Weaver, M. J. Exploration of the Ionizable Metal Cluster-Electrode Surface

Analogy: Infrared Spectroelectrochemistry of $[\text{Pt}_{24}(\text{CO})_{30}]^n$, $[\text{Pt}_{26}(\text{CO})_{32}]^n$, and $[\text{Pt}_{38}(\text{CO})_{44}]^n$ ($n = 0$ to -10) and Comparisons with Potential-Dependent Spectra of CO Adlayers on Platinum Surfaces. *J. Am. Chem. Soc.* **114**, 6159-6169 (1992).

- ⁶² Weaver, M. J. & Gao, X. Molecular Capacitance: Sequential Electron-Transfer Energetics for Solution-Phase Metallic Clusters in Relation to Gas-Phase Clusters and Analogous Interfaces. *J. Phys. Chem.* **97**, 332-338 (1993).
- ⁶³ Ingram, R. S., Hostetler, M. J., Murray, R. W., Schaaff, T. G., Khoury, J. T., Whetten, R. L., Bigioni, T. P., Guthrie, D. K. & First, P. N. 28 kDa Alkanethiolate-Protected Au Clusters Give Analogous Solution Electrochemistry and STM Coulomb Staircases. *J. Am. Chem. Soc.* **119**, 9279-9280 (1997).
- ⁶⁴ Chen, S., Murray, R. W. & Feldberg, S. W. Quantized Capacitance Charging of Monolayer-Protected Au Clusters. *J. Phys. Chem. B* **102**, 9898-9907 (1998).
- ⁶⁵ Chen, S., Ingram, R. S. H., Hostetler, M. J., Pietron, J. J., Murray, R. W., Schaaff, T. G., Khoury, J. T., Alvarez, M. M. & Whetten, R. L. Gold nanoelectrodes of varied size: transition to molecule-like charging. *Science* **120**, 2098-2101 (1998).

Chapter II

Discovery and Identification of a Carbon-Free Molecular Cobalt Oxide

Water Oxidation Catalyst and Its Characterization

Published in part in “A soluble molecular fast organic-structure-free water oxidation catalyst based on abundant metals,” *Science*. **2010**, 328, 342–345

With Tan, J. M.; Besson, C; Geletii, Y. V.; Musaev, D. G.; Kuznetsov, A. E.; Luo, Z.; Hardcastle, K. I.; Hill, C. L.

Abstract

Development of a carbon-free water oxidation catalyst based on earth-abundant elements is reported. This cobalt-based polyoxometalate is capable of fast water oxidation (fastest molecular catalyst currently reported). This complex, $[\text{Co}_4(\text{H}_2\text{O})_2(\text{PW}_9\text{O}_{34})_2]^{10-}$, is essentially a $\text{Co}_4^{\text{II}}\text{O}_4$ cluster stabilized by oxidatively resistant polyoxotungstate ligands. The synthesis of said complex is straightforward and based on principles of metal-oxo cluster self-assembly. This finding reinforces metal oxides as efficient water oxidation catalysts. This finding also establishes polyoxometalates as molecular metal oxide clusters very capable of water oxidation chemistry.

Introduction

The importance of oxidation resistant WOCs in artificial photosynthesis was discussed in the last chapter. Studies regarding an all-inorganic WOC were also discussed. Also apparent is the general need for oxidatively resistant WOCs.¹⁻¹⁹ Polyoxometalates (POMs) are metal oxyanions with a metal-oxygen-metal frame. They present a unique solution as oxidative catalysts because they are able to incorporate various transition metals and are tunable both structurally and electronically.²⁰⁻³¹ Most importantly, POMs are known to be thermally and oxidatively stable, which are core requisites for potential WOCs.^{4,5,20-25,29-31}

Transition-metal-substituted POMs can be understood as d-electron metal centers ligated by molecular metal-oxo polychelating ligands. A more illustrative way to depict POMs is to describe them as molecular dirt. POM frames are generally assembled from d^0 metal oxides. Consider for example complex **1** described in the last chapter. The polytungstate frame [γ -SiW₁₀O₃₆] consists of W^{VI}O₆ subunits. These octahedral subunits self-assemble in water into corner-sharing, edge-sharing, or face-sharing configurations, all of which may be controlled by varying the reaction conditions. The assembly terminates due to decreased negative charge density on the terminal oxo groups which reduce intermolecular reactions.^{24,25,28-37} These traits of POMs serve to stabilize them as discrete molecular units. Moreover, these inorganic ligands are based on fully oxidized metals (d^0 W^{VI}), allowing POMs to be oxidatively robust.

Upon the discovery of water oxidation activity of **1**,⁸ effort was dedicated to identify other POMs that might act as WOCs. Complex **1** was based on

ruthenium, a rare metal. It is significantly more desirable to develop WOCs based on first-row transition metals by virtue of their relative abundance.^{2,5} This chapter focuses on the identification of a cobalt based POM capable of water oxidation: $[\text{Co}_4(\text{H}_2\text{O})_2(\text{PW}_9\text{O}_{34})_2]^{10-}$ (**2**).

Experimental

Synthesis of $\text{Na}_{10}[\text{Co}_4(\text{H}_2\text{O})_2(\text{PW}_9\text{O}_{34})_2] \cdot 27\text{H}_2\text{O}$

The preparation of **Na₁₀-2** is derived from that of **K₁₀-2** reported in literature.³⁸ A higher yield preparation of **K₁₀-2** was reported by Finke *et al.*³⁹ To synthesize **Na₁₀-2**, $\text{Na}_2\text{WO}_4 \cdot 2\text{H}_2\text{O}$ (35.62 g, 0.108 mol), $\text{Na}_2\text{HPO}_4 \cdot 7\text{H}_2\text{O}$ (3.22 g, 0.012 mol), and $\text{Co}(\text{NO}_3)_2 \cdot 6\text{H}_2\text{O}$ (6.98 g, 0.024 mol) were mixed in 100 mL water. After adjusting the pH from 9 to 7, this purple suspension was then refluxed at 100 °C for two hours. A dark purple solution resulted within minutes of heating. After reflux, the solution was saturated with NaCl and allowed to cool to room temperature. The resulting purple crystals were collected, quickly washed with approximately 30 mL of water, and recrystallized from hot water (35% mass yield based on Co). Thermogravimetric analysis gave 27 water molecules of hydration (figure 2.1). FT/IR (cm^{-1}): 1037 (m), 939 (m), 882 (w), 767 (w) (figure 2.2). UV-Vis (H_2O , pH 3.5 to 9): λ_{max} , 579 nm ($\epsilon_{579} = 330 \text{ M}^{-1} \text{ cm}^{-1}$) (figure 2.3). ³¹P-NMR: 1855 ppm, $\Delta\nu_{1/2} = 400 \text{ Hz}$; Elemental analysis calculated (%) for $\text{Na}_{10}[\text{Co}_4(\text{H}_2\text{O})_2(\text{PW}_9\text{O}_{34})_2] \cdot 27\text{H}_2\text{O}$: Co, 4.33; Na, 4.22; P, 1.14; W, 60.76. Found: Co, 4.49; Na, 4.24; P, 1.06; W, 58.7.

Synthesis of all other POMs used in this study were done according to literature procedures.⁴⁰⁻⁴⁶ The product purity was confirmed using IR spectroscopy.

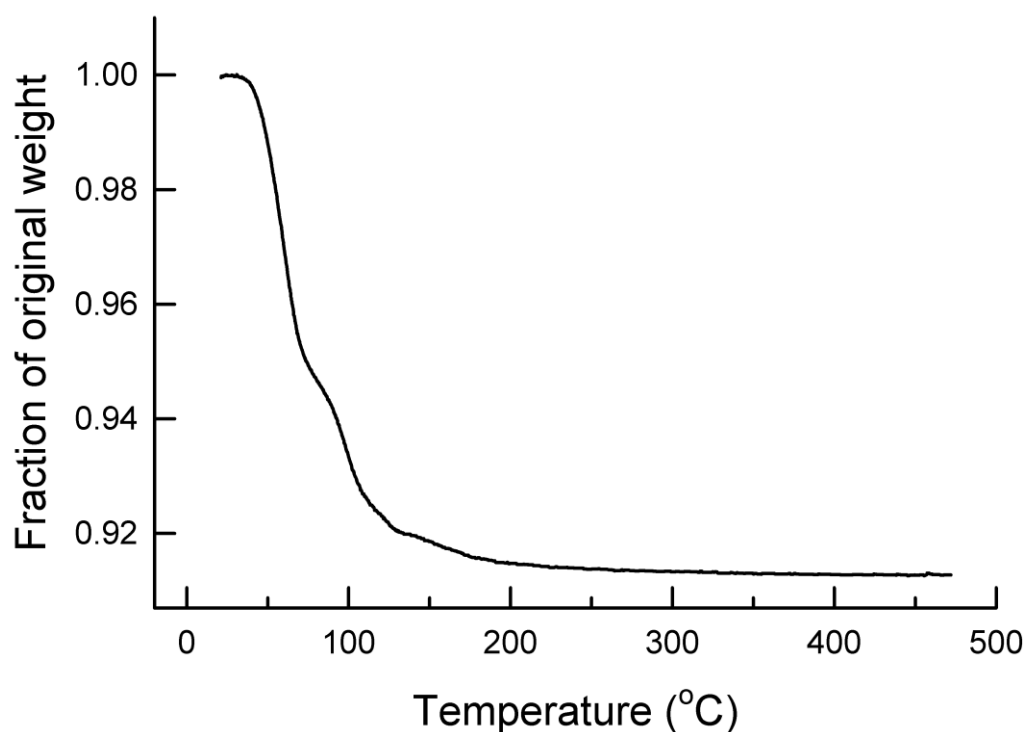


Figure 2.1 Thermogravimetric Analysis (TGA) of crystalline **Na₁₀-2**. The weight loss observed (9%) is attributed to waters of hydration. Given that $\text{Na}_{10}\text{Co}_4(\text{H}_2\text{O})_2\text{P}_2\text{W}_{18}\text{O}_{68}$ has a formula weight of 4962 dalton, there are approximately 27 waters of hydration as determined by TGA.

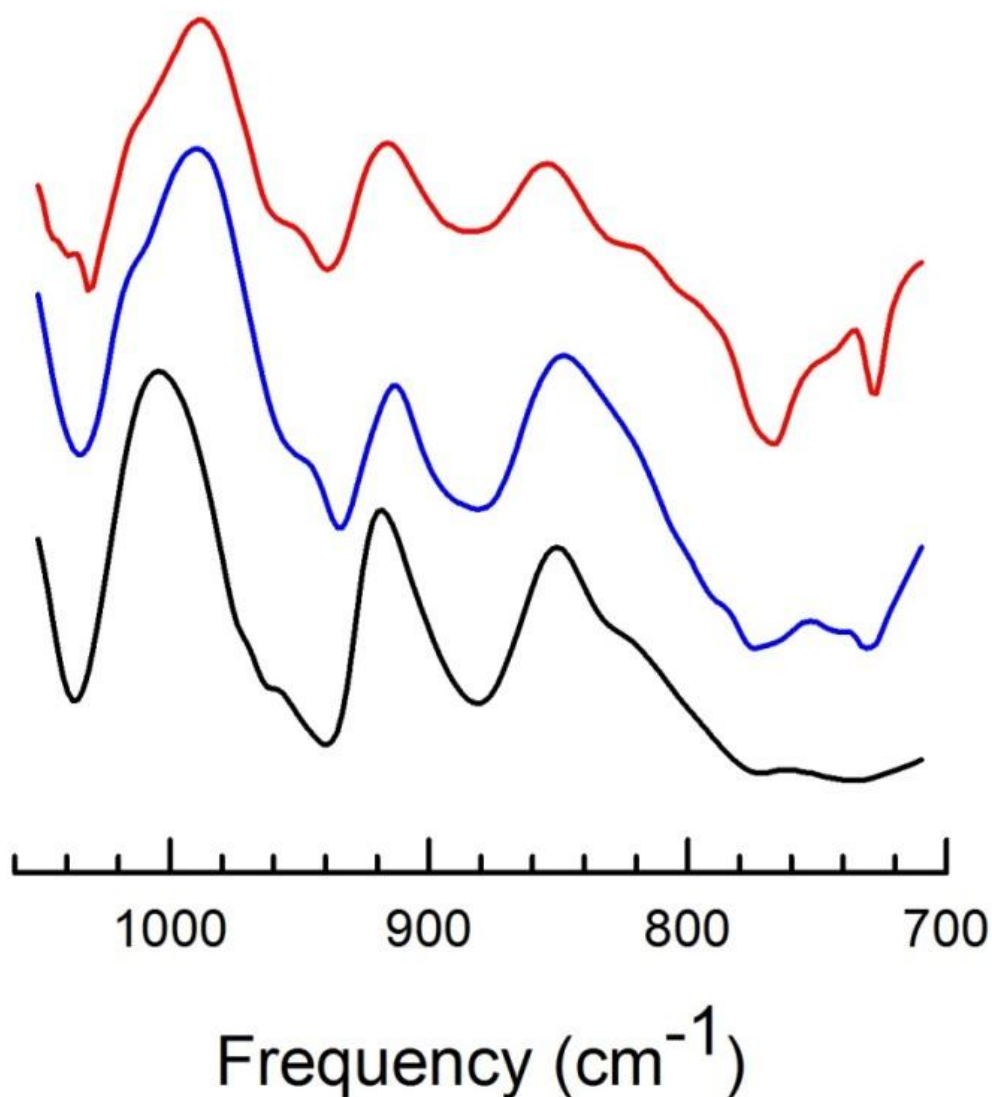


Figure 2.2 FT-Infrared spectrum of **Na₁₀₋₂** (black), the light-yellow precipitate re-isolated from a “post-chemical reaction” solution (red), and the dark-yellow precipitate obtained from mixing two concentrated solutions of **Na₁₀₋₂** and $[\text{Ru}(\text{bpy})_3]^{2+}$ (blue). All FT-IR spectroscopy were performed using 1 wt% sample in KBr pellet. All three spectra show the characteristic P-O stretching (1037 cm^{-1}), terminal W-O stretching (939 cm^{-1}), and W-O-W bending (882 and 767 cm^{-1}) bands.

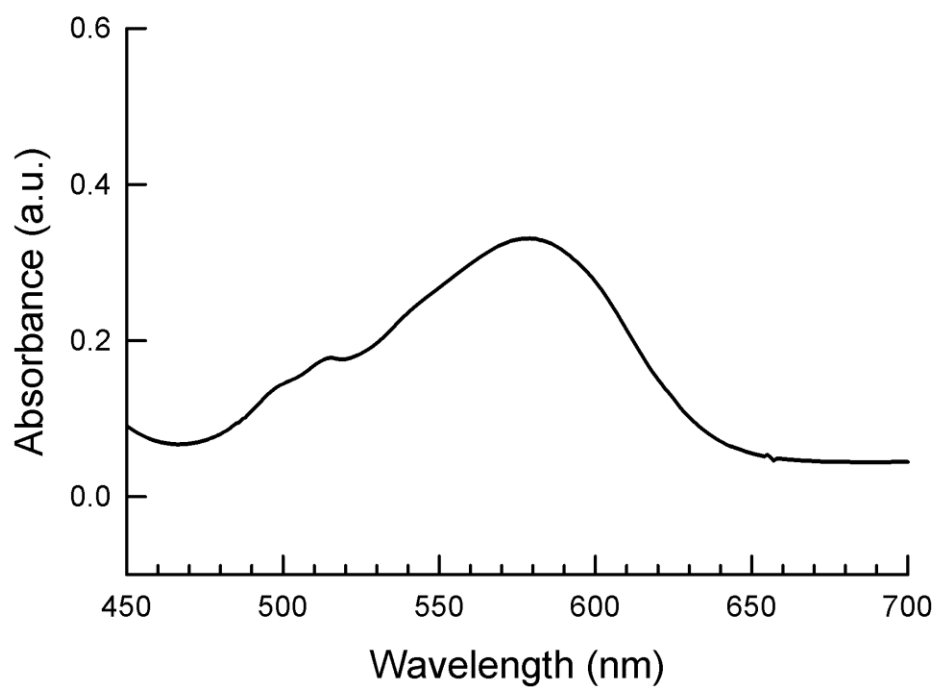


Figure 2.3 UV-Visible spectrum of 1 mM **2** in 30 mM pH 8 NaPi buffer. The spectrum does not change with variation in solution age and solution pH. The calculated extinction coefficient at λ_{\max} (579 nm) is $\epsilon_{579} = 330 \text{ M}^{-1} \text{ cm}^{-1}$.

X-ray diffraction

The complete datasets for **Na₁₀-2** were collected at Emory University. A suitable crystal of **Na₁₀-2** was coated with Paratone N oil, suspended in a small fiber loop and placed in a cooled nitrogen gas stream at 173 K on a Bruker D8 APEX II CCD sealed tube diffractometer with graphite monochromated MoK α (0.71073 Å) radiation. Data were measured using a series of combinations of phi and omega scans with 10 s frame exposures and 0.5° frame widths. Data collection, indexing and initial cell refinements were all carried out using APEX II software.⁴⁷ Frame integration and final cell refinements were done using SAINT software.⁴⁸ The final cell parameters were determined from least-squares refinement on 9978 reflections.

The structure was solved using Direct methods and difference Fourier techniques (SHELXTL, V6.12).⁴⁹ Only the Co, Na and W atoms were refined anisotropically; no hydrogen atoms were included in the final structure. Scattering factors and anomalous dispersion corrections are taken from the *International Tables for X-ray Crystallography*.⁵⁰ Structure solution, refinement, graphics and generation of publication materials were performed by using SHELXTL, V6.12 software. Additional details of data collection and structure refinement are given in Table 2.1.

Table 2.1 Crystal data and refinement parameters for the X-ray structure of **Na₁₀-2**

complex	Na₁₀-2
molecular formula	Na ₁₀ Co ₄ O _{98.66} P ₂ W ₁₈
formula wt. (g mol ⁻¹)	5415.42
temperature (K)	172(2)
radiation (λ, Å)	0.71073
crystal system	Triclinic
space group	<i>P</i> -1
<i>a</i> (Å)	11.539(3)
<i>b</i> (Å)	12.807(4)
<i>c</i> (Å)	17.259(5)
<i>α</i> (°)	98.019(4)
<i>β</i> (°)	106.639(4)
<i>γ</i> (°)	111.205(4)
Volume (Å ³)	2192.3(11)
<i>Z</i>	1
<i>μ</i> (mm ⁻¹)	24.451
F(000)	2369
crystal size (mm ³)	0.38 x 0.32 x 0.20
reflections collected	40531
independent reflections	11692 [R(int) = 0.0469]
absorption correction	semi-empirical from equivalents
refinement method	full-matrix least-squares on F ²
goodness-of-fit on F ²	1.078
final R indices	R1 ^a = 0.0814
[R > 2σ (I)]	wR2 ^b = 0.2374
R indices (all data)	R1 ^a = 0.0951, wR2 ^b = 0.2643

$$^a R_1 = \frac{\sum ||F_o| - |F_c||}{\sum |F_o|}$$

$$^b wR_2 = \left\{ \frac{\sum [w(F_o^2 - F_c^2)^2]}{\sum [w(F_o^2)]} \right\}^{0.5}$$

Analysis of O₂ content using gas chromatography (GC)

A round-bottom flask with a total volume of ~17 mL was used to hold 8 mL of aqueous [Ru(bpy)₃]³⁺ solution. A thick-wall tube was used to hold 2 mL of the catalyst in buffered solution. Both containers were capped with a rubber stopper and extensively deaerated by bubbling argon gas through the solution for over 10 minutes. The 2 mL solution in the thick-wall tube was then quickly

transferred into the round-bottom flask using a cannula. This affords 10 mL of reaction solution. We report the species concentrations in this solution. A fully deaerated 250 μL Hamilton gas-tight syringe was used to withdraw a sample of the gas from the reaction vessel headspace. Aliquots (100 μL) of this gas were immediately injected into a Hewlett-Packard 5890 gas chromatograph fitted with a thermal conductivity detector for analysis. For timed reactions, a stopwatch was used to measure the time elapsed from the time of solution transfer via cannula to the time at which gas was withdrawn from the headspace. TOF for **1** is given as the final TON divided by the time elapsed.

Calibration of this system was performed using the exact same procedures substituting the reaction solutions with water. Four reference volumes of O_2 were used in constructing a multipoint calibration slope. After mixing, 0 μL , 23.5 μL , 47 μL , or 70.5 μL of pure O_2 (corresponding to 0, 1, 2, or 3 $\mu\text{mol O}_2$) were injected into the headspace of the reaction vessel. The reaction vessel was shaken to allow equilibration of O_2 between gas and aqueous phases. The retention times of oxygen and nitrogen were separated by approximately 20 seconds. The oxygen peak was seen first a little under 1 minute. Contamination from air was minimal ($< 0.07 \mu\text{mol O}_2$ for the chemical oxidation of water) and accounted for by subtracting half of the nitrogen peak area from the total oxygen peak area. This is a conservative estimate, as the gas chromatograph gives an oxygen to nitrogen ratio of 1 : 2.8 for a sample of air. The amount of O_2 was plotted against the integration area for the adjusted oxygen peak. A linear correlation between the two was found and the slope was used as the conversion factor for the

quantification of O₂ – yield in future experiments. Three data points were taken for each reference volume and the average O₂ peak area was used in the calibration, giving a Pearson r-value of > 0.99.

Cyclic voltammetry

Cyclic voltammograms (CVs) were obtained at room temperature in buffered solutions using BAS CV-50W voltammetric analyzer. A saturated Ag/AgCl reference electrode from BAS was calibrated using the [Fe(CN)₆]³⁻/[Fe(CN)₆]⁴⁻ couple, for which accurate published data are available (SI4). On the basis of this calibration, potentials in the CV are reported relative to the NHE by the addition of 200 mV to the BAS electrode values.

UV-Visible spectroscopy

All UV-Vis spectroscopy was performed with an Agilent 8453 spectrometer at 25 °C using a quartz cell with a 1 cm pathlength. The UV-Vis spectroscopy of **1** is shown in figure 2.3. No changes in its spectrum were observed during any of the hydrolytic stability studies.

³¹P NMR

The ³¹P (243 MHz) NMR spectra were obtained at 300 K in 5 mm o. d. tubes on a Unity Plus 600 spectrometer equipped with a Varian 600 SW/PF6 probehead. The chemical shifts are given with respect to 85 % H₃PO₄. Acquisition parameters are as follows: pulsewidth 4 μs (~40° flip angle), time domain window 100 kHz (412 ppm), 1500 (for diluted solutions) or 3000 (for concentrated solutions) points, resulting in acquisition times of 7.5 or 15 μs respectively.

Characterization of the post-catalysis solution

(a) Preparation of solution for ^{31}P -NMR

Tris(2,2'-bipyridyl)triperchlororuthenium(III) ($[\text{Ru}(\text{bpy})_3]^{3+}$, 11.0 mg, 11.3 μmol) was dissolved in D_2O (15 mL). A separate solution containing **2** (0.075 mM) and sodium phosphate (NaPi) (0.16 M, pH 8.0) was prepared in in 1:5 $\text{D}_2\text{O}/\text{H}_2\text{O}$. A 2 mL aliquot of the latter solution was then added to 8 mL of the former solution, resulting in 0.6 mM $[\text{Ru}(\text{bpy})_3]^{3+/2+}$, 0.015 mM **2**, and 32 mM NaPi dissolved in 5:1 $\text{D}_2\text{O}/\text{H}_2\text{O}$. After the reaction was completed, $\text{Na}[\text{BPh}_4]$ (18 mg, 52.6 μmol) was added to this solution. The resulting light yellow precipitate was filtered off using a micro-filter. The completely colorless filtrate was used for ^{31}P NMR (figure 2.4).

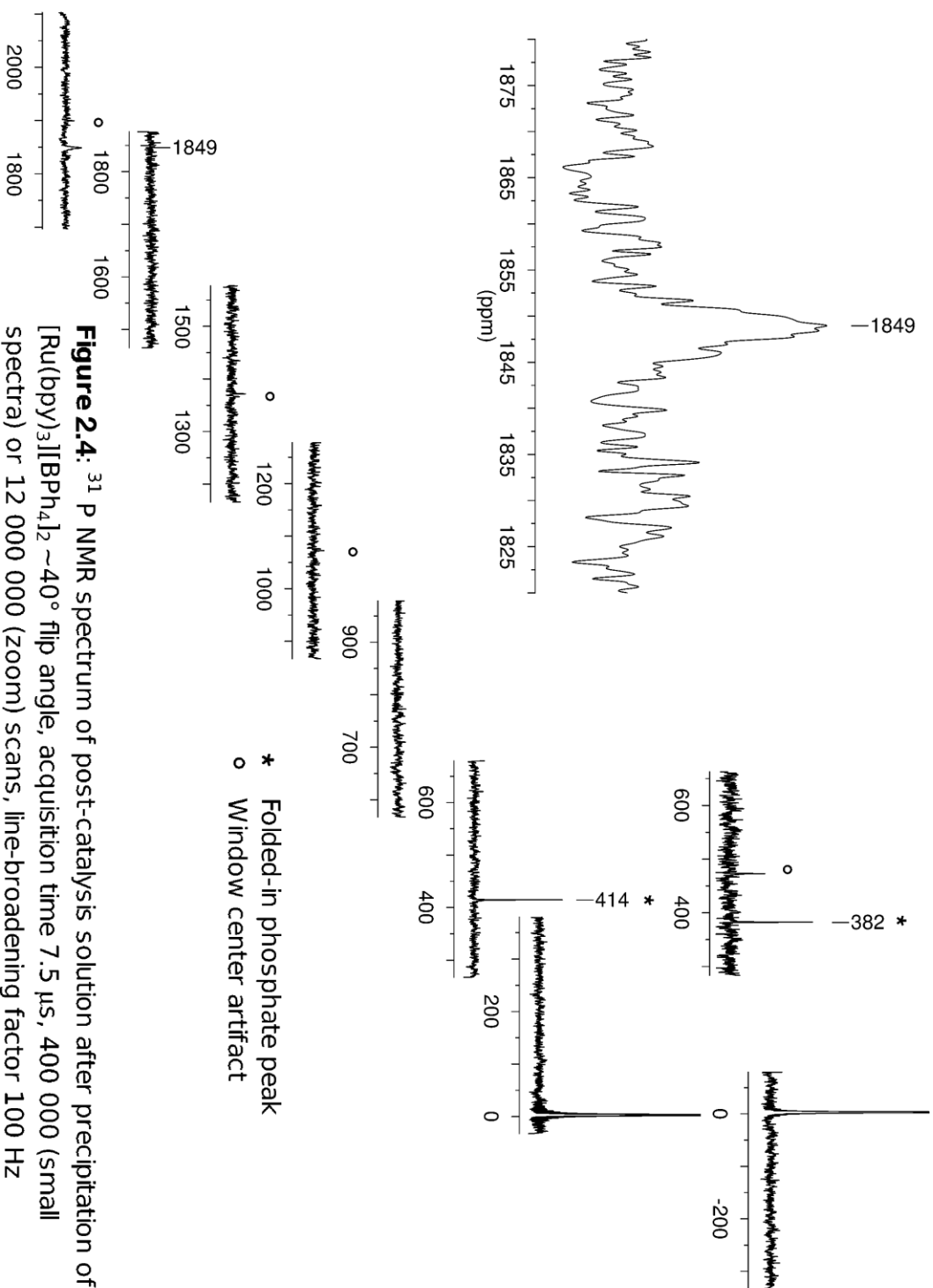


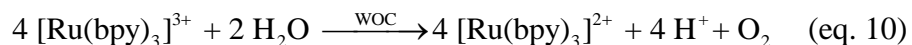
Figure 2.4: ^{31}P NMR spectrum of post-catalysis solution after precipitation of $[\text{Ru}(\text{bpy})_3][\text{BPh}_4]_2$ ~40° flip angle, acquisition time 7.5 μs , 400 000 (small spectra) or 12 000 000 (zoom) scans, line-broadening factor 100 Hz

(b) Re-isolation of catalytically active species

[Ru(bpy)₃]³⁺ (276.7 mg, 0.285 mmol) was dissolved in water (152 mL). A separate aqueous solution of **2** (0.016 mM **2** in 0.153 M NaPi at pH 8.0, 38 mL) was then added. After reaction completion, the solution was concentrated via evaporation. When the solution volume was approximately 50-60 mL, tris(2,2'-bipyridyl)dichlororuthenium(II) hexahydrate ([Ru(bpy)₃]²⁺, 150 mg, 0.20 mmol) was added to this solution, inducing the formation of a light yellow precipitate. The yellow precipitate (1.1 mg) was collected by centrifugation and dried under vacuum, characterized using FT-IR spectroscopy (figure 2.2) and tested for WOC activity.

Results and Discussion

B-type [Co₄(H₂O)₂(α-PW₉O₃₄)₂]¹⁰⁻ (**2**) can be readily prepared from salts and oxides containing cobalt, tungsten and phosphorus.^{5,38} Complex **2** was found to be a WOC through a trial of multiple cobalt-containing POMs (complexes **2-9**). In this process, tris(2,2'-bipyridyl)ruthenium(III), [Ru(bpy)₃]³⁺, was used as a stoichiometric oxidant (eq. 10) and the total oxygen yield was monitored by analyzing the reaction vessel headspace using gas chromatography.^{4,5,8}



Eight cobalt-containing POMs were examined as potential WOCs (Table 2.2). Only complex **2** was active. Cyclic voltammetry of 1 mM **2** also shows a large catalytic current onset at 0.95 V vs. saturated Ag/AgCl reference electrode, indicating a low overpotential for electrochemical water oxidation (figure 2.5). This electrochemical feature is not observed for complexes **3** through **9**.

Table 2.2 Co-containing POMs as potential WOCs. All reactions were run in pH 8 NaPi buffer. 1.5 mM [Ru(bpy)₃]³⁺, ambient temperature; bpy = 2,2'-bipyridine;

$$\text{turnover number, TON} = n_{\text{O}_2}/n_{\text{catalyst}}; \text{O}_2\text{-yield} = \frac{4n_{\text{O}_2}}{n_{\text{Ru(bpy)}_3}}$$

Complex	Complex concentration (mM)	bpy (mM)	TON	O ₂ yield (%)
[Co ₄ (H ₂ O) ₂ (PW ₉ O ₃₄) ₂] ¹⁰⁻ (2)	0.0032	0.06	75	64
[Co ₄ (H ₂ O) ₂ (P ₂ W ₁₅ O ₅₆) ₂] ¹⁰⁻ (3) ⁴⁰	0.0064	0.06	0	0
[Co(H ₂ O)PW ₁₁ O ₃₉] ⁵⁻ (4) ⁴¹	0.0064	0.06	0	0
[Co(H ₂ O)SiW ₁₁ O ₃₉] ⁶⁻ (5) ⁴²	0.0064	0.06	0	0
[Co ₃ (H ₂ O) ₃ (PW ₉ O ₃₄) ₂] ¹²⁻ (6) ⁴³	0.0064	0.06	0	0
[Co ₃ (H ₂ O) ₃ SiW ₉ O ₃₇] ¹⁰⁻ (7) ⁴⁴	0.0064	0.06	0	0
[WCo ₃ (H ₂ O) ₂ (CoW ₉ O ₃₄) ₂] ¹²⁻ (8) ⁴⁵	0.0064	0.06	0	0
[Co ₇ (H ₂ O) ₂ (OH) ₂ P ₂ W ₂₅ O ₉₄] ¹⁶⁻ (9) ⁴⁶	0.0064	0.06	0	0

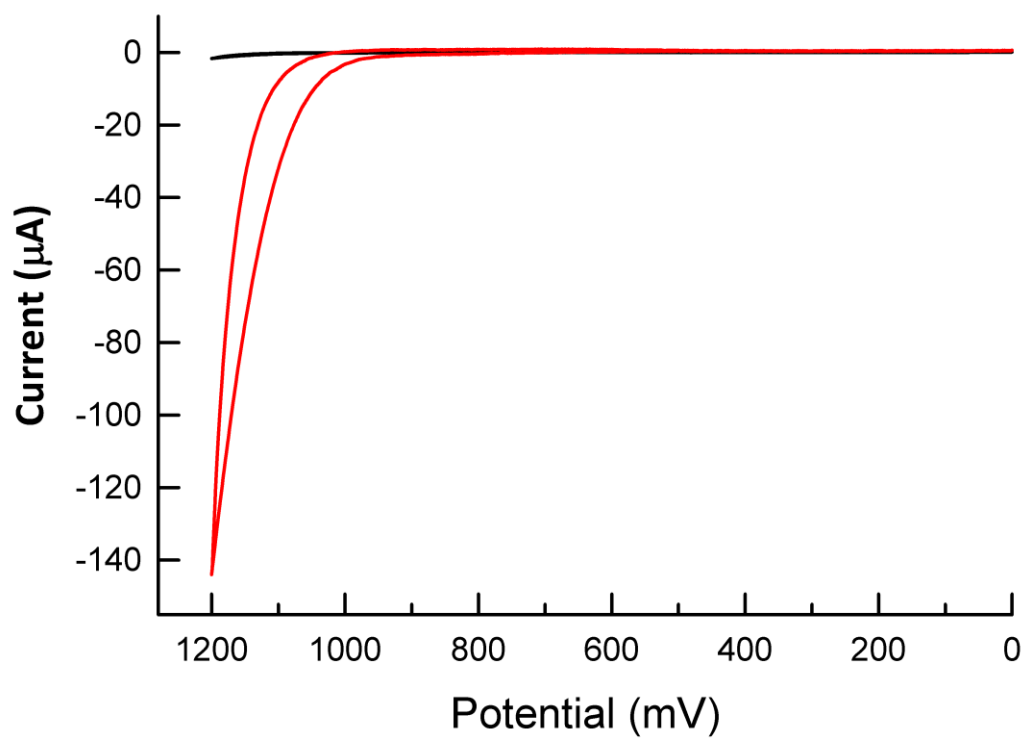


Figure 2.5 Cyclic voltammogram (CV) of 50 mM sodium phosphate solution at pH 8 without **2** (black curve) and with 1 mM **2** (red curve).

The structure of **2** is characterized using x-ray crystallography (figure 2.6). It is interesting to note the structure of the tetracobalt core. Whether this structure remains unchanged in the higher oxidation states is unknown. However, should the active species be geometrically similar to the structure shown in figure 2.6, it would imply that the key water oxidation step occurs at a single cobalt center. Recent studies have suggested that water oxidation indeed may occur at single metal centers.^{7,13,51,52} All the same, few experiments have currently been done to clarify the actual mechanism of water oxidation using **2** and any speculations at this point would be unsubstantiated. It should be noted that in a currently unpublished work, Daniel Nocera's group have identified the active species in his previously published CoPi WOC paper.² It is identified as a solution phase polyoxoheptacobaltate species near the electrode surface. All cobalt centers in this structure also purportedly have edge sharing μ -oxos, similar to that of complex **2**. Such a result would indicate that polyoxocobaltate structures are naturally capable WOCs and POM stabilized multi-cobalt-oxo structure are simply all-inorganic molecular versions of these WOCs. In fact, it is well-known that aqueous cobalt will form cobalt oxide/hydroxide clusters *in situ* under highly oxidizing or basic conditions.^{2,4,53-56} These cobalt oxide/hydroxide clusters are proposed to be WOCs.

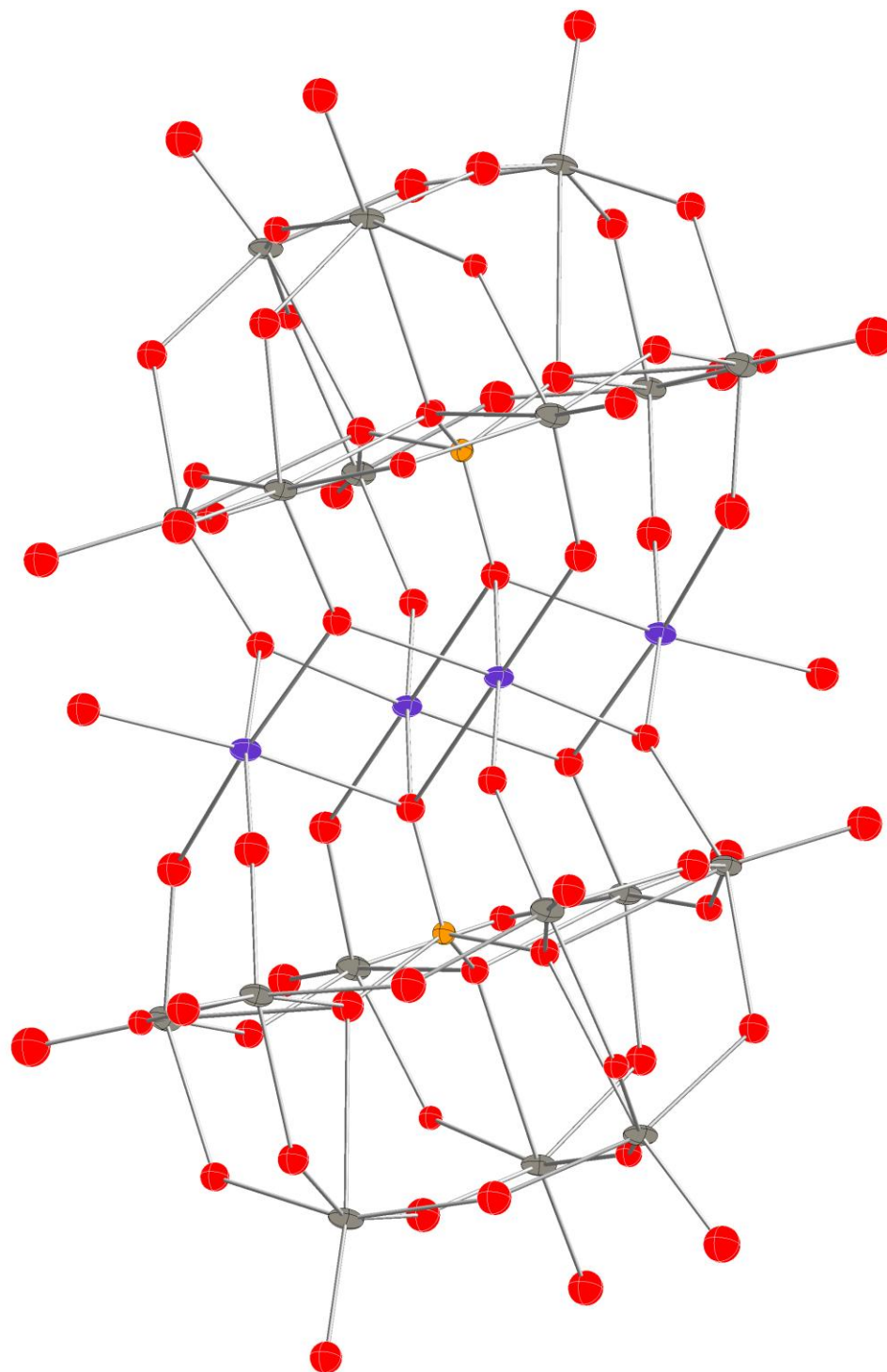


Figure 2.6 X-ray structure of $\text{Na}_{10}\text{-2}$ in thermal ellipsoids. Co: purple, O/OH₂ (terminal): red; P: orange; W: gray. Hydrogen atoms, water molecules and sodium cations are omitted for clarity.

Examination of the structures of complexes **3-9** shows different cobalt-core compositions than **2** with the exception of $[\text{Co}_4(\text{H}_2\text{O})_2(\text{P}_2\text{W}_{15}\text{O}_{56})_2]^{16-}$ (**3**) (figure 2.7). However, because **3** is synthesized and crystallized at a much lower pH than **2** and known to be unstable under higher pH corresponding to our catalytic conditions (pH 7.5 to 8.0),⁵⁷ it was not surprising that **3** is inactive as a WOC. The total oxygen yield must always be less than 100% per oxidant due to significant competing bipyridyl ligand oxidation.⁵⁴ A first-order hyperbolic fit of the O_2 -yield to the concentration of **2** is consistent with this description (figure 2.8).

Water oxidation catalysis by **2** (eq. 10) has a rate highly sensitive to pH. Increasing pH from the initial value of 7.5 to 8.0 in NaPi drops the reaction time down from 270 s to 90 s (respective final pHs after reactions: 7.3 and 7.5). The reaction is made faster in a solution with a higher buffer capacity at pH 8.0 (a mixed buffer of 30 mM NaPi and 30 mM sodium borate buffer; final pH > 7.9). The turnover frequency (TOF) observed for **2** thusly is $> 5.5 \text{ s}^{-1}$. Using initial concentrations of $1.2 \times 10^{-4} \text{ mM}$ **2** and 2.4 mM $[\text{Ru}(\text{bpy})_3]^{3+}$, a TON $\sim 10^3$ in under three minutes was obtained. Consequently, the apparent TON also increases sharply at higher pH due to the faster rate of water oxidation (figure 2.8). The TON in this system is ultimately limited by the formation of an insoluble adduct between **2** and $[\text{Ru}(\text{bpy})_3]^{3+/2+}$, which is in turn determined by the concentration of the $[\text{Ru}(\text{bpy})_3]^{3+}$.

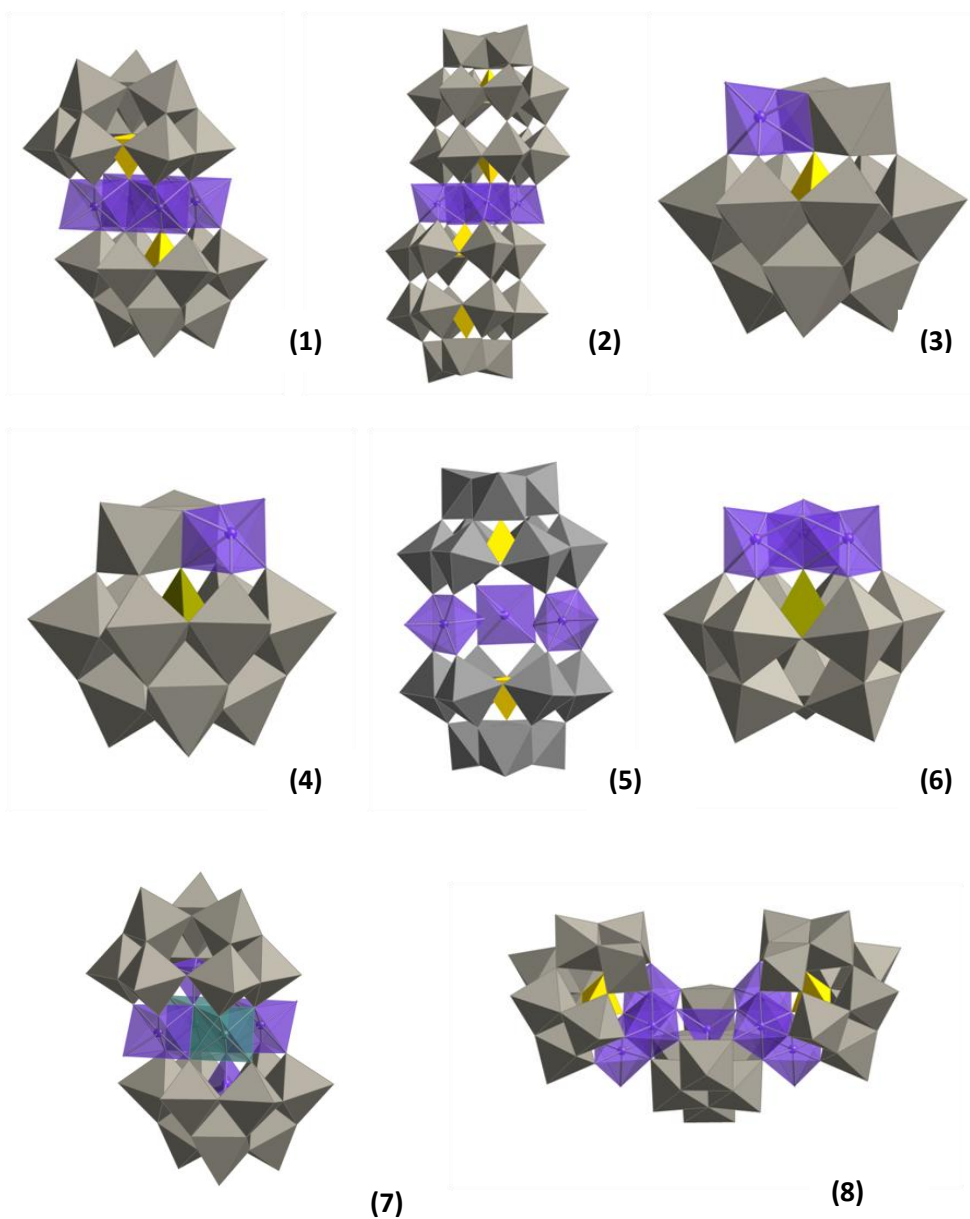


Figure 2.7a Polyhedral representation of the cobalt-containing polytungstate complexes **2-9**. Purple: Co; Grey: WO_6 ; Yellow: PO_4 ; Green: SiO_4 ; Blue: Co and W are disordered in the two positions.

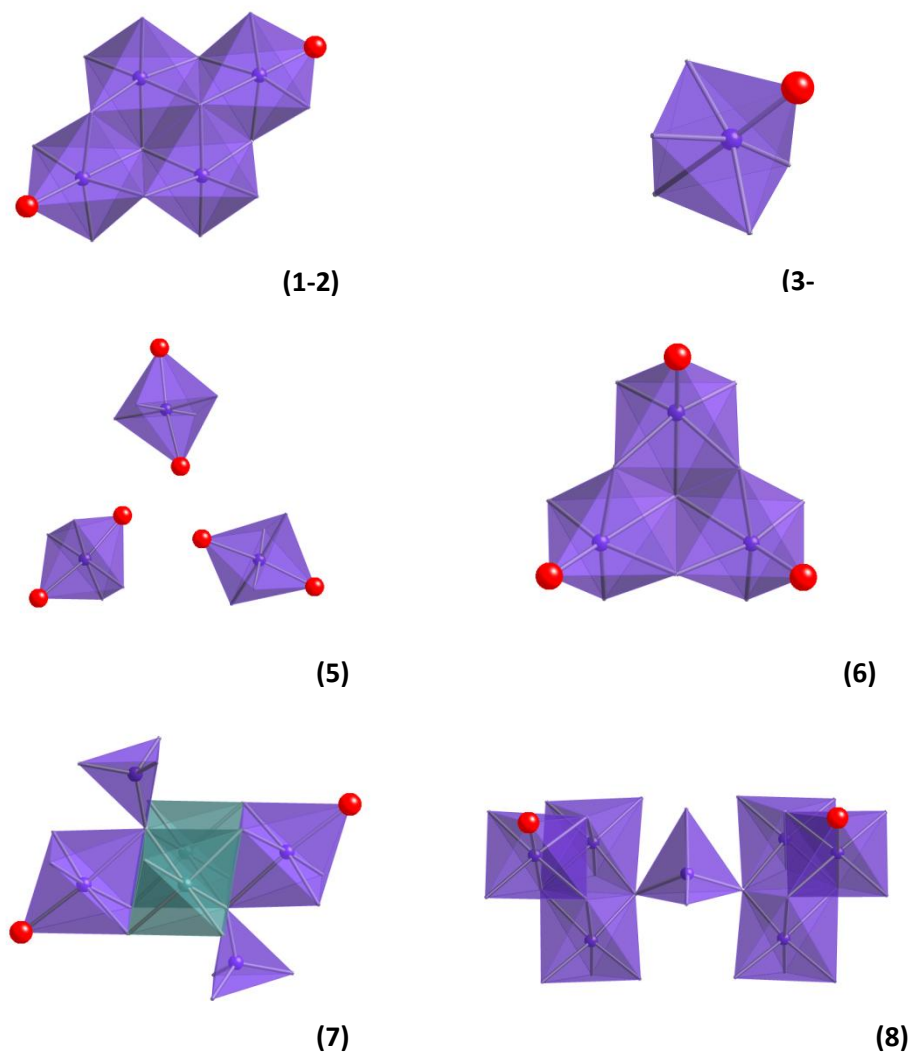


Figure 2.7b Polyhedral representation of the Co core structures of the cobalt-containing polytungstate complexes, **2-9**. Purple ball: Co; Red ball: Terminal O; Blue ball: Co and W disordered in the two positions. All bridging oxygen atoms were omitted.

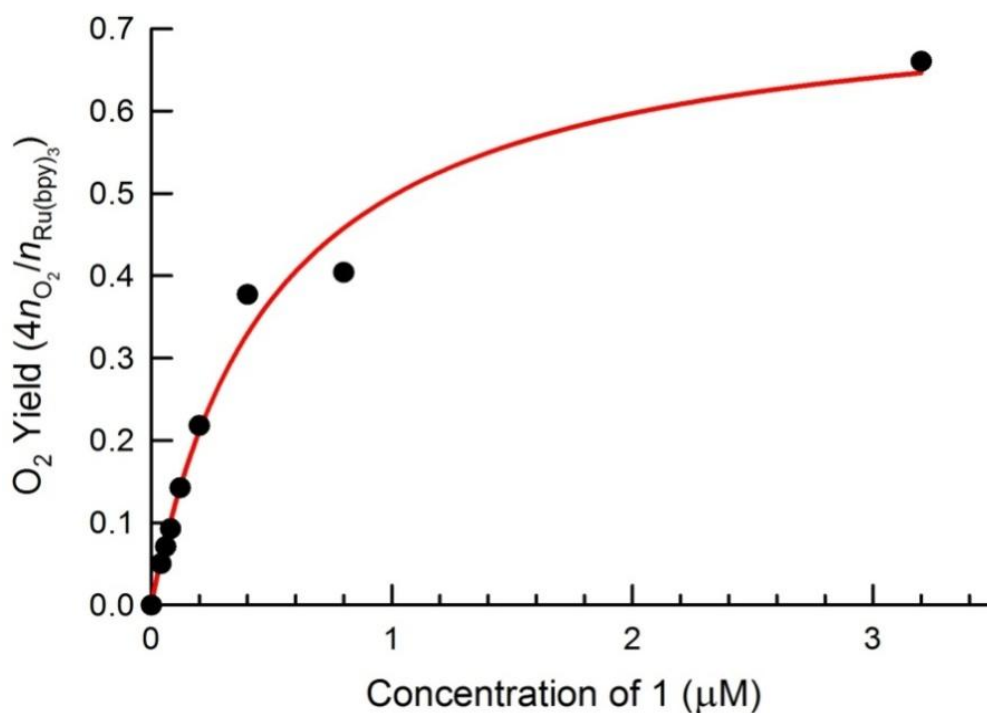
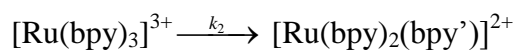
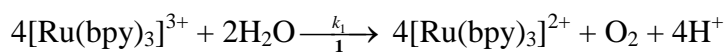


Figure 2.8 The O₂ yield as defined in table 2.2 versus the concentration of **2** (solid circles) and its hyperbolic fit (red line), Pearson correlation coefficient is 0.99. Reactions took place in 30 mM NaPi buffer, initial pH 8.0, 1.5 mM [Ru(bpy)₃]³⁺, r.t. The hyperbolic fit is consistent with a simplified reaction mechanism written below using the steady-state approximation for the catalyst concentration and assumptions that $r_{1S} = 4k_1[\mathbf{2}]f([\text{Ru}(\text{bpy})_3]^{3+})$ and $r_{2S} = k_2 g([\text{Ru}(\text{bpy})_3]^{3+}, \text{Ru}(\text{bpy})_2(\text{bpy}')^{2+})$, where (bpy') is oxidatively damaged bpy:



A simple derivation results in a hyperbolic function of y versus [2]:

$$y = \frac{n_{O_2}}{\frac{1}{4}n_{Ru(bpy)_3}} = \frac{\int_0^\infty 4k_1[\mathbf{1}]f([Ru(bpy)_3]^{3+})dt}{\int_0^\infty 4k_1[\mathbf{1}]f([Ru(bpy)_3]^{3+})dt + \int_0^\infty k_2g([Ru(bpy)_3]^{3+}, [Ru(bpy)_3]^{2+})dt}$$

$$y = \frac{4k_1[\mathbf{1}]\int_0^\infty f([Ru(bpy)_3]^{3+})dt}{4k_1[\mathbf{1}]\int_0^\infty f([Ru(bpy)_3]^{3+})dt + k_2\int_0^\infty g([Ru(bpy)_3]^{3+}, [Ru(bpy)_3]^{2+})dt} = \frac{[\mathbf{1}]}{[\mathbf{1}] + \frac{k_2\int_0^\infty g([Ru(bpy)_3]^{3+}, [Ru(bpy)_3]^{2+})dt}{4k_1\int_0^\infty f([Ru(bpy)_3]^{3+})dt}}$$

$$y = \frac{4n_{O_2}}{n_{Ru(bpy)_3}} = \frac{[\mathbf{1}]}{[\mathbf{1}] + C}$$

The cobalt-containing POM, **2**, is remarkably straightforward to synthesize as shown in the experimental section. It can be crystallized in over 35% yield in a one-pot equilibration synthesis that entails simply heating Co^{2+} , phosphate, and tungstate in the stoichiometric ratio (2:1:9) in water at reflux.³⁸ This synthesis of **2** implies a possible mechanism for self-repair, an important strategy to improve TON in previous works by the Hill group and the Nocera group.^{2,58,59} Homogeneous catalysts like **2** have an advantage over heterogeneous ones in that they utilize a higher percentage of the metal sites for turnover than heterogeneous ones. This is a likely factor in a 500-fold higher observed efficiency of catalytic water oxidation per cobalt atom in the case of **2** when compared to the heterogeneous cobalt phosphate catalyst.

As stated above, aqueous cobalt hydroxide/oxides are known to be WOCs.^{2,54-56} However, these tend to aggregate and deactivate. In fact, this can be demonstrated in a simple experiment. Adding a few drops of 1 M aqueous NaOH

to a 1 mM solution of $\text{Co}(\text{NO}_3)_2$ turned the solution slightly blue. This color quickly disappears and a white precipitate was observed, indicating the formation of cobalt oxide/hydroxide aggregate. However, if the aqueous cobalt can be bound molecularly, aggregation is prevented. To demonstrate, 6 equivalents of bpy was added to a 1 mM solution of $\text{Co}(\text{NO}_3)_2$, a yellow solution results (figure 2.9). Adding aqueous NaOH to this solution does not yield any precipitate. This demonstrates that bpy prevents the formation of catalytically active cobalt oxide/hydroxides.

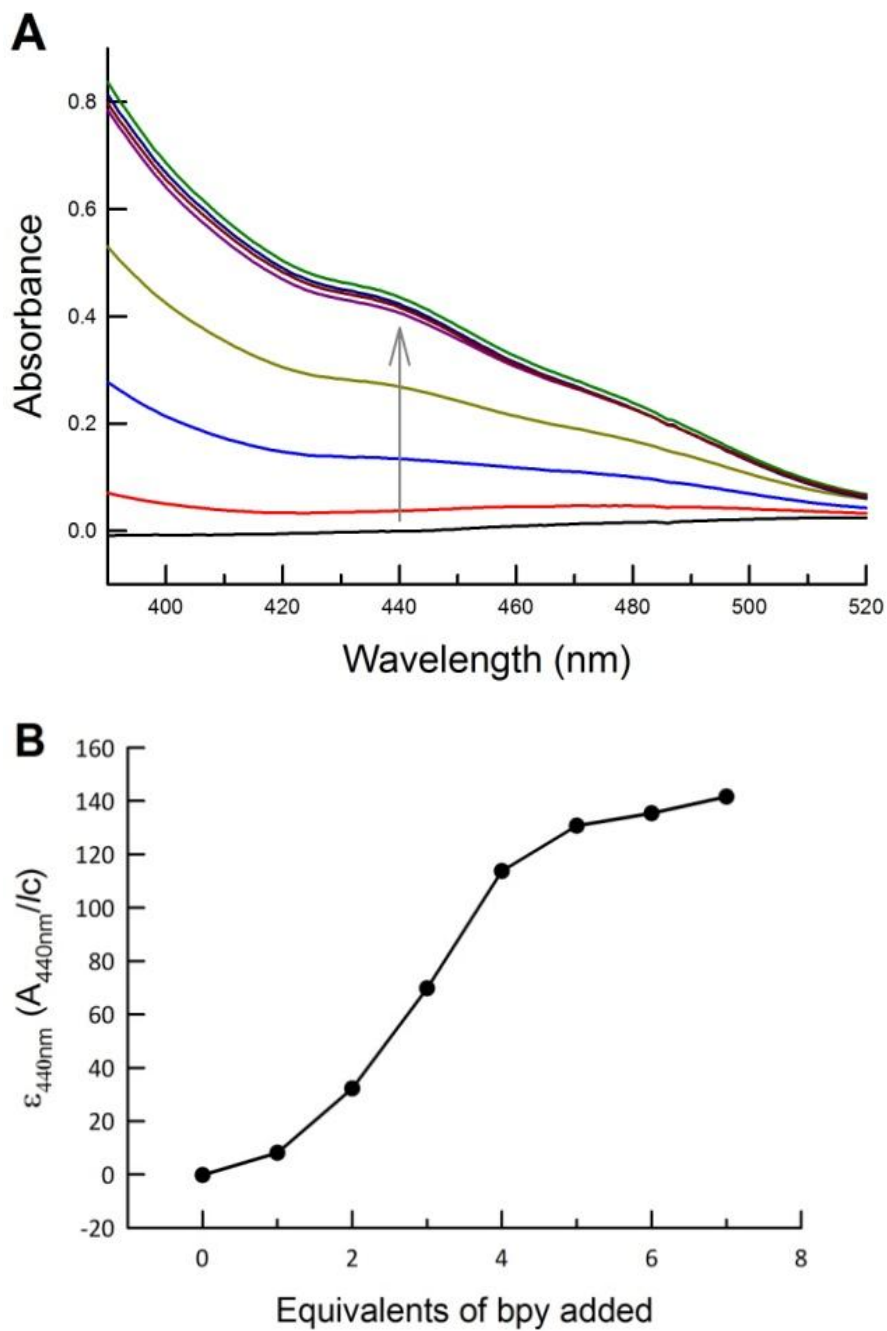


Figure 2.9 (A) UV-Visible spectroscopy indicating the appearance of the bpy cobalt complex with increasing amounts of added bpy. A 5 mM solution of $\text{Co}(\text{NO}_3)_2$ is titrated using a 50 mM solution of bpy. (B) The extinction coefficient ($\text{M}^{-1} \text{cm}^{-1}$) at 440 nm versus the equivalents of bpy added (corrected for a 1/10 dilution factor after each addition).

To prove that **2** is a stable molecular WOC in this system and not its decomposition, I now describe seven lines of experimental evidence. The first two arguments pertain to the hydrolytic stability of **2**. No changes are observed in either the UV/Visible or ^{31}P NMR spectra of a solution of **2** at pH 8 over a one month period (figure 2.3 and figure 2.10). UV-Vis and ^{31}P NMR spectra also both establish that **2** is stable for at least one day within the pH range of 3.5 to 9 (figure 2.10 to figure 2.13).

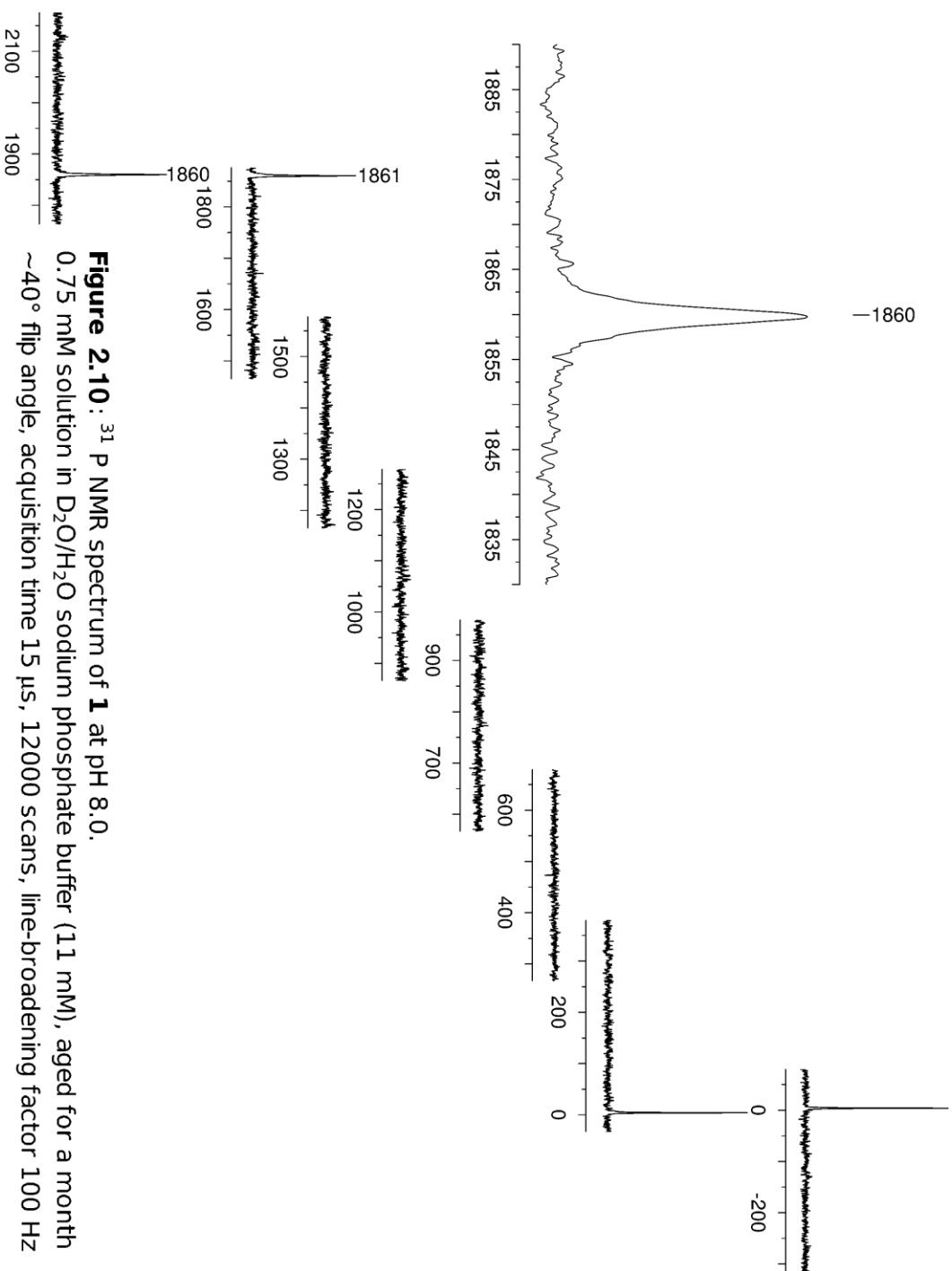


Figure 2.10 : ^{31}P NMR spectrum of **1** at pH 8.0.
0.75 mM solution in $\text{D}_2\text{O}/\text{H}_2\text{O}$ sodium phosphate buffer (11 mM), aged for a month
 $\sim 40^\circ$ flip angle, acquisition time 15 μs , 12000 scans, line-broadening factor 100 Hz

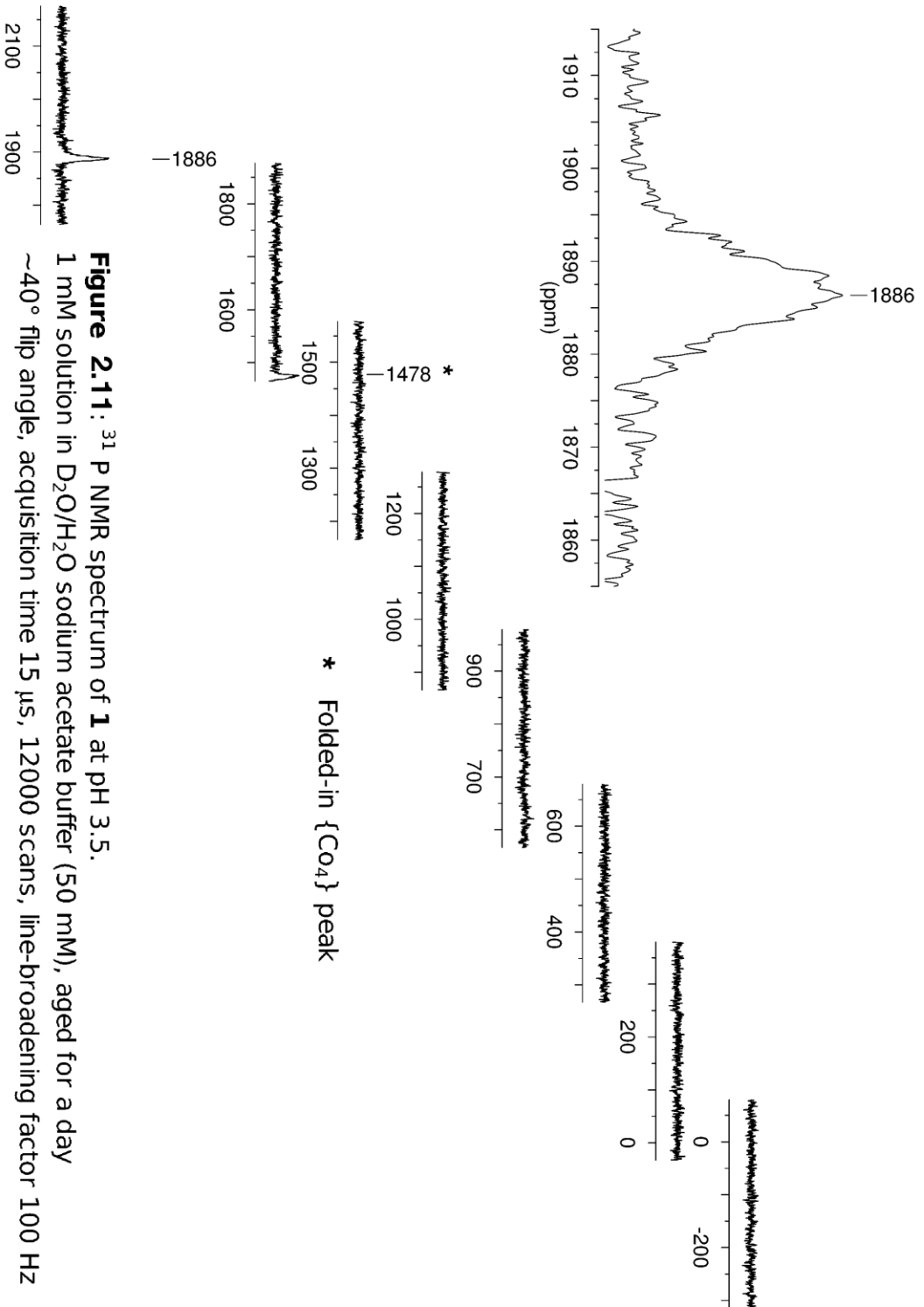
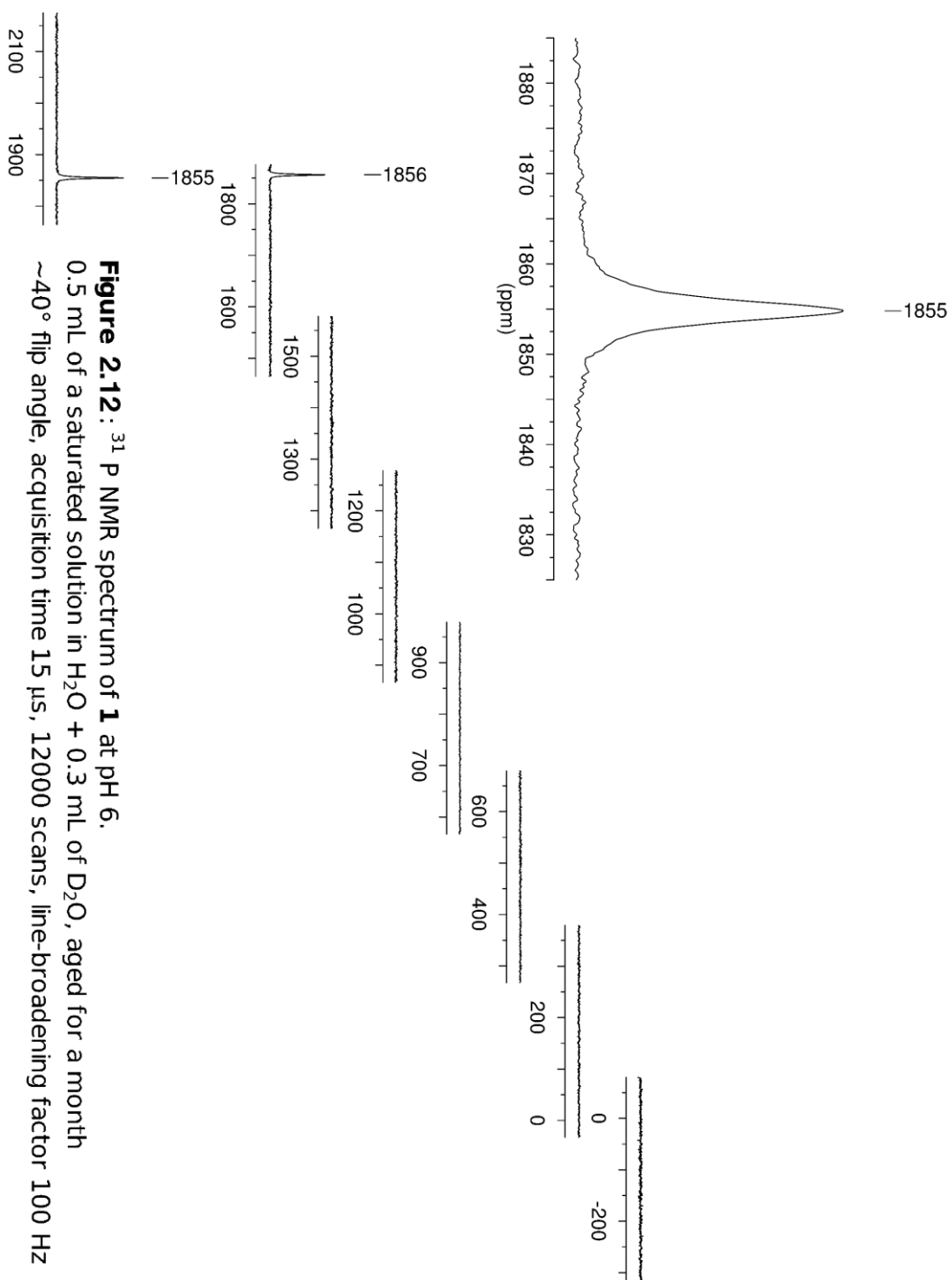


Figure 2.11: ³¹P NMR spectrum of **1** at pH 3.5.
1 mM solution in D₂O/H₂O sodium acetate buffer (50 mM), aged for a day
~40° flip angle; acquisition time 15 μs, 12000 scans, line-broadening factor 100 Hz



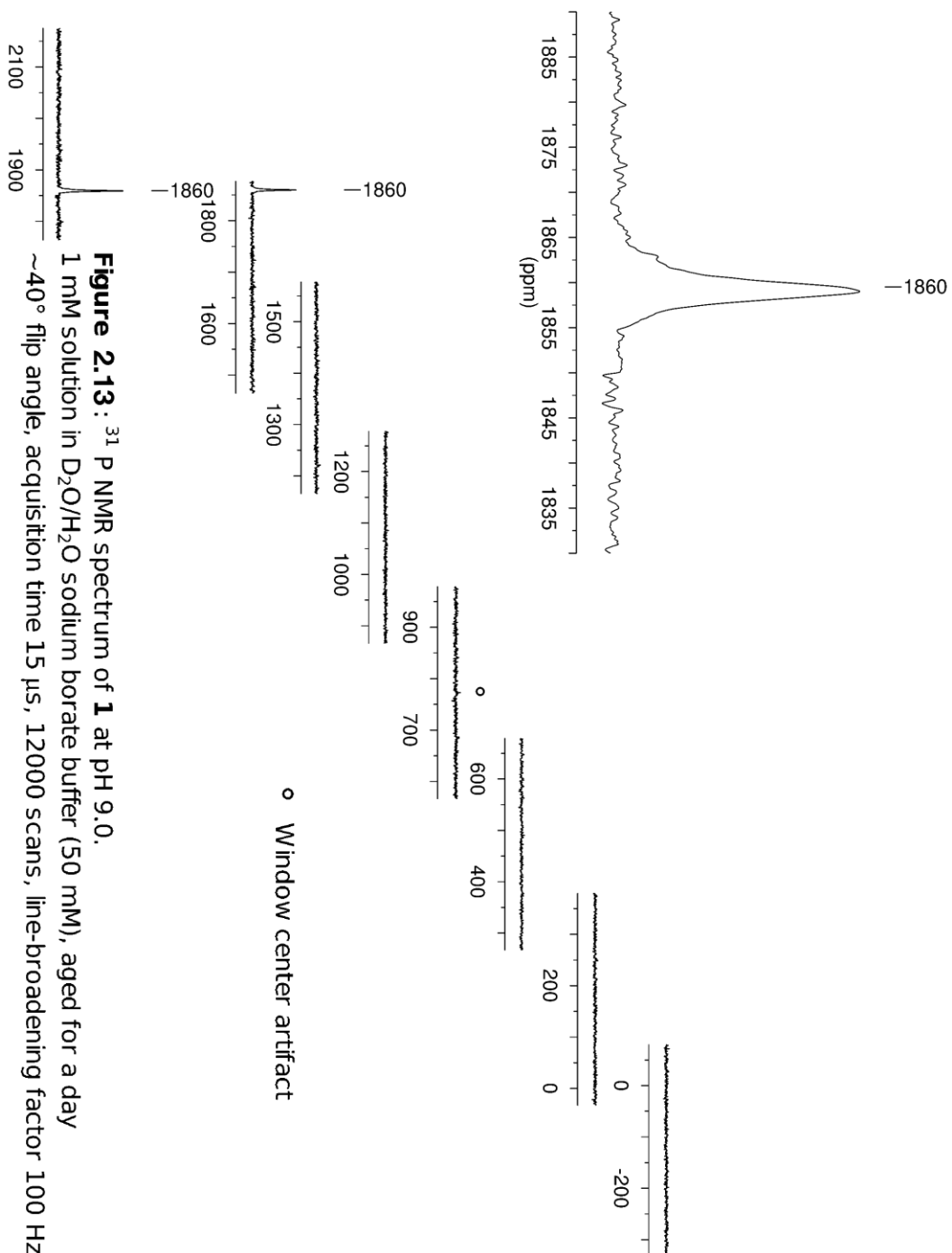


Figure 2.13: ^{31}P NMR spectrum of **1** at pH 9.0.

1 mM solution in $\text{D}_2\text{O}/\text{H}_2\text{O}$ sodium borate buffer (50 mM), aged for a day

~40° flip angle, acquisition time 15 μs , 12000 scans, line-broadening factor 100 Hz

The third argument for the stability of **2** are a series of selective catalyst poisoning experiments using 2,2'-bipyridine (bpy) as an inhibitor (figure 2.9). Bpy reacts with Co(aq)^{2+} to form $[\text{Co(bpy)}_3]^{2+}$,⁶⁰ inhibiting the formation of cobalt oxide/hydroxide clusters and thus all water oxidation activity. In contrast, the addition of the same molar equivalent excess of bpy to solutions of **2** has a relatively minor effect on the apparent water oxidation activity (table 2.3). The observed slight decrease in activity can be attributed to bpy competitively coordinating to the cobalt core of **2**, or the irreversible oxidative degradation of bpy, which is proportional to the bpy concentration. In a similarly telling experiment, aging **1** under reaction conditions for 3 days has no effect on its catalytic water oxidation activity (table 2.3), whereas aging $\text{Co(NO}_3)_2$ under the same conditions for 3 days significantly decreases its catalytic activity. This observation tracks with well-known cobalt hydroxide/oxide formation above neutral pH,⁶¹ decreasing the effective surface area and therefore catalytic activity. In addition, at pH 6.2, no water oxidation is observed for reactions catalyzed by **2**, whereas $\text{Co(NO}_3)_2$ is still capable of catalyzing a small extent of water oxidation (table 2.3). These results are consistent with **2** being a catalytically active species completely different from aqueous cobalt. One can also conclude that the polydentate polytungstate ligands of **2** stabilize it as a WOC by preventing the formation of cobalt hydroxide/oxide clusters.

Table 2.3 The effect of bpy on the catalytic water oxidation activity of **2** and Co(aq)^{2+} .

Run	Complex	Complex concentration (mM)	bpy (mM)	Buffer	TON	O ₂ yield (%)
1	2	0.0032	0	pH 8 NaPi	78.1	66.7
2	2	0.0032	0.3012	pH 8 NaPi	56	48
3	$\text{Co(NO}_3)_2$	0.013 [*]	0.3012	pH 8 NaPi	0	0
4	$\text{Co(NO}_3)_2$	0.060 [†]	0.3012	pH 8 NaPi	0.2	<4
5	$\text{Co(NO}_3)_2$	0.013	0	pH 8 NaPi	23.4	80
6	no catalyst	--	0	pH 8 NaPi	0	0
7	2	0.0032	0	pH 6.2 NaPi/phthalic acid [‡]	0	0
8	$\text{Co(NO}_3)_2$	0.013	0	pH 6.2 NaPi/phthalic acid	10	35
9	2	0.0032	0.135	pH 8 NaPi	70.3	60
10	2 (aged) [§]	0.0032	0.135	pH 8 NaPi	71.2	60.8
11	$\text{Co(NO}_3)_2$ (aged) [§]	0.013	0	pH 8 NaPi	9.8	33.6
12	CoO^{\parallel}	0.0032	0	pH 8 NaPi	0	0

^{*}Same theoretical cobalt concentration as 0.0032 mM **1**; [†] Same solid mass as 0.0032 mM **1**; [‡] A mixed buffer of 30 mM NaPi and 30 mM phthalic acid at pH 6.2 was used; [§] A 1 mM stock solution in 30 mM pH 8 NaPi was left for 72 hours before use; ^{||} not soluble, suspension obtained after 10 minutes of sonication.

In the fourth line of argument for the stability of **2**, the post-reaction solution containing **2** was characterized using ³¹P NMR despite the low solubility of **2** in the presence of excess $[\text{Ru}(\text{bpy})_3]^{2+}$. When $[\mathbf{2}] = 0.015$ mM, as few as 40 equivalents of $[\text{Ru}(\text{bpy})_3]^{3+/2+}$ make the post-reaction solution supersaturated, forming a light yellow precipitate in minutes to hours. To prevent precipitation, $[\text{Ru}(\text{bpy})_3]^{2+}$ was removed from the post-reaction solution by adding NaBPh_4 and removing solid $[\text{Ru}(\text{bpy})_3][\text{BPh}_4]_2$ by filtration. In the ³¹P NMR spectrum of this

solution, **2** (1850 ppm, $\Delta v_{1/2} = 600$ Hz) was the only species detected besides the free phosphate originating from the buffer solution. This strongly suggests that **2** remains intact under catalytic water oxidation conditions (figure 2.4).

The fifth and sixth lines of experimental evidence for the stability of **2** utilizes IR characterization and recycling of the WOC after an initial water oxidation reaction. After the reaction was complete, the solution was saturated with $[\text{Ru}(\text{bpy})_3]^{2+}$, which acts as a counter-ion for complex **2**, resulting in its precipitation. The infrared spectrum of the precipitate showed the characteristic peaks of **2**, a B-type sandwich polytungstate, at 1037 cm^{-1} , 939 cm^{-1} , 882 cm^{-1} , and 767 cm^{-1} (figure 2.2), indicating that the POM framework remains intact after catalysis. For simplicity, we assumed a 1:1 ratio of the $[\text{Ru}(\text{bpy})_3]^{2+}$ and **2** in the precipitate, and assigned the molecular formula of the precipitate to be **Na₈Ru(bpy)₃-2**. Using the corresponding molecular weight, we recycled *ca.* 0.0032 mM **Na₈Ru(bpy)₃-2** as catalyst in the reaction of $[\text{Ru}(\text{bpy})_3]^{3+}$ with water in the presence of bpy at pH 8. This reaction yielded 49.3% O₂ and a TON of 58 per **2**, exactly reproducing the activity of pure crystalline **Na₁₀-2** (run #2, Table 2.3).

The seventh indication of the stability of **2** during catalysis is its voltammetric behavior. In summary, catalytic current is retained after chemical water oxidation, demonstrating that catalytic activity of the active species is undiminished after turnover. In a cyclic voltammogram of unreacted $[\text{Ru}(\text{bpy})_3]^{2+}$ and a catalytic concentration of **2**, an increased anodic current peak and decreased cathodic current peak is observed for the $[\text{Ru}(\text{bpy})_3]^{3+}/[\text{Ru}(\text{bpy})_3]^{2+}$ couple,

indicating the catalytic reduction of $[\text{Ru}(\text{bpy})_3]^{3+}$ (figure 2.14). The observed catalytic current increases with catalyst concentration.⁸ As shown in figure 2.14, the catalytic current for the solution after chemical water oxidation and for an analogous solution incapable of chemical water oxidation ($[\text{Ru}(\text{bpy})_3]^{2+}$ and **2** alone) match each other under similar conditions. This result indicates no evident catalyst deactivation and implies that concentration of **2** remains constant after catalysis. In contrast, the same cyclic voltammetric experiment using $\text{Co}(\text{NO}_3)_2$ in place of **2** shows a marked decrease in the catalytic water oxidation current for the solution after chemical water oxidation when compared to that of analogous solution incapable of chemical water oxidation ($[\text{Ru}(\text{bpy})_3]^{2+}$ and $\text{Co}(\text{NO}_3)_2$ alone; see figure 2.15). Once again, this finding is consistent with aqueous cobalt hydrolyzing and condensing to hydroxide/oxide particles under oxidative conditions, decreasing the effective catalyst concentration.

In conclusion, this chapter presents numerous lines of evidence for the stability and structural integrity of **2** during water oxidation turnover. Discussions of metal-oxide WOCs indicate that POMs are a uniquely interesting class of oxidatively stable WOCs. In fact, as molecular metal oxides, POMs may be the solution to preventing *in situ* metal oxide/hydroxide cluster aggregations.

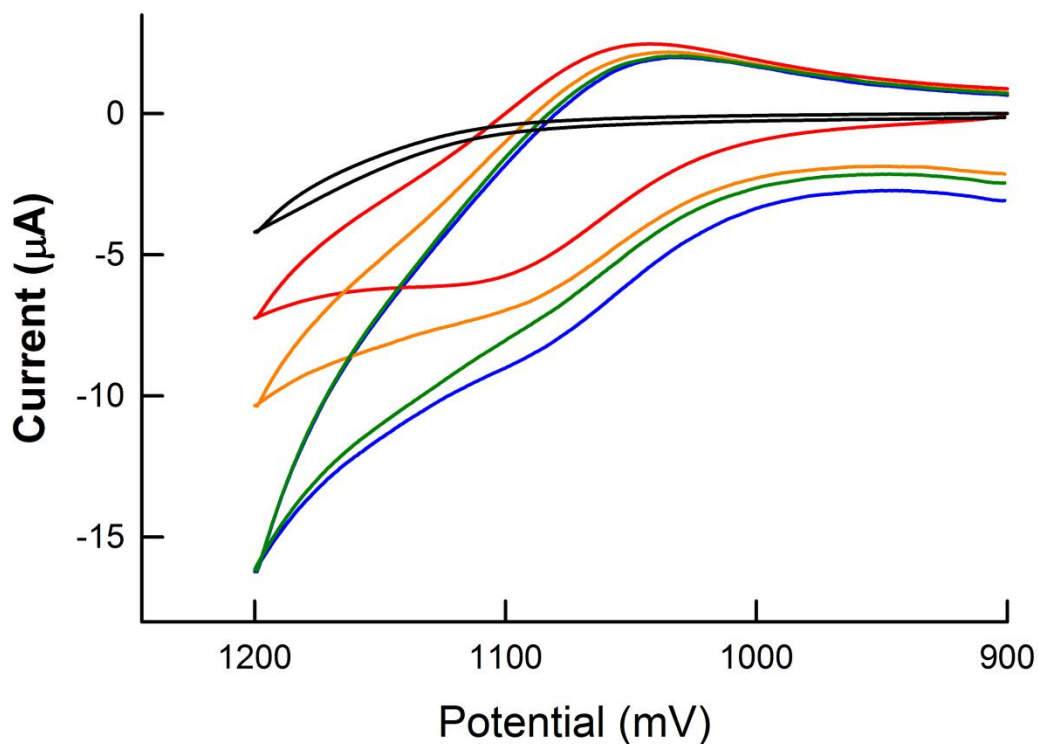


Figure 2.14 Cyclic voltammogram of 0.857 mM $[\text{Ru}(\text{bpy})_3]^{2+}$ (red), 3.2 μM **1** (black), a solution incapable of chemical water oxidation comprising 0.857 mM $[\text{Ru}(\text{bpy})_3]^{2+}$ and 3.2 μM **1** (green) or 1.6 μM **1** (yellow), and a post-reaction solution containing 0.857 mM $[\text{Ru}(\text{bpy})_3]^{3+}$ reduced in the presence of 3.2 μM **1** (blue). The series of CVs for 0 μM **1** (red), 1.6 μM **1** (yellow), and 3.2 μM **1** (green) added to 0.857 mM $[\text{Ru}(\text{bpy})_3]^{2+}$ shows increasing anodic current and decreasing cathodic current, demonstrating the correlation between increasing catalytic current and the concentration of **1**. Conditions: 60 mM NaPi, pH 8, scan rate 25 mV/s; potentials measured and reported versus an Ag/AgCl reference electrode.

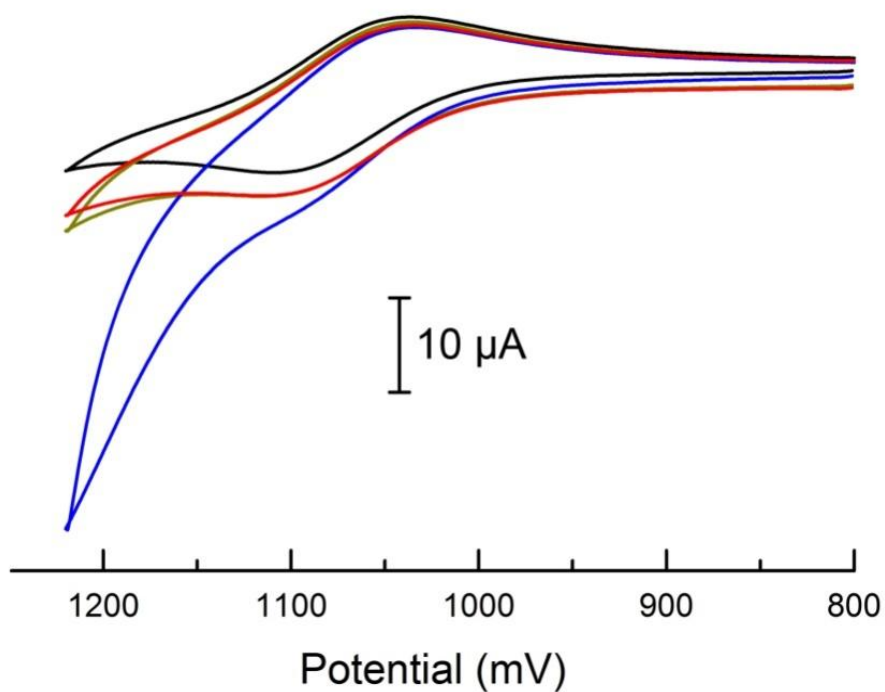


Figure 2.15 Cyclic voltammograms: 0.857 mM $[\text{Ru}(\text{bpy})_3]^{2+}$ (black); a “post-chemical reaction” solution containing 0.857 mM $[\text{Ru}(\text{bpy})_3]^{2+}$ and 0.0128 mM $\text{Co}(\text{NO}_3)_2$ (red); an “unreacted” model solution containing 0.857 mM $[\text{Ru}(\text{bpy})_3]^{2+}$ and 0.0128 mM $\text{Co}(\text{NO}_3)_2$ (blue); or 0.0064 mM $\text{Co}(\text{NO}_3)_2$ (yellow). The solutions are buffered using 60 mM NaPi, pH 8, scan rate 25 mV/s.

Reference

- ¹ Eisenberg, R. & Gray, H. B. Preface on Making Oxygen. *Inorg. Chem.* **47**, 1697-1699 (2008).
- ² Kanan, M. W. & Nocera, D. G. In Situ Formation of an Oxygen-Evolving Catalyst in Neutral Water Containing Phosphate and Co^{2+} . *Science* **321**, 1072-1075, doi:[10.1126/science.1162018](https://doi.org/10.1126/science.1162018) (2008).
- ³ Kanan, M. W., Surendranath, Y. & Nocera, D. G. Cobalt–phosphate oxygen-evolving compound. *Chem. Soc. Rev.* **38**, 109-114 (2009).
- ⁴ Geletii, Y. V., Besson, C., Hou, Y., Yin, Q., Musaev, D. G., Quinonero, D., Cao, R., Hardcastle, K. I., Proust, A., Kögerler, P. & Hill, C. L. Structural, Physicochemical and Reactivity Properties of an All-Inorganic, Highly Active Tetraruthenium Homogeneous Catalyst for Water Oxidation. *J. Am. Chem. Soc.* **131**, 17360-17370 (2009).
- ⁵ Yin, Q., Tan, J. M., Besson, C., Geletii, Y. V., Musaev, D. G., Kuznetsov, A. E., Luo, Z., Hardcastle, K. I. & Hill, C. L. A fast soluble carbon-free molecular water oxidation catalyst based on abundant metals. *Science*, Printed online March 11, 2010, doi:[10.1126/science.1185372](https://doi.org/10.1126/science.1185372) (2010).
- ⁶ Tagore, R., Crabtree, R. H. & Brudvig, G. W. Oxygen Evolution Catalysis by a Dimanganese Complex and Its Relation to Photosynthetic Water Oxidation. *Inorganic Chemistry* **47**, 1815-1823, doi:[10.1021/ic062218d](https://doi.org/10.1021/ic062218d) (2008).
- ⁷ Yagi, M. & Kaneko, M. Molecular Catalysts for Water Oxidation. *Chemical Reviews* **101**, 21-36, doi:[10.1021/cr980108l](https://doi.org/10.1021/cr980108l) (2000).

- ⁸ Geletii, Y. V., Botar, B., Kögerler, P., Hillesheim, D. A., Musaev, D. G. & Hill, C. L. An All-Inorganic, Stable, and Highly Active Tetra-ruthenium Homogeneous Catalyst for Water Oxidation. *Angew. Chem. Int. Ed.* **47**, 3896-3899. Selected as the VIP Article by the reviewers and editor. Published online 3893/3820/3808 DOI: 3810.1002/anie.200705652, doi:DOI: 10.1002/anie.200705652 (2008).
- ⁹ Gersten, S. W., Samuels, G. J. & Meyer, T. J. Catalytic Oxidation of Water by an Oxo-Bridged Ruthenium Dimer. *J. Am. Chem. Soc.* **104**, 4029-4030 (1982).
- ¹⁰ Wada, T., Tsuge, K. & Tanaka, K. Electrochemical Oxidation of Water to Dioxygen Catalyzed by the Oxidized Form of the Bis(ruthenium-hydroxo) Complex in H₂O *Angew. Chem. Int. Ed.* **39**, 1479-1482 (2000).
- ¹¹ Limburg, J., Vrettos, J. S., Chen, H., Paula, J. C. d., Crabtree, R. H. & Brudvig, G. W. Characterization of the O₂-Evolving Reaction Catalyzed by [(terpy)(H₂O)Mn^{III}(O)₂Mn^{IV}(OH₂)(terpy)](NO₃)₃ (terpy) 2,2':6,2''-Terpyridine). *J. Am. Chem. Soc.* **123**, 423-430 (2001).
- ¹² Hurst, J. K. Water oxidation catalyzed by dimeric μ -oxo bridged ruthenium diimine complexes *Coord. Chem. Rev.* **249**, 313-328 (2005).
- ¹³ Zong, R. & Thummel, R. A New Family of Ru Complexes for Water Oxidation. *J. Am. Chem. Soc.* **127**, 12802-12803 (2005).
- ¹⁴ Muckerman, J. T., Polyansky, D. E., Wada, T., Tanaka, K. & Fujita, E. Water Oxidation by a Ruthenium Complex with Noninnocent Quinone

- Ligands: Possible Formation of an O-O Bond at a Low Oxidation State of the Metal. *Inorg. Chem.* **47**, 1787-1802 (2008).
- ¹⁵ Brimblecombe, R., Swiegers, G. F., Dismukes, G. C. & Spiccia, L. Sustained Water Oxidation Photocatalysis by a Bioinspired Manganese Cluster. *Angew. Chem. Int. Ed.* **47**, 7335-7338 (2008).
- ¹⁶ Romain, S., Bozoglian, F., Sala, X. & Llobet, A. Oxygen—Oxygen Bond Formation by the Ru-Hbpp Water Oxidation Catalyst Occurs Solely via an Intramolecular Reaction Pathway. *J. Am. Chem. Soc.* **131**, 2768-2769 (2009).
- ¹⁷ Kohl, S. W., Weiner, L., Schwartsburd, L., Konstantinovski, L., Shimon, L. J. W., Ben-David, Y., Iron, M. A. & Milstein, D. Consecutive Thermal H₂ and Light-Induced O₂ Evolution from Water Promoted by a Metal Complex. *Science* **324**, 74-77 (2009).
- ¹⁸ Hull, J. F., Balcells, D., Blakemore, J. D., Incarvito, C. D., Eisenstein, O., Brudvig, G. W. & Crabtree, R. H. Highly Active and Robust Cp* Iridium Complexes for Catalytic Water Oxidation. *J. Am. Chem. Soc.* **131**, 8730-8731 (2009).
- ¹⁹ Kunkely, H. & Vogler, A. Water Splitting by Light with Osmocene as Photocatalyst. *Angew. Chem. Int. Ed.* **48**, 1685-1687, doi:10.1002/anie.200804712 (2009).
- ²⁰ Hill, C. L. & Prosser-McCartha, C. M. Homogeneous catalysis by transition metal oxygen anion clusters. *Coord. Chem. Rev.* **143**, 407-455 (1995).

- 21 Hill, C. L. in *Polyoxometalates in Catalysis* Vol. J. Mol. Catal. A: Chem (ed Craig L. Hill) 2–6 (Elsevier, 2007).
- 22 Hill, C. L. Foreword, Polyoxometalates in Catalysis. *J. Mol. Catal. A: Chem. Special Issue* **262**, 1, doi:<http://dx.doi.org/10.1016/j.molcata.2006.08.041> (2007).
- 23 Hill, C. L. Progress and challenges in polyoxometalate-based catalysis and catalytic materials chemistry. *J. Mol. Catal. A: Chem.* **262**, 2-6 (2007).
- 24 Hill, C. L. Polyoxometalates in Catalysis. *J. Mol. Catal. A* **262**, 1-242 (2007 Special Issue).
- 25 Hill, C. L., Delannoy, L., Duncan, D. C., Weinstock, I. A., Renneke, R. F., Reiner, R. S., Atalla, R. H., Han, J. W., Hillesheim, D. A., Cao, R., Anderson, T. M., Okun, N. M., Musaev, D. G. & Geletii, Y. V. Complex catalysts from self-repairing ensembles to highly reactive air-based oxidation systems. *C.R. Chimie* **10**, 305-312 (2007).
- 26 Neumann, R. & Dahan, M. A ruthenium-substituted polyoxometalate as an inorganic dioxygenase for activation of molecular oxygen. *Nature* **388**, 353-355 (1997).
- 27 Besson, C., Huang, Z., Geletii, Y. V., Lense, S., Hardcastle, K. I., Musaev, D. G., Lian, T., Proust, A. & Hill, C. L. Cs₉[(Y-PW₁₀O₃₆)₂Ru₄O₅(OH)(H₂O)₄], a new all-inorganic, soluble catalyst for the efficient visible-light-driven oxidation of water. *Chem. Commun.*, in press (2010).

- 28 Pope, M. T. in *Comprehensive Coordination Chemistry II: From Biology to Nanotechnology* Vol. 4 *Comprehensive Coordination Chemistry II* (ed A. G. Wedd) 635-678 (Elsevier Ltd., 2004).
- 29 Hill, C. L. in *Comprehensive Coordination Chemistry-II: From Biology to Nanotechnology* Vol. 4 *Comprehensive Coordination Chemistry II* (ed A. G. Wedd) 679-759 (Elsevier Ltd., 2004).
- 30 Hill, C. L. Stable, Self-Assembling, Equilibrating Catalysts for Green Chemistry. *Angew. Chem. Int. Ed.* **43**, 402-404 (2004).
- 31 Pope, M. T. & Müller, A. (Kluwer Academic Publishers, Dordrecht, 2001).
- 32 Pope, M. T. & Müller, A. Chemistry of polyoxometallates. Actual variation on an old theme with interdisciplinary references. *Angew. Chem. Int. Ed. Engl.* **30**, 34-48 (1991).
- 33 Yamase, T. & Pope, M. T. in *Nanostructure Science and Technology* Vol. 2 (ed David J. Lockwood) (Kluwer Academic/Plenum Publishers, New York, 2002).
- 34 Pope, M. T. in *Comprehensive Coordination Chemistry* Vol. 3 eds G. Wilkinson, R. D. Gillard, & J. A. McCleverty) Chapter 38 (Pergamon Press, 1987).
- 35 Pope, M. T. & Müller, A. (Kluwer Academic Publishers, Dordrecht, Netherlands, 1993).
- 36 Pope, M. T. & Müller, A. Introduction to polyoxymetalates. *Molecular Engineering* **3**, 1-8 (1993).

- 37 Borrás-Almenar, J. J., Coronado, E., Müller, A. & Pope, M. T. *Polyoxometalate Molecular Science*. Vol. 98 (Kluwer Academic Publishers, 2003).
- 38 Weakley, T. J. R., Evans, H. T., Jr., Showell, J. S., Tourné, G. F. & Tourné, C. M. 18-Tungstotetracobalto(II)diphosphate and related Anions: a Novel Structural Class of Heteropolyanions. *J. Chem. Soc. Chem. Comm.* **4**, 139-140 (1973).
- 39 Finke, R. G., Droege, M. W. & Domaille, P. J. Trivalent Heteropolytungstate Derivatives. 3.¹ Rational Syntheses, Characterization, Two-Dimensional ¹⁸³W NMR, and properties of $P_2W_{18}M_4(H_2O)_2O_{68}^{10-}$ and $P_4W_{30}M_4(H_2O)_2O_{112}^{16-}$ (M=Co, Cu, Zn). *Inorg. Chem.* **26**, 3886-3896 (1987).
- 40 Finke, R. G. & Droege, M. W. Trivalent Heteropolytungstate Derivatives. 2. Synthesis, Characterization, and ¹⁸³W NMR of $P_4W_{30}M_4(H_2O)_2O_{112}$ (M = Co, Cu, Zn). *Inorg. Chem.* **22**, 1006-1008 (1983).
- 41 Weakley, T. J. R. Heteropolyanions Containing Two Different Heteroatoms. Part III. Cobalto(II)undecatungstophosphate and Related Anions. *J. Chem. Soc., Dalton Trans. Inorg. Chem.* **3**, 341-346 (1973).
- 42 Weakley, T. J. R. & Malik, S. A. Heteropolyanions containing two different heteroatoms - Part I. *J. Inorg. Nucl. Chem.* **29**, 2935-2944 (1967).
- 43 Knoth, W. H., Domaille, P. J. & Farlee, R. D. Anions of the Type $(RMOH_2)_3W_{18}P_2O_{68}^{9-}$ and $[H_2OCo]_3W_{18}P_2O_{68}^{12-}$. A Reinvestigation of "B,b-W₉PO₃₄⁹⁻". *Organometallics* **4**, 62-68 (1985).

- 44 Liu, J. G., Ortega, F., Sethuraman, P., Katsoulis, D. E., Costello, C. E. & Pope, M. T. Trimetallo Derivatives of Lacunary 9-Tungstosilicate Heteropolyanions. 1. Synthesis and Characterization. *J. Chem. Soc., Dalton Trans.*, 1901-1906 (1992).
- 45 Tourné, C. M., Tourné, G. F. & Zonnevijlle, F. Chiral Polytungstometalates $[\text{WM}_3(\text{H}_2\text{O})_2(\text{XW}_9\text{O}_{34})_2]^{12-}$ ($\text{X} = \text{M} = \text{Zn}$ or Co^{II}) and their M-Substituted Derivatives. Syntheses, Chemical, Structural and Spectroscopic Study of some D, L Sodium and Potassium Salts. *J. Chem. Soc., Dalton Trans.* **1**, 143-155 (1991).
- 46 Clemente-Juan, J. M., Coronado, E., Forment-Aliaga, A., Galan-Mascaros, J. R., Gimenez-Saiz, C. & Gomez-Garcia, C. J. A New Heptanuclear Cobalt(II) Cluster Encapsulated in a Novel Heteropolyoxometalate Topology: Synthesis, Structure, and Magnetic Properties of $[\text{Co}_7(\text{H}_2\text{O})_2(\text{OH})_2\text{P}_2\text{W}_{25}\text{O}_{94}]^{16-}$. *Inorganic Chemistry* **43**, 2689-2694, doi:10.1021/ic0354872 (2004).
- 47 Bruker APEX 2 SAINT Version 6.45A. *Bruker AXS Inc.* (2003).
- 48 Bruker SAINT. *Bruker AXS Inc.*
- 49 Sheldrick, G. M. *Acta Cryst* **A64** (2008).
- 50 Wilson, A. J. C. *International Tables for X-ray Crystallography*. Vol. C (Academic Publishers, 1992).
- 51 Rodríguez, M., Romero, I., Sens, C. & Llobet, A. RuO complexes as catalysts for oxidative transformations, including the oxidation of water to

- molecular dioxygen. *Journal of Molecular Catalysis A: Chemical* **251**, 215-220 (2006).
- ⁵² Sala, X., Romero, I., Rodríguez, M., Escriche, L. & Llobet, A. Molecular Catalysts that Oxidize Water to Dioxygen. *Angewandte Chemie International Edition* **48**, 2842-2852 (2009).
- ⁵³ Brown, G. M. & Sutin, N. A Comparison of the Rates of Electron Exchange Reactions of Ammine Complexes of Ruthenium(II) and -(III) with the Predictions of Adiabatic, Outer-Sphere Electron Transfer Models. *J. Am. Chem. Soc.* **101**, 883-892 (1979).
- ⁵⁴ Ghosh, P. K., Brunschwig, B. S., Chou, M., Creutz, C. & Sutin, N. Thermal and Light-Induced Reduction of Ru(bpy)₃³⁺ in Aqueous Solution. *J. Am. Chem. Soc.* **106**, 4772-4783 (1984).
- ⁵⁵ Harriman, A., Pickering, I. J., Thomas, J. M. & Christensen, P. A. Metal Oxides as Heterogeneous Catalysts for Oxygen Evolution under Photochemical Conditions. *J. Chem. Soc. Faraday Trans. 1*, **84**, 2795-2806 (1988).
- ⁵⁶ Harriman, A., Richoux, M.-C., Christensen, P. A., Mosseri, S. & Neta, P. Redox Reactions with Colloidal Metal Oxides: Comparison of Radiation-generated and Chemically generated RuO₂•2H₂O and MnO₂ Colloids. *J. Chem. Soc., Faraday Trans. 1* **83**, 3001-3014 (1987).
- ⁵⁷ Ruhlmann, L., Nadjo, L., Canny, J., Contant, R. & Thouvenot, R. Di- and Tetranuclear Dawson-Derived Sandwich Complexes: Synthesis,

- Spectroscopic Characterization, and Electrochemical Behavior. *Eur. J. Inorg. Chem.*, 975-986 (2002).
- ⁵⁸ Weinstock, I. A., Atalla, R. H., Reiner, R. S., Moen, M. A., Hammel, K. E., Houtman, C. J., Hill, C. L. & Harrup, M. K. A New Environmentally Benign Technology for Transforming Wood Pulp Into Paper. Engineering Polyoxometalates As Catalysts for Multiple Processes. *J. Mol. Catal. A: Chem.* **116**, 59-84 (1997).
- ⁵⁹ Weinstock, I. A., Barbuzzi, E. M. G., Wemple, M. W., Cowan, J. J., Reiner, R. S., Sonnen, D. M., Heintz, R. A., Bond, J. S. & Hill, C. L. Equilibrating Metal-oxide Cluster Ensembles for Oxidation Reactions Using Oxygen in Water. *Nature* **414**, 191-195 (2001).
- ⁶⁰ Burstall, F. H. & Nyholm, R. S. Studies in co-ordination chemistry. Part XIII. Magnetic moments and bond types of transition-metal complexes. *J. Chem. Soc.*, 3570-3579, doi:10.1039/JR9520003570 (1952).
- ⁶¹ Baes, J., Charles F. & Mesmer, R. E. *The Hydrolysis of Cations*. (John Wiley & Sons, 1976).

Chapter III

Coupling of Photosensitizers with Molecular Water Oxidation Catalysts for use in Artificial Photosynthesis, and Light-driven Water Splitting via Photoelectrochemical Cells

Published in part in “Insights into Photoinduced Electron Transfer Between

$[\text{Ru}(\text{mptpy})_2]^{4+}$ (mptpy = 4'(4-methylpyridinio)-2,2':6',2''-terpyridine) and

$[\text{S}_2\text{O}_8]^{2-}$: Computational and Experimental Studies,” *J. Phys. Chem. C.* **2010**, in
revision.

With Musaev, D. G.; Kaledin, A.; Huang, Z.; Yin, Q.; Geletii, Y. V.; Constable, E.;
Dunphy, E.; Housecroft, C.; Lian, T.; Hill, C. L.

Abstract

The combination of the previously-mentioned water oxidation catalysts and photosensitizer is explored. Systems that model possible artificial photosynthesis schemes are employed to demonstrate the compatibility of the POM-based water oxidation catalysts (WOCs), **1** and **2**, with light-driven water splitting systems. The capability of WOC coupled photosensitizers to harvest light energy is evaluated. While the oxidative stability of organic containing metal to ligand charge transfer (MLCT) complex is not ideal, they remain attractive light-capturing complexes due to a broad visible light absorption range and relatively long excited state lifetimes. Alternatively, the possibility of utilizing photoelectrochemical cells in conjunction with complexes **1** and **2** as WOCs to split water via light energy is explored. Such a system could be potentially useful. Discussions of the photoanode reveal the need to synthesize better photosensitive semiconductor metal oxides as well as improving their functionalization.

Introduction

Artificial photosynthesis involves harvesting light energy to split water, ultimately, at a much higher efficiency than plants do.¹⁻¹³ The water oxidation event must be coupled to photon absorption in order to be useful. Both photovoltaics (PV) and photosensitizers (PS) operate on the same fundamental principle. When PV or PS absorb photons, electrons are promoted to excited states, generating an electron and hole pair. This corresponds to a rise in potential energy. These excited states are short lived (10^{-8} s to 10^{-4} s).¹⁴⁻¹⁷ Relaxation to the ground electronic state occurs rapidly. PV materials eject electrons using incident light energy, generating a direct current. However, as discussed in Chapter I, electrical energy is difficult to store and PV cells present unique challenges in production cost as well as environmental concerns.^{2,3,6,8,9,18-26} While development of PV materials is very much viable and valuable, my research has focused on coupling PS with WOCs directly.

As shown in figure 1.2, the PS scheme needs to trap both the electron and the hole generated through light absorption in a redox pair (as in the classic Gratzel cell).¹³ A light-driven water oxidation scheme can trap the hole generated through oxidizing the WOC. After four holes are transferred to the WOC, four electron oxidation of water as previously described may occur to trap the potential energy in a stable diradical oxygen molecule. The electrons must be similarly trapped in a stable reductant, thus completing the requisite charge separation.

Four-electron oxidation of water is one of the most, if not the most, thermodynamically and kinetically challenging reactions in nature.²⁷⁻³³ The

naturally occurring Oxygen Evolving Complex (OEC) in Photosystem II has a peak TOF of about 1000 s^{-1} .³⁴ It also rapidly decomposes due to photo-bleaching and self-oxidation. The best artificial systems are almost two orders of magnitude slower. Given that the longest living PS excited states have lifetimes of less than 1 ms, it is currently impossible to trap the holes generated in diradical oxygen before quenching the excited electrons. The excited electron in the PS must be quenched first to generate an oxidizing PS thermodynamically capable of water oxidation. This can be done through a terminal oxidant or electrochemically.

Using a terminal oxidant other than O_2 is practically undesirable and energetically costly. However, it can be used as a first step proof-of-concept experiment to demonstrate the viability of such a scheme.³⁵ This reaction system has been employed both heterogeneously and homogeneously. Catalyst complex **1** described in chapter 1 has been coupled with $[\text{Ru}(\text{bpy})_3]^{2+}$ to catalyze light-driven water oxidation (figure 3.1).

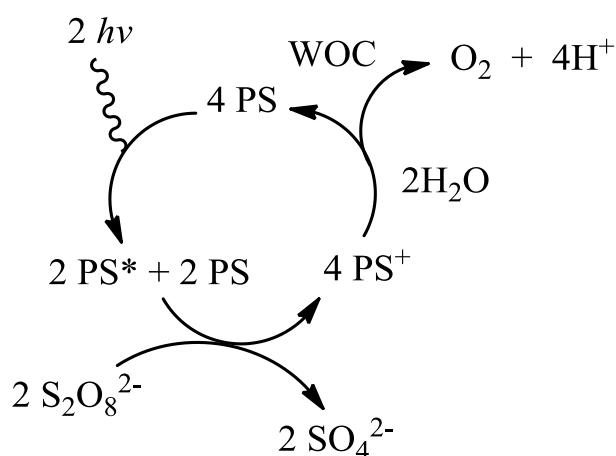


Figure 3.1 A generalized chemical scheme for the given light-driven water oxidation. PS: photosensitizer, PS*: photoexcited photosensitizer, PS⁺: oxidized photosensitizer, WOC: water oxidation catalyst. The chemical scheme is balanced.

An excited PS can be oxidized at the anode of an electrochemical cell. Ideally, the excited electron will travel to the cathode, where it will reduce water. The hole remaining on the PS can then oxidize the WOC, which will then oxidize water. While the excited states of most PS are reducing enough to reduce protons to hydrogen thermodynamically, it is nonetheless kinetically difficult.¹¹⁻¹³ Also taking the inefficiency of current WOCs into consideration, it is not surprising that such systems generally require an external bias potential in addition to light in order to split water.³⁶⁻⁴¹ Nevertheless, such systems are capable of using light energy to split water, netting an overall positive energy gain.

A number of molecules and materials are capable photosensitizers for water oxidation. The most widely used ones are ruthenium based metal-ligand charge transfer (MLCT) complexes.^{40,42-45} In this chapter, a homogenous water oxidation system induced by light using such MLCT complexes is reported, thus demonstrating the possibility of coupling WOC complexes **1** and **2** with PS. Construction of a photoelectrochemical cell is also reported. I will also briefly discuss possible modifications and improvements to the photosensitive anode surface.

Experimental

Analysis of O₂ content using gas chromatography (GC)

In the photocatalytic system, a 10 mL round-bottom flask with a total volume of ~17 mL was used to hold 8 mL of aqueous reaction solution. The reaction vessel was capped with a rubber stopper and extensively deaerated by bubbling argon gas through the solution for over 10 minutes. Stirring was

accomplished using a Teflon-coated stirrer. A fully deaerated 250 μL Hamilton gas-tight syringe was used to withdraw a sample of the gas in the round-bottom headspace. Aliquots (100 μL) of this gas were immediately injected into a Hewlett-Packard 5890 gas chromatograph fitted with a thermal conductivity detector for analysis. Illumination was achieved using a 150 W Hamamatsu Xenon lamp fitted with a cutoff filter. The reaction was paused at different time intervals by shielding the reaction vessel from the light beam. A sample of the headspace gas was taken at each of these intervals.

Calibration of this system is done using the exact same procedures substituting the reaction solutions with water. After mixing, 23.5 μL , 47 μL , or 70.5 μL of pure O_2 (corresponding to 1, 2, or 3 $\mu\text{mol O}_2$) are injected into the headspace of the reaction vessel. The reaction vessel is shaken to allow adequate mixing. Aliquots (100 μL) of the reaction vessel headspace are then transferred using a deaerated Hamilton gas-tight syringe into the gas chromatograph for analysis. The retention times of oxygen and nitrogen are separated by approximately 20 seconds. The oxygen peak is seen first a little less than 1 minute. Contamination from air is minimal and accounted for by subtracting half of the nitrogen peak area from the total oxygen peak area. This is a conservative estimate, as the gas chromatograph gives an oxygen to nitrogen ratio of 1 : 2.8 for a sample of air. The amount of O_2 is plotted against the integration area for the adjusted oxygen peak. A linear correlation between the two is found and the slope is used as the conversion factor for the quantification of O_2 in future injections.

Synthesis of $[\text{Ru}(\text{mptpy})_2]^{4+}$

[Ru(mptpy)₂][PF₆]₄ (0.03 M) was dissolved in a mixture of 9:1 MeCN:CH₂Cl₂. Tetrabutylammonium hydrogen sulfate (0.12 M) was added and the resulting mixture stirred for 30 min. A red precipitate was collected by filtration, washed with MeCN (2 x 10 mL), redissolved in H₂O, and the solvent removed under reduced pressure to give a dark red solid (0.13 g, 0.12 mmol, 78 %).

Photoelectrochemistry

Current-potential scans were done using a three-electrode system at room temperature in buffered solution. Working electrode potential was controlled using a VersaStat II potentiostat. A saturated Ag/AgCl was used as the reference electrode. A platinum wire was used as the counter electrode. Illumination of the working electrode materials was achieved using a 300 W Hamamatsu Xenon lamp fitted with a 420 nm – 520 nm cutoff filter.

Synthesis of the semiconductor metal oxide working electrode

The working electrode is taken as the anode. A fluorine doped tin oxide (FTO) layer forms a transparent conductive glass layer. α -Fe₂O₃ (hematite) nanoparticles suspended in an aqueous colloidal solution were then doctor-bladed onto half of the FTO surface to form a thin uniform layer. Once air dried, this film is baked at 450°C for two and a half hours to achieve thermal annealing. This film is then refluxed in toluene overnight with a trimethoxysilyl-quaternary-ammonium reagent. The modified surface is soaked in a saturated solution of complex **1** to adsorb said POM.

Results and Discussion

Visible-light-driven water oxidation using **1** has previously been reported. As seen in figure 3.1, this scheme is dependent upon the presence of photons,

$[\text{Ru}(\text{bpy})_3]^{2+}$ (a PS), **1** (a WOC), and $\text{S}_2\text{O}_8^{2-}$ (the terminal oxidant). Here, $\text{S}_2\text{O}_8^{2-}$ serves as an electron sink. It allows for separation of charges in this homogeneous system and demonstrates that **1** may be coupled with a PS to catalyze water oxidation.

As compatibility of **2** with a completely homogeneous light-driven water oxidation system is crucial in the further development of artificial photosynthesis involving **2** as a WOC. A similar study as that described above was conducted using an analogous scheme and complex **2**. Following the scheme described in figure 3.1, complex **2** catalyzes light-driven water oxidation. Figure 3.2 shows the oxygen yield in this system with three different concentrations of **2**.

Much of the loss in the quantum yield of this system occurs due to the inefficient quenching of photoexcited $[\text{Ru}(\text{bpy})_3]^{*2+}$ with persulfate. This results from a relatively short lifetime of the excited $[\text{Ru}(\text{bpy})_3]^{*2+}$ state as well as a relatively small window of light absorption. Attempts at finding a better PS was centered around a $[\text{Ru}(\text{mptpy})_2]^{4+}$ complex (mptpy = 4'-(4-methylpyridinio)-2,2':6,2''-terpyridine; figure 3.3).⁴⁶ This dye was shown to have a high oxidation potential (1.39 V vs. NHE), a relatively long excited state lifetime, a high extinction coefficient over a wide absorption range that overlaps well with the solar spectrum, and a high positive charge allowing for stronger ion pairing and electronic interaction with negatively charged POMs.

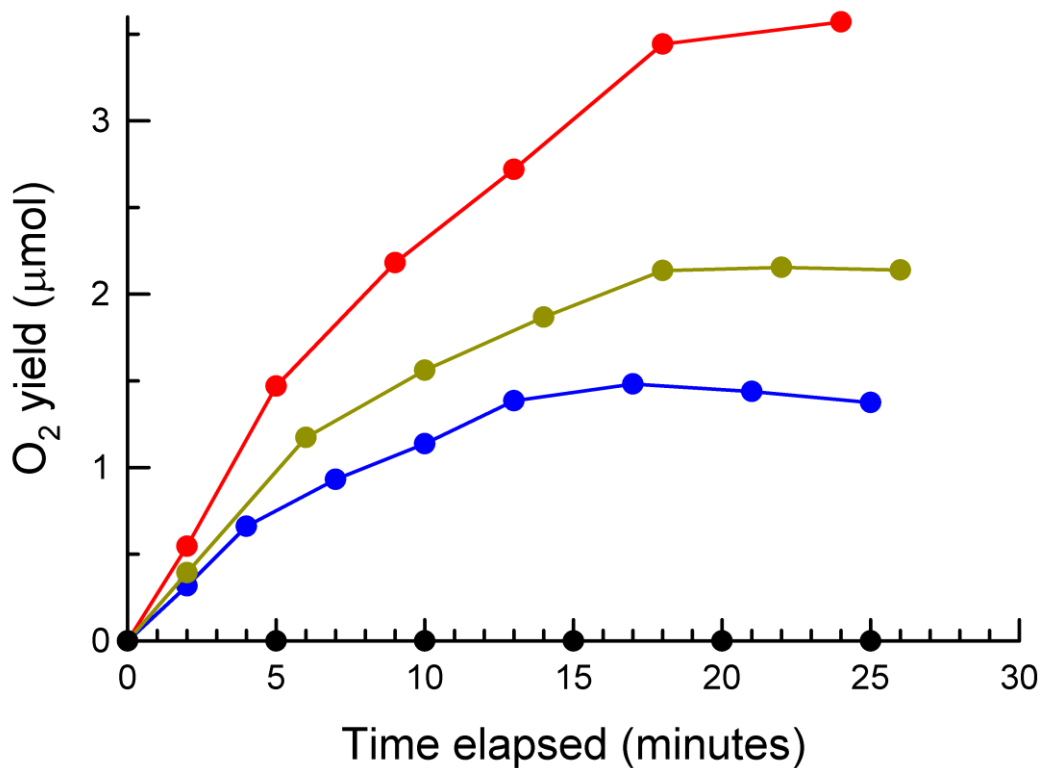


Figure 3.2 The time-profile of oxygen yield using **2** as the WOC in figure 3.1, with 0.0032 mM **1** (red), 0.00128 mM **1** (yellow), and 0.000512 mM **1** (blue). An 8 mL solution of 2.5 mM of sodium persulfate, 30 mM NaPi buffer at pH 8, and 1 mM $[\text{Ru}(\text{bpy})_3]^{2+}$ was used.

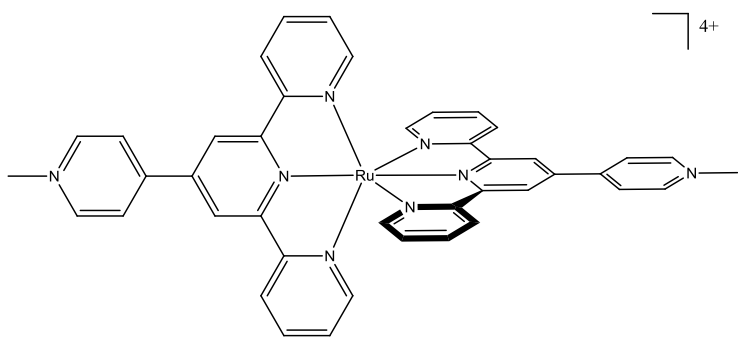


Figure 3.3 Structure of $[\text{Ru}(\text{mptpy})_2]^{4+}$

It would seem that $[\text{Ru}(\text{mptpy})_2]^{4+}$ is an ideal PS for light energy capture and would be extremely efficient in the scheme summarized in figure 3.1. However, experiments involving complex **1** and $[\text{Ru}(\text{mptpy})_2]^{4+}$ reveal numerous problems. First, solubility of the highly positively charged $[\text{Ru}(\text{mptpy})_2]^{4+}$ with the negatively charged persulfate and POM is low in solution. Adequate PS concentration is therefore difficult to achieve. Second, charge transfer from the excited $[\text{Ru}(\text{mptpy})_2]^{4+}$ to $\text{S}_2\text{O}_8^{2-}$ is slower than that of the $[\text{Ru}(\text{bpy})_3]^{2+}$ because of a lower excitation energy. Most importantly, the mptpy ligands in $[\text{Ru}(\text{mptpy})_2]^{4+}$ are much less oxidatively stable than the bpy ligands in $[\text{Ru}(\text{bpy})_3]^{2+}$. This is probably due to the reduced aromatic stabilization of the ligands or the tendency for the oxidized $[\text{Ru}(\text{mptpy})_2]^{5+}$ to hydrolyze due to a smaller metal center and the tridenticity of the ligands. As a result, experiments show that $[\text{Ru}(\text{mptpy})_2]^{4+}$ likely decomposes into RuO_x particles, as evidenced by black precipitates, which catalyze water oxidation. Small amounts of water oxidation activity are gained after the addition of complex **1** as a WOC (figure 3.4).

This result confirms that oxidative stability is of key importance in a water oxidation system. The instability of organic containing PS is unavoidable and undesirable. Therefore, attempts have been made to move towards a photoelectrochemical cell in which a semiconductor metal oxide (SMO) is used as a PS, charge separation is achieved with the application of a small positive bias potential. The desired reaction is summarized in figure 3.5.

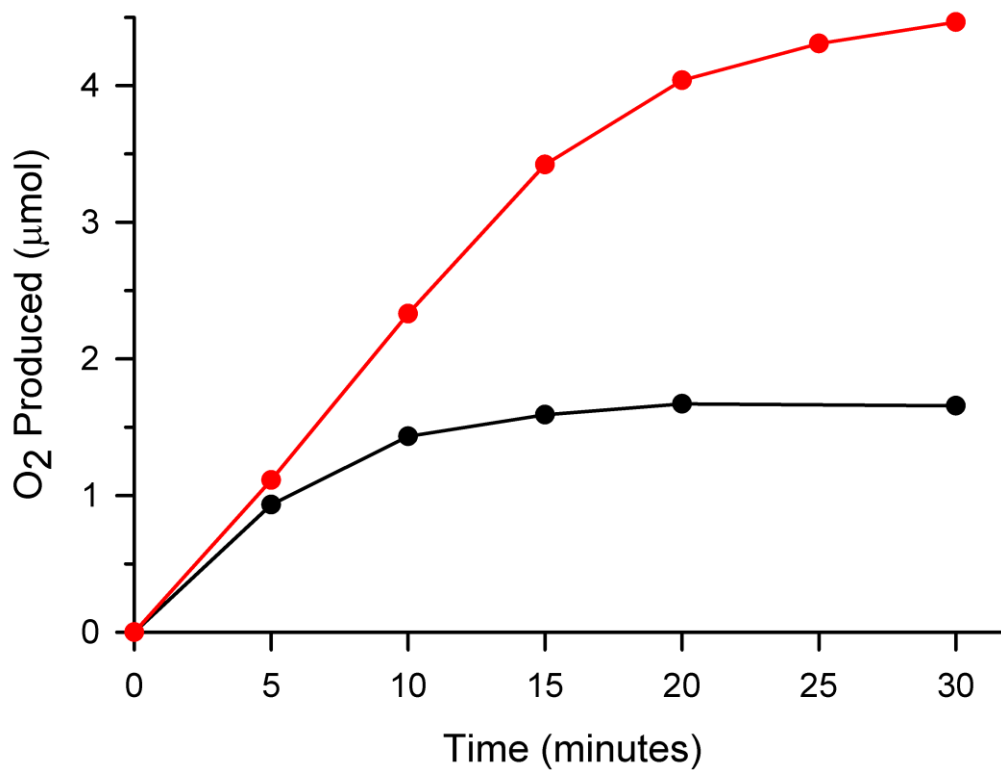


Figure 3.4 The time-profile of oxygen yield using $[\text{Ru}(\text{mptpy})_2]^{4+}$ as the PS in figure 3.1. Reaction was carried out using 5 mM persulfate, 0.2 mM $[\text{Ru}(\text{mptpy})_2]^{4+}$, 20 mM sodium phosphate buffer in 8 mL of solution with no added WOC (black) or 0.008 mM **1** (red). All persulfate was consumed at the end of the reaction.

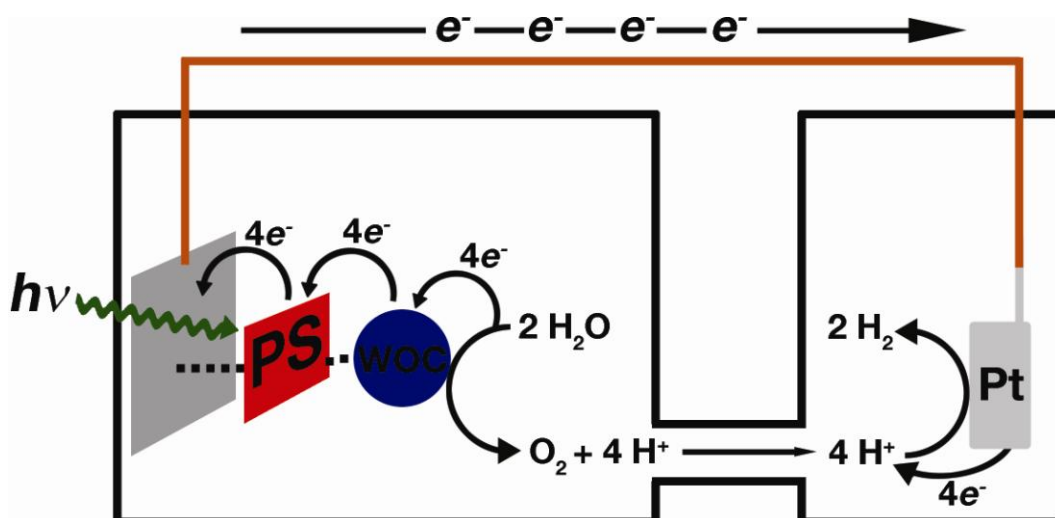


Figure 3.5 A generalized chemical scheme for photoelectrochemical splitting of water, showing the charge separation process.^{39-45,47-57} PS: photosensitizer, WOC: water oxidation catalyst. The chemical scheme is balanced.

Hematite, $\alpha\text{-Fe}_2\text{O}_3$, nanoparticles are used as PS to absorb light in the visible region (figure 3.6). To immobilize POM WOCs such as **1** on the surface of the Fe_2O_3 nanoparticles, a trimethoxysilyl-quaternary-ammonium reagent was used to functionalize the SMO surface (reaction summarized in figure 3.7). The quaternary ammonium can then act as an ion exchange resin to immobilize the POMs. Evidence of this is given by the reflectance IR spectroscopy in figure 3.8. Using this film, a catalytic photocurrent can be obtained in water at pH 7 (20 mM NaPi) with 1 M KNO_3 as the electrolyte (figure 3.9). This catalytic photocurrent may be attributable to water splitting using light energy. Previous reports are consistent with this interpretation. It should be noted that a relatively large bias potential and a relative low current density is observed using this setup. This is probably attributable to the fact that the $\alpha\text{-Fe}_2\text{O}_3$ nanoparticles employed are large

in size and not doped with silicon, which should improve electron transport through the SMO and thus facilitate charge separation. In any case, this experiment seems to demonstrate a system capable of capturing light energy to split water. More experiments are needed to optimize the system.

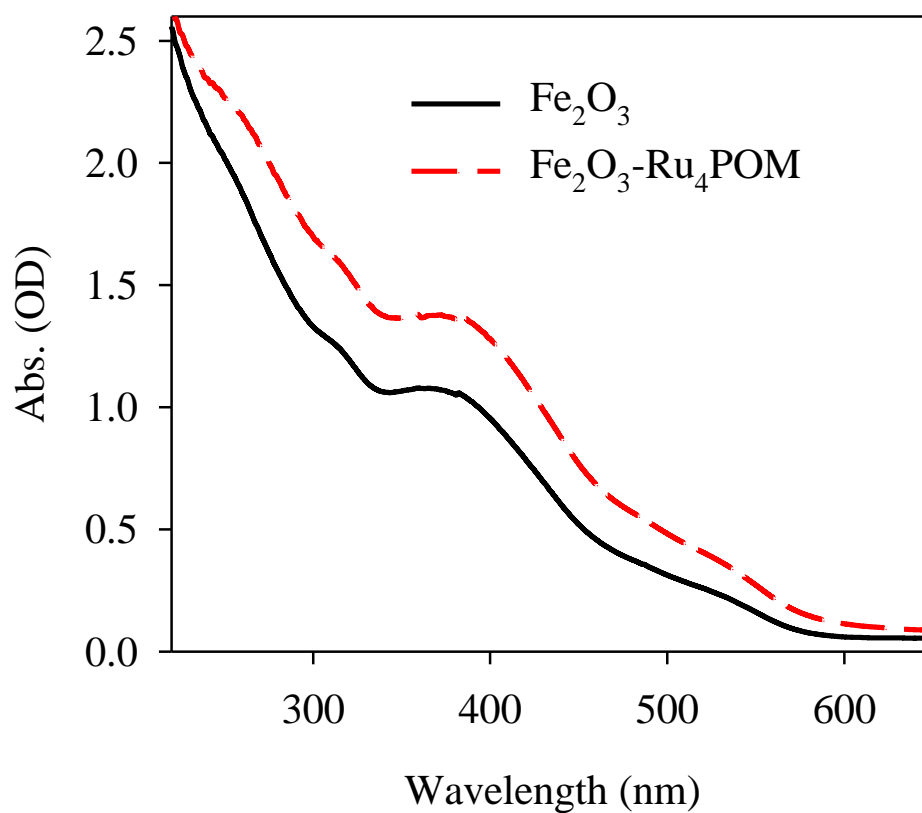


Figure 3.6 UV-visible absorption spectra of a Fe₂O₃ nanoparticle film (black) and after it has been functionalized with **1**.

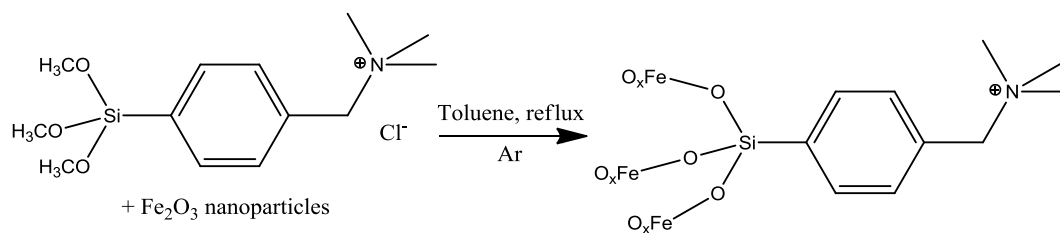


Figure 3.7 Reaction scheme for the functionalization of SMO surface using a silylating reagent with a terminal quaternary ammonium group.

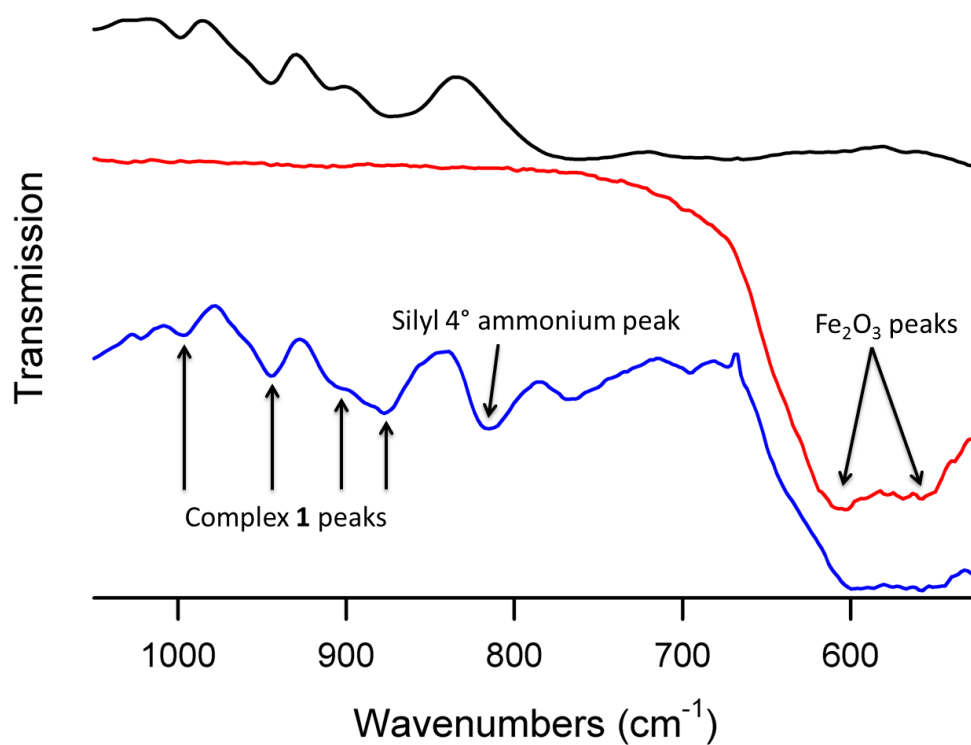


Figure 3.8 Reflectance IR spectrum of crystalline **1** (black), unmodified homogeneous Fe₂O₃ nanoparticle film (red), and Fe₂O₃ film surface modified with **1** via silyl quaternary ammonium.

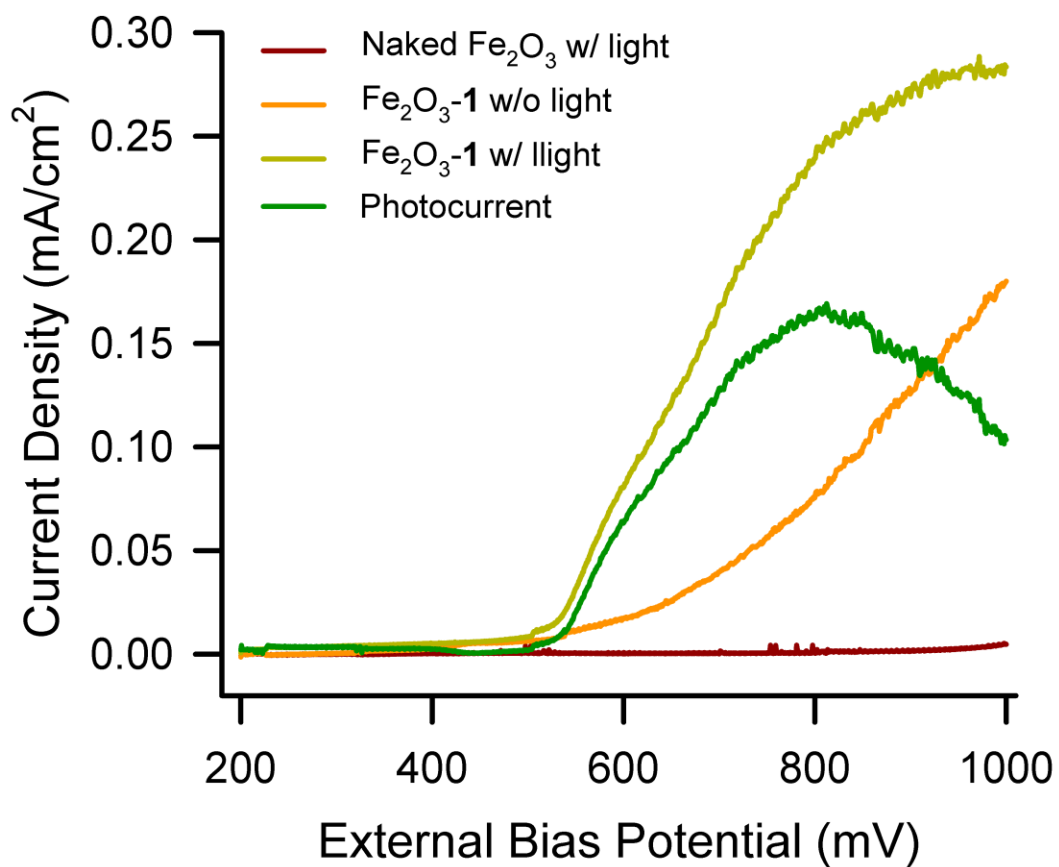


Figure 3.9 A linear current vs. potential sweep using unmodified Fe₂O₃ under illumination (red) and modified Fe₂O₃ both with (yellow) and without (orange) illumination. A plot of the photocurrent (yellow minus orange) is also plotted (green). Aqueous KNO₃ (1 M solution) was used as the electrolyte, and the solution is buffered at pH 7 with 20 mM NaPi. Scan speed is 30 mV/s.

The attachment of the POM WOCs to the surface of the SMO electrode in the previous experiment still involved organic species. These organic linkers will not be stable in an oxidative system. A more promising and scientifically interesting system involves creating a metal-to-metal charge transfer (MMCT) chromophore that can simultaneously act as a PS and bind POM electrostatically. Previous reports of MMCT complexes by Heinz Frei do not allow for simple translation into photoanodes.⁵⁸⁻⁶⁰ Therefore, efforts were made to synthesize a Cr(III)→Ti(IV) MMCT film. Melt synthesis at 100°C of Cr(NO₃)₃ in the presence of a TiO₂ nanoparticle film formed a yellow layer on the surface of the film (figure 3.10). This is likely due to O→Cr(VI) ligand metal charge transfer, which indicates a tetravalent Cr(VI) oxide on the surface of TiO₂ and thus the formation of Ti-O-Cr bonds.^{61,62} Reduction of Cr(VI) to Cr(III) should generate the desired MMCT species.

Ultimately, carbon-free POM-based WOCs can be coupled to photosensitizing light harvesters. Nonetheless, extensive research is still required in order to improve the efficiency and viability of systems based on the design shown in figure 3.5. Realizing efficient artificial photosynthesis in the form of water splitting requires basic research into the coupling of PS and WOCs. Fundamentally, the issues present in light harvesting are chemistry problems. Therefore, chemical research in related areas will facilitate a better understanding of the problems and afford possible solutions.

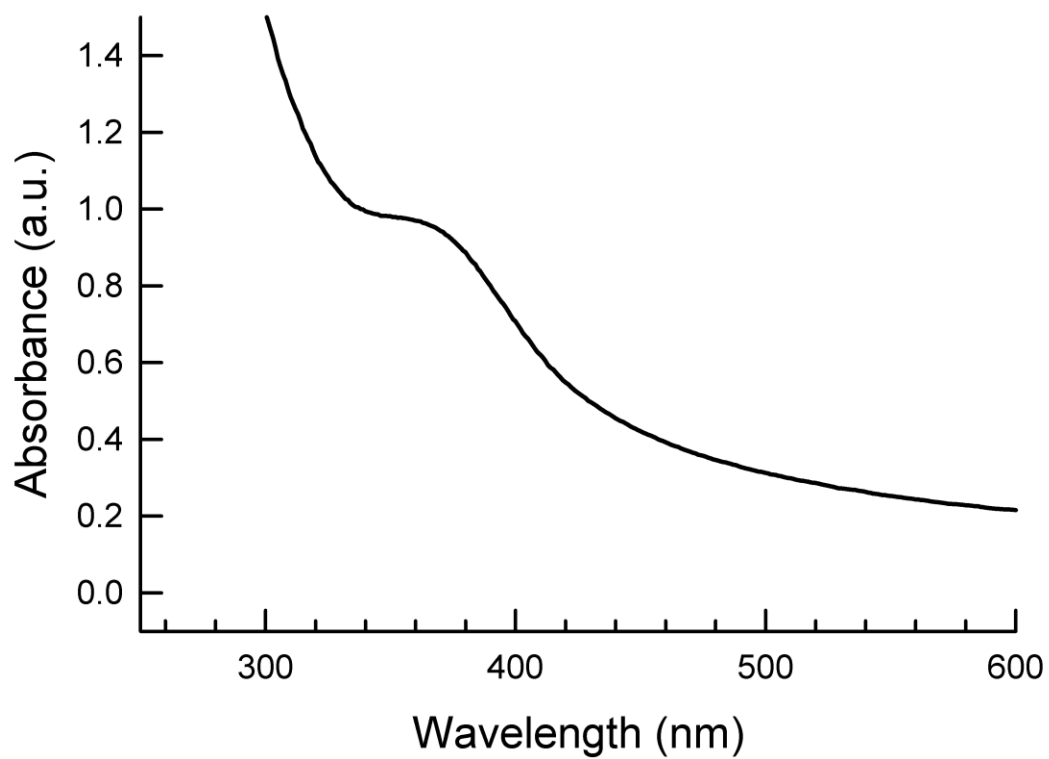


Figure 3.10 UV-visible spectrum of a TiO₂ nanoparticle film deposited on a sapphire window functionalized with chromium oxide. The peak at *ca.* 360 nm is attributable to LMCT transitions of tetravalent chromium oxide.

References

- ¹ Chow, J., Kopp, R. J. & Portney, P. R. Energy Resources and Global Development. *Science* **302**, 1528-1531 (2003).
- ² Balzani, V., Credi, A. & Venturi, M. Photochemical Conversion of Solar Energy. *ChemSusChem* **1**, 26-58, doi:DOI: [10.1002/cssc.200700087](https://doi.org/10.1002/cssc.200700087) (2008).
- ³ Painuly, J. P. Barriers to renewable energy penetration; a framework for analysis. *Renewable Energy* **24**, 73-89, doi:Doi: [10.1016/s0960-1481\(00\)00186-5](https://doi.org/10.1016/s0960-1481(00)00186-5) (2001).
- ⁴ Hoffert, M. I., Caldeira, K., Benford, G., Criswell, D. R., Green, C., Herzog, H., Jain, A. K., Kheshgi, H. S., Lackner, K. S., Lewis, J. S., Lightfoot, H. D., Manheimer, W., Mankins, J. C., Mauel, M. E., Perkins, L. J., Schlesinger, M. E., Volk, T. & Wigley, T. M. L. Advanced Technology Paths to Global Climate Stability: Energy for a Greenhouse Planet. *Science* **298**, 981-987, doi:10.1126/science.1072357 (2002).
- ⁵ Twidell, J. & Weir, T. *Renewable Energy Resources*. (Taylor & Francis, 2006).
- ⁶ Barnham, K. W. J., Mazzer, M. & Clive, B. Resolving the energy crisis: nuclear or photovoltaics? *Nat Mater* **5**, 161-164 (2006).
- ⁷ Granqvist, C. G., Niklasson, G. A. & Azens, A. Electrochromics: Fundamentals and energy-related applications of oxide-based devices. *Applied Physics A: Materials Science & Processing* **89**, 29-35 (2007).

- 8 Lewis, N. S. Powering the Planet. *MRS Bulletin* **32**, 208-820 (2007).
- 9 Lewis, N. S. & Nocera, D. G. Powering the planet: Chemical challenges in solar energy utilization. *Proc. Nat. Acad. Sci.* **103(43)**, 15729-15735 (2006).
- 10 Pimentel, D. Ethanol fuels: Energy security, economics, and the environment. *Journal of Agricultural and Environmental Ethics* **4**, 1-13 (1991).
- 11 Meyer, T. J. Chemical approaches to artificial photosynthesis. *Accounts of Chemical Research* **22**, 163-170, doi:10.1021/ar00161a001 (1989).
- 12 Bard, A. J. & Fox, M. A. Artificial Photosynthesis: Solar Splitting of Water to Hydrogen and Oxygen. *Accounts of Chemical Research* **28**, 141-145, doi:10.1021/ar00051a007 (1995).
- 13 Graetzel, M. Artificial photosynthesis: water cleavage into hydrogen and oxygen by visible light. *Accounts of Chemical Research* **14**, 376-384, doi:10.1021/ar00072a003 (1981).
- 14 Hagfeldt, A. & Gratzel, M. Molecular Photovoltaics. *Accounts of Chemical Research* **33**, 269-277, doi:10.1021/ar980112j (2000).
- 15 Kaledin, A. L., Huang, Z., Geletii, Y. V., Lian, T., Hill, C. L. & Musaev, D. G. Insights into photoinduced electron transfer between $[\text{Ru}(\text{bpy})_3]^{2+}$ and $\text{S}_2\text{O}_8^{2-}$ in water: computational and experimental studies. *J. Phys. Chem. A* **114**, 73-80 (2010).

- 16 Howard, I. A., Zutterman, F., Deroover, G., Lamoen, D. & Van Alsenoy,
C. Approaches to calculation of exciton interaction energies for molecular
dimer. *J. Phys. Chem. B* **108**, 19155-19162 (2004).
- 17 Scholes, G. D. *In Resonance Energy Transfer*. (Wiley, 1998).
- 18 Johansson, T. B., Kelly, H., Reddy, A. K. N. & Williams, R. H.
Renewable energy: Sources for fuels and electricity. (1993).
- 19 Rosa, A. d. *Fundamentals of Renewable Energy Processes*. (Academic
Press, 2009).
- 20 The future is not black. *Nat Mater* **5**, 159-159 (2006).
- 21 Materials for clean energy. *Nature* **414**, 331-331 (2001).
- 22 Laboratory, O. R. N. Basic Research Needs To Assure A Secure Energy
Future. *U.S. Department of Energy* (2008).
- 23 Miles, R. W., Hynes, K. M. & Forbes, I. Photovoltaic solar cells: An
overview of state-of-the-art cell development and environmental issues.
Progress in Crystal Growth and Characterization of Materials **51**, 1-42
(2005).
- 24 Fthenakis, V. M. & Moskowitz, P. D. Photovoltaics: environmental, health
and safety issues and perspectives. *Progress in Photovoltaics: Research
and Applications* **8**, 27-38 (2000).
- 25 Knapp, K. & Jester, T. Empirical investigation of the energy payback time
for photovoltaic modules. *Solar Energy* **71**, 165-172 (2001).
- 26 Kazmerski, L. L. Photovoltaics: A review of cell and module technologies.
Renewable and Sustainable Energy Reviews **1**, 71-170.

- ²⁷ Eisenberg, R. & Gray, H. B. Preface on Making Oxygen. *Inorg. Chem.* **47**, 1697-1699 (2008).
- ²⁸ Kanan, M. W. & Nocera, D. G. In Situ Formation of an Oxygen-Evolving Catalyst in Neutral Water Containing Phosphate and Co^{2+} . *Science* **321**, 1072-1075, doi:[10.1126/science.1162018](https://doi.org/10.1126/science.1162018) (2008).
- ²⁹ Geletii, Y. V., Besson, C., Hou, Y., Yin, Q., Musaev, D. G., Quinonero, D., Cao, R., Hardcastle, K. I., Proust, A., Kögerler, P. & Hill, C. L. Structural, Physicochemical and Reactivity Properties of an All-Inorganic, Highly Active Tetra-ruthenium Homogeneous Catalyst for Water Oxidation. *J. Am. Chem. Soc.* **131**, 17360-17370 (2009).
- ³⁰ Yin, Q., Tan, J. M., Besson, C., Geletii, Y. V., Musaev, D. G., Kuznetsov, A. E., Luo, Z., Hardcastle, K. I. & Hill, C. L. A fast soluble carbon-free molecular water oxidation catalyst based on abundant metals. *Science*, Printed online March 11, 2010, doi:[10.1126/science.1185372](https://doi.org/10.1126/science.1185372) (2010).
- ³¹ Yagi, M. & Kaneko, M. Molecular Catalysts for Water Oxidation. *Chemical Reviews* **101**, 21-36, doi:[10.1021/cr980108l](https://doi.org/10.1021/cr980108l) (2000).
- ³² Geletii, Y. V., Botar, B., Kögerler, P., Hillesheim, D. A., Musaev, D. G. & Hill, C. L. An All-Inorganic, Stable, and Highly Active Tetra-ruthenium Homogeneous Catalyst for Water Oxidation. *Angew. Chem. Int. Ed.* **47**, 3896-3899. Selected as the VIP Article by the reviewers and editor. Published online 3893/3820/3808 DOI: [10.1002/anie.200705652](https://doi.org/10.1002/anie.200705652), doi:[DOI: 10.1002/anie.200705652](https://doi.org/10.1002/anie.200705652) (2008).

- 33 Romain, S., Bozoglian, F., Sala, X. & Llobet, A. Oxygen—Oxygen Bond Formation by the Ru-Hbpp Water Oxidation Catalyst Occurs Solely via an Intramolecular Reaction Pathway. *J. Am. Chem. Soc.* **131**, 2768-2769 (2009).
- 34 Bricker, T. M. Oxygen evolution in the absence of the 33-kilodalton manganese-stabilizing protein. *Biochemistry* **31**, 4623-4628, doi:10.1021/bi00134a012 (1992).
- 35 Henbest, K., Douglas, P., Garley, M. S. & Mills, A. Persulfate quenching of the excited state of ruthenium(II) tris-bipyridyl dication: thermal reactions. *J. Photochem. Photobiol, A: Chem.* **80**, 299-305 (1994).
- 36 Youngblood, W. J., Lee, S.-H. A., Kobayashi, Y., Hernandez-Pagan, E. A., Hoertz, P. G., Moore, T. A., Moore, A. L., Gust, D. & Mallouk, T. E. Photoassisted Overall Water Splitting in a Visible Light-Absorbing Dye-Sensitized Photoelectrochemical Cell. *J. Am. Chem. Soc.* **131**, 926-927, doi:10.1021/ja809108y (2009).
- 37 Youngblood, W. J., Lee, S.-H. A., Maeda, K. & Mallouk, T. E. Visible Light Water Splitting Using Dye-Sensitized Oxide Semiconductors. *Accounts of Chemical Research* **42**, 1966-1973, doi:10.1021/ar9002398 (2009).
- 38 Heller, A. Conversion of sunlight into electrical power and photoassisted electrolysis of water in photoelectrochemical cells. *Accounts of Chemical Research* **14**, 154-162, doi:10.1021/ar00065a004 (1981).

- 39 Brimblecombe, R., Dismukes, G. C., Swiegers, G. F. & Spiccia, L. Molecular water-oxidation catalysts for photoelectrochemical cells. *Dalton Trans.*, 9374 - 9384 (2009).
- 40 Grätzel, M. Photoelectrochemical cells. *Nature* **414**, 338-344 (2001).
- 41 Sivula, K., Formal, F. L. & Grätzel, M. WO₃-Fe₂O₃ Photoanodes for Water Splitting: A Host Scaffold, Guest Absorber Approach. *Chem. Mater.* **21**, 2862-2867 (2009).
- 42 Grätzel, M. Conversion of sunlight to electric power by nanocrystalline dye-sensitized solar cells. *J. Photochem. Photobiol. A: Chem.* **164**, 3-14 (2004).
- 43 Grätzel, M. Solar Energy Conversion by Dye-Sensitized Photovoltaic Cells. *Inorg. Chem.* **44**, 6841-6851 (2005).
- 44 Nazeeruddin, M. K., Kay, A., Rodicio, I., Humphry-Baker, R., Müller, E., Liska, P., Vlachopoulos, N. & Grätzel, M. Conversion of Light to Electricity by *cis*-X₂Bis(2,2'-bipyridyl-4,4'-dicarboxylate)ruthenium(II) Charge-Transfer Sensitizers (X = Cl⁻, Br⁻, I⁻, CN⁻, and SCN⁻) on Nanocrystalline TiO₂ Electrodes. *J. Am. Chem. Soc.* **115**, 6382-6390 (1993).
- 45 Rotzinger, F. P., Munavalli, S., Comte, P., Hurst, J. K., Gratzel, M., Pern, F.-J. & Frank, A. J. A Molecular Water-Oxidation Catalyst Derived from Ruthenium Diaqua Bis(2,2'-bipyridyl-5,5'-dicarboxylic acid). *J. Am. Chem. Soc.* **109**, 6619-6626 (1987).

- ⁴⁶ Musaev, D., Kaledin, A., Huang, Z., Yin, Q., Geletii, Y., Constable, E., Dunphy, E., Housecroft, C., Lian, T. & Hill, C. Insights into Photoinduced Electron Transfer Between $[\text{Ru}(\text{mptpy})_2]^{4+}$ (mptpy = 4'(4-methylpyridinio)-2,2':6',2''-terpyridine) and $[\text{S}_2\text{O}_8]^{2-}$: Computational and Experimental Studies. *J. Phys. Chem.* **In submission** (2010).
- ⁴⁷ Bonhôte, P., Moser, J.-E., Humphry-Baker, R., Vlachopoulos, N., Zakeeruddin, S. M., Walder, L. & Grätzel, M. Long-Lived Photoinduced Charge Separation and Redox-Type Photochromism on Mesoporous Oxide Films Sensitized by Molecular Dyads. *J. Am. Chem. Soc.* **121**, 1324-1336 (1999).
- ⁴⁸ Borgarello, E., Kiwi, J., Pelizzetti, E., Visca, M. & Grätzel, M. Sustained water cleavage by visible light. *J. Am. Chem. Soc.* **103**, 6324-6329 (1981).
- ⁴⁹ Brown, G. E., Henrich, V. E., Casey, W. H., Clark, D. L., Eggleston, C., Felmy, A., Goodman, D. W., Grätzel, M., Maciel, G., McCarthy, M. I., Nealson, K. H., Sverjensky, D. A., Toney, M. F. & Zachara, J. M. Metal oxide surfaces and their interactions with aqueous solutions and microbial organisms. *Chem. Rev.* **99**, 77-174 (1999).
- ⁵⁰ Cesar, I., Kay, A., Martinez, J. A. G. & Grätzel, M. Translucent Thin Film Fe_2O_3 Photoanodes for Efficient Water Splitting by Sunlight: Nanostructure-Directing Effect of Si-Doping. *J. Am. Chem. Soc.* **128**, 4582-4583 (2006).
- ⁵¹ Clifford, J. N., Palomares, E., Nazeeruddin, M. K., Grätzel, M., Nelson, J., Li, X., Long, N. J. & Durrant, J. R. Molecular Control of Recombination

- Dynamics in Dye-Sensitized Nanocrystalline TiO₂ Films: Free Energy vs Distance Dependence. *J. Am. Chem. Soc.* **126**, 5225-5233 (2004).
- 52 Comte, P., Nazeeruddin, M. K., Rotzinger, F. P., Frank, A. J. & Grätzel, M. Artificial analogues of the oxygen-evolving complex in photosynthesis: the oxo-bridged ruthenium dimer L₂(H₂O)Ru^{III}-O-Ru^{III}(H₂O)L₂, L = 2,2'-bipyridyl-4,4'-dicarboxylate. *J. Mol. Catal.* **52**, 63-84 (1989).
- 53 Duret, A. & Grätzel, M. Visible Light-Induced Water Oxidation on Mesoscopic α-Fe₂O₃ Films Made by Ultrasonic Spray Pyrolysis. *J. Phys. Chem. B* **109**, 17184-17191 (2005).
- 54 Grätzel, M. *Heterogeneous Photochemical Electron Transfer*. (CRC Press, 1989).
- 55 Nazeeruddin, M. K. & Grätzel, M. Transition Metal Complexes for Photovoltaic and Light Emitting Applications. *Struct. Bond.* **123**, 113-173 (2007).
- 56 Serpone, N., E. Pelizzetti & Grätzel, M. Photosensitization of Semiconductors with Transition Metal Complexes - A Route to the Photoassisted Cleavage of Water. *Coord. Chem. Rev.* **64**, 225-245 (1985).
- 57 Ghosh, A. K. & Maruska, H. P. Photoelectrolysis of Water in Sunlight with Sensitized Semiconductor Electrodes. *J. Electrochem. Soc.* **124**, 1516-1522 (1977).
- 58 Han, H. & Frei, H. Controlled Assembly of Hetero-binuclear Sites on Mesoporous Silica: Visible Light Charge-Transfer Units with Selectable Redox Properties. *J. Phys. Chem.* **112**, 8391-8399 (2008).

- 59 Jiao, F. & Frei, H. Nanostructured Cobalt Oxide Clusters in Mesoporous Silica as Efficient Oxygen-Evolving Catalysts. *Angew. Chem. Int. Ed.* **48**, 1841 (2009).
- 60 Nakamura, R. & Frei, H. Visible Light-Driven Water Oxidation by Ir Oxide Clusters Coupled to Single Cr Centers in Mesoporous Silica. *J. Am. Chem. Soc.* **128**, 10668-10669 (2006).
- 61 Khaddar-Zine, S., Ghorbel, A. & Naccache, C. EPR and UV–visible spectroscopic studies of alumina-supported chromium oxide catalysts. *Journal of Molecular Catalysis A: Chemical* **150**, 223-231 (1999).
- 62 Malecki, A., Ma³ecka, B., Gajerski, R. & Labus, S. THERMAL DECOMPOSITION OF CHROMIUM(III) NITRATE(V) NANOHYDRATE Different chromium oxides CrO_{1.5+y} formation. *Journal of Thermal Analysis and Calorimetry* **72**, 135-144 (2003).